ACCELERATED DISTRIBUTION DEMONSTRATION SYSTEM

REGULATORY INFORMATION DISTRIBUTION SYSTEM (RIDS)

ACCESSION NBR:9008070270 DOC.DATE: 90/08/02 NOTARIZED: NO DOCKET #
FACIL:50-275 Diablo Canyon Nuclear Power Plant, Unit 1, Pacific Ga 05000275
50-323 Diablo Canyon Nuclear Power Plant, Unit 2, Pacific Ga 05000323
AUTH.NAME AUTHOR AFFILIATION
SHIFFER,J.D. Pacific Gas & Electric Co.
RECIP.NAME RECIPIENT AFFILIATION
Document Control Branch (Document Control Desk)

SUBJECT: Forwards response to NRC questions re long term seismic program geology,seismology & geophysics issues.

DISTRIBUTION CODE: D031D COPIES RECEIVED:LTR 1 ENCL 1 SIZE: 139
TITLE: Diablo Canyon Long-Term Seismic Program

NOTES: See Reports

	RECIPIENT ID CODE/NAME	COPIES LTTR	COPIES ENCL	RECIPIENT ID CODE/NAME	COPIES LTTR	COPIES ENCL
	PD5 LA	1	0	PD5 PD	5	5
	ROOD,H	1	1			
INTERNAL:	ACRS	~~0~~ 1	~~0~~ 1	ADM/LFMB	1	0
	NRR ASHAR,H	1	1	NRR BAGCHI,G	1	1
	NRR JENG,D	1	1	NRR PICHUMANI,R	1	1
	NRR ROTHMAN,R	1	1	NRR/DST 8E2	1	1
	~~NRR/PMAS/ILRB12~~	1	1	OGC/HDS2	1	0
	REG FILE 01	1	1	RES/DE/SSEB/SES	1	1
EXTERNAL:	LPDR	1	1	NRC PDR	1	1
	NSIC	1	1			

NOTE TO ALL "RIDS" RECIPIENTS:

PLEASE HELP US TO REDUCE WASTE! CONTACT THE DOCUMENT CONTROL DESK, ROOM P1-37 (EXT. 20079) TO ELIMINATE YOUR NAME FROM DISTRIBUTION LISTS FOR DOCUMENTS YOU DON'T NEED!

TOTAL NUMBER OF COPIES REQUIRED: LTTR 27 ENCL ~~24~~ 19

RIDS/ADDS

RIDS/ADDS

Pacific Gas and Electric Company
77 Beale Street
San Francisco, CA 94106
415/973-4684
TWX 910-372-6587

James D. Shiffer
Senior Vice President and
General Manager
Nuclear Power Generation

August 2, 1990

PG&E Letter No. DCL-90-201

U.S. Nuclear Regulatory Commission
ATTN: Document Control Desk
Washington, D.C. 20555

Re: Docket No. 50-275, OL-DPR-80
Docket No. 50-323, OL-DPR-82
Diablo Canyon Units 1 and 2
Long Term Seismic Program - Geology/Seismology/Geophysics

Gentlemen:

We are responding to the NRC Staff request dated February 23, 1990, for information relating to Long Term Seismic Program geology, seismology, and geophysics issues. Enclosed are PG&E's responses to questions 2 through 8 and 10 through 13. Questions 1 and 9 relate to ground motions and will be answered in our forthcoming submittal on those issues.

The responses to questions 3 and 4 contain proprietary geophysical data that are exempt from public disclosure in accordance with 10 CFR 2.790(a)(9). The proprietary information is appropriately marked and has been transmitted only to the NRC Project Manager (2 copies) and to NRC consultants (R. D. Brown and D. B. Slemmons). We request that this material be handled in accordance with NRC procedures for proprietary material.

Kindly acknowledge receipt of this material on the enclosed copy of this letter and return it in the enclosed addressed envelope.

Sincerely,

JD Shiffer/RC Anderson

J. D. Shiffer

cc w/enc.: R. D. Brown, Jr.
D. Clark
H. Rood (2)
D. B. Slemmons

cc wo/enc.: A. P. Hodgdon
J. B. Martin
P. J. Morrill
P. P. Narbut
B. Norton
CPUC
Diablo Distribution

3285S/0084K/DWO/1587

A031
1/1

RESPONSE TO GSG QUESTIONS
LP 2 THROUGH LP 8 AND LP 10 THROUGH LP 13

July 1990

This volume responds to 11 geology/seismology/geophysics questions asked of PG&E by the Nuclear Regulatory Commission (NRC) on February 23, 1990. These responses provide data requested to augment or clarify information presented in the Final Report of the Long Term Seismic Program, submitted by PG&E to the NRC on July 31, 1988, information presented in responses to previous NRC questions and information obtained as a result of the Loma Prieta earthquake.

QUESTION LP 2

The seismic velocity model used in the analysis of reflection seismology data may greatly influence the geological interpretation. Therefore, describe and analyze the methods used to derive the velocity model on which the depth sections shown in the montages were based. Of importance are the range of horizontal and vertical velocity gradients near the Hosgri fault zone and also those elsewhere in the offshore Santa Maria basin. Also, discuss the degree of sensitivity of the geologic interpretation of the seismic data (e.g., dip of fault, earthquake potential) to the likely variations in the velocity model used.

METHODS USED TO DERIVE THE VELOCITY MODEL FOR THE MONTAGE

We used a "layer cake" velocity model to depth-convert the interpreted seismic records presented in the montages submitted in Response to Question GSG 1, March 1990. The model is designed to be versatile, allow rapid recalculation, and produce reproducible results. The "layers" were based on the interpretation of the rock units on the seismic reflection time records. The velocities in the model were derived using a combination of stacking velocity information, well data, and seismic refraction data, as well as published velocities from data in the offshore Santa Maria Basin (Hatton and others, 1981).

More complete descriptions of the velocity data, velocity determination techniques, and depth-conversion method are given in Section 3.7 of Attachment GSG Q1-A, submitted in March 1990. The effects of velocity variations are discussed quantitatively. Attachment GSG Q1-A also addresses the specifics of the interpretational procedures used to develop the montages, including the depth conversion process, and most of the information requested in the current question. Additional data on lateral velocity variations in the vicinity of the Hosgri fault zone are given below.

VELOCITY VARIATIONS IN THE VICINITY OF THE HOSGRI FAULT ZONE

Detailed data regarding velocity variations in the vicinity of the Hosgri fault zone are limited. We previously submitted the stacking velocities printed at the top of some of the seismic reflection records that cross the Hosgri fault zone. Additional data on such variations can be derived from the following sources: sonic logs of two Phillips wells, one on each side of the fault zone, and the results of detailed velocity analyses of two seismic reflection records using an iterative prestack depth migration program (Migpack).

Sonic logs are available from Phillips wells 397-1 on the east side of the Hosgri fault zone, and 397-2 on the west side (Figures LP Q2-1 and LP Q2-2). These two wells are approximately 3.5 kilometers apart, about 15.5 kilometers northwest of Point Sal. The wells are discussed further in the Response to Question LP 6, and their locations are shown on Figure LP Q6-1, as well as on the panels for the Point Sal montage. The thinner Monterey and upper Miocene sections on the east side of the Hosgri are evident. Average velocities for the horizons marked on the logs compare favorably between the wells and with the layer-cake model used in the depth conversions. Of course there is a much thicker section of mid- to late-Miocene rocks on the west side of the Hosgri fault zone, but changes in thickness are accommodated directly in the conversion process. The velocities used in the models are presented in Table LP Q2-1 and can be compared with those from the Phillips wells.

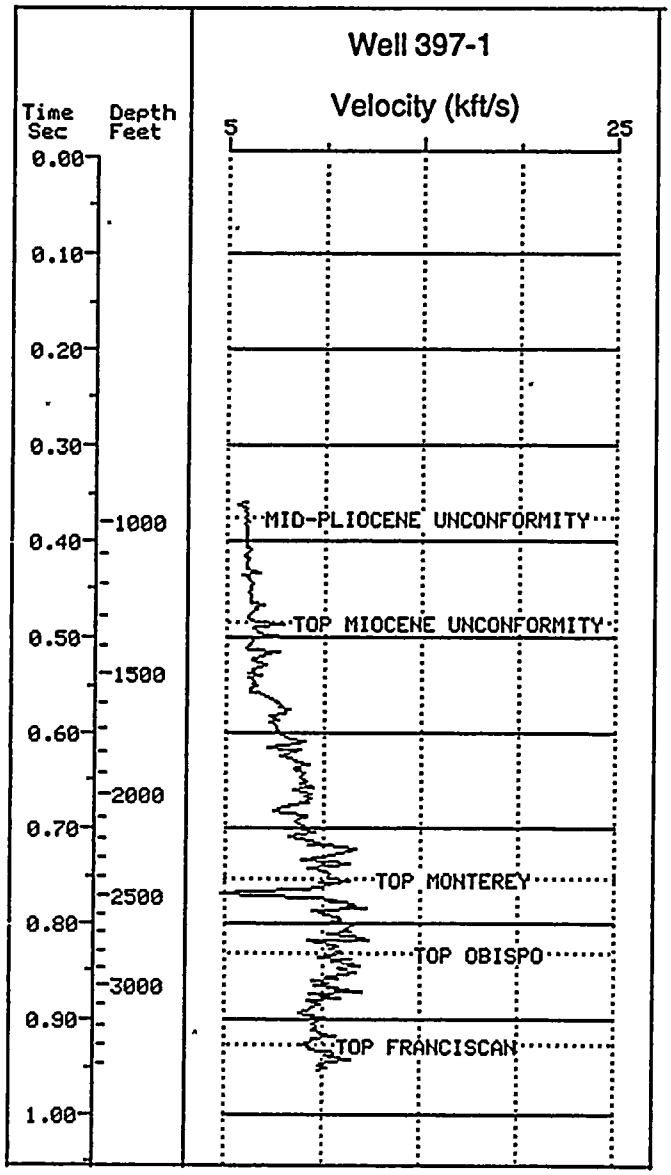

Figure LP Q2-1

Velocity versus depth curve from Phillips well 397-1 on the east side of the Hosgri fault zone. Velocity data are from a sonic log. Horizon boundaries are marked at depths interpreted by PG&E based on additional well log data. Refer to the Response to Question LP 6 for a discussion of the criteria used to identify horizon depths in the wells.

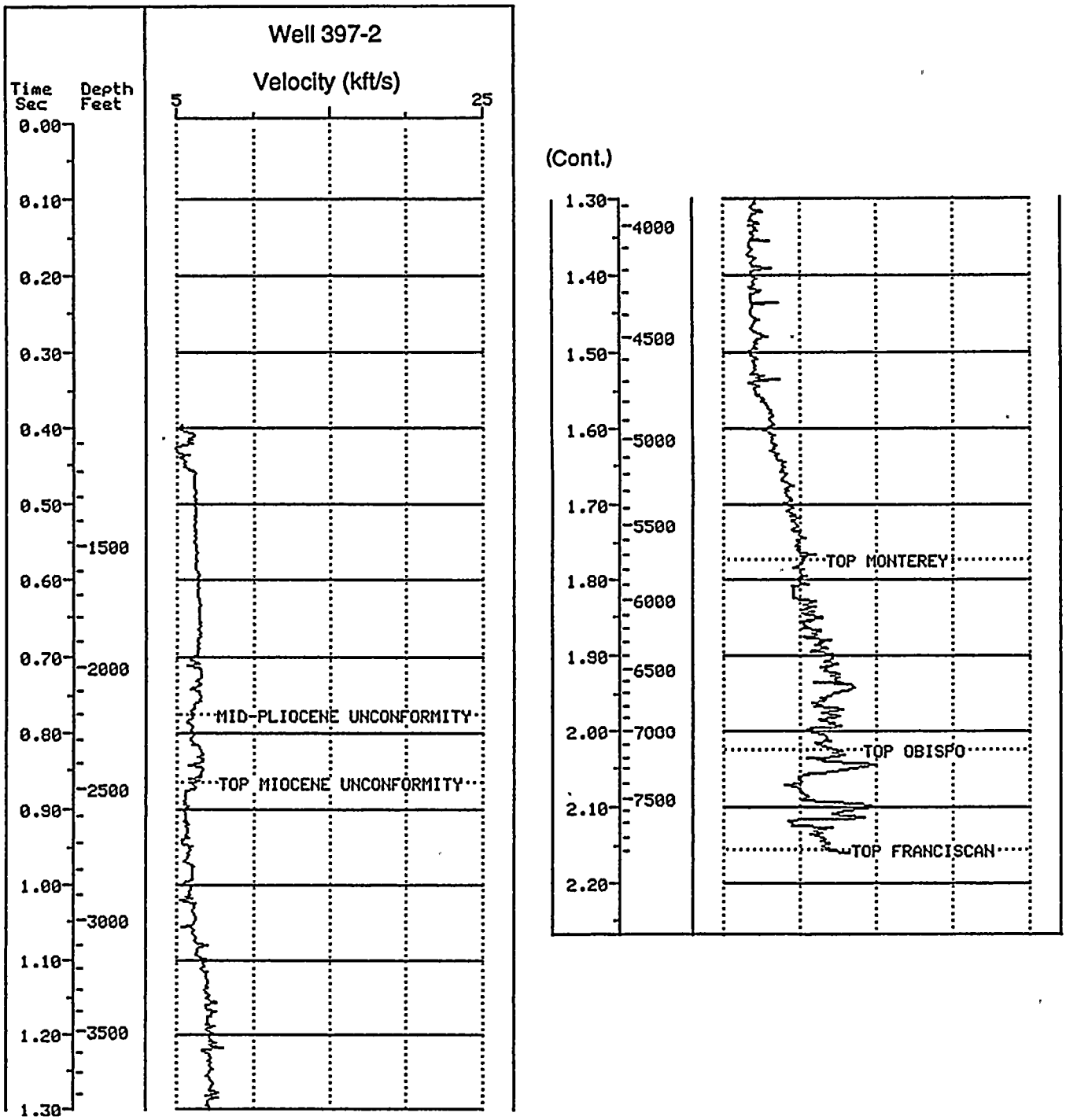

Figure LP Q2-2

Velocity versus depth curve from Phillips well 397-2 on the west side of the Hosgri fault zone. Velocity data are from a sonic log. Horizon boundaries are marked at depths interpreted by PG&E based on additional well log data. Refer to the Response to Question LP 6 for a discussion of the criteria used to identify horizon depths in the wells.

Table LP Q2-1

COMPARISON OF VELOCITY VALUES

Unit	Migpack GSI-87A	Migpack GSI-100	Phillips 397-1	Phillips 397-2	Hatton 1981	PG&E (1988)	Montage
Water	1500	1500	--	--	1500	1500	1500
Sea Floor/Mid-Pliocene	1714	1648	--	1900	1770	1770	1770
Mid-Pliocene/Top Miocene	2182	1824	2000	2100	2130	2230	↓
Top Miocene/Top Monterey Formation	1917	2200	2500	2400	2440	↓	2638
Top Monterey/Opal Ct/ Quartz Diagenitic Front	2378	2341	3000	3000	2740	↓	↓
Lower Monterey Formation	2866	2551	3100	3400	↓	2910	↓
Paleogene Sedimentary and Volcanic Rocks	--	3453	3100	3500	3050	↓	↓
Franciscan Basement	3800	3800	3050	3600	--	4500	3800

NOTES:

1. Velocities are averages for the zones, exclusive of thin layers. All values are in meters/second.
2. Hatton and others' (1981) data are from Queenie structure, 30 kilometers southwest of the Hosgri fault zone.

Additional insight into velocity variations in the vicinity of the Hosgri fault zone is provided by the results of the Migpack program, which was run as a test process on lines GSI-87A and GSI-100. Migpack is an interactive prestack depth migration program that was developed by the French petroleum company, TOTAL. The program is available in the United States through the Houston Area Research Center. The program allows a high level of geologic input into the processing effort. The seismic velocity structure, which is the basis for migration (see also the Response to Question LP 3), is modeled based on a geologic scenario. The Migpack program returns information on the accuracy of the model based upon the ability to provide good seismic imaging, and the interpreter can adjust the model accordingly. The iterative procedure allows convergence to a detailed and accurate velocity structure. Further details are given in Fay and Jeannot (1986), who describe it as one of the most powerful means of subsurface structure imaging available in the presence of lateral velocity variations.

The results derived from the Migpack analysis of GSI lines 87A and 100 are given in Tables LP Q2-2 and LP Q2-3, respectively. The tables provide information on both lateral and vertical velocity variations for each layer used in the model, as well as an "average" value. The heading "curve type" provides information on the form of the velocity distribution curve needed to fit the observed horizontal variations most accurately.

The average velocities provided in the table match closely the values used in the "layer cake" depth-conversion process. The maximum variation for a given layer is about 15 percent; several zones have average values identical to the "layer cake" model.

INTERPRETATIONAL SENSITIVITY ANALYSIS

Section 3.7 of Attachment GSG Q1-A provides quantitative estimates of the variations in estimated thicknesses of units and dips of fault traces that would be computed based on observed variations in velocities used in the "layer-cake" model. Such variations were shown not to be of significance as far as the basic interpretation of the structures are concerned. That is, the velocity model was accurate enough to provide a reasonable depth conversion of interpreted seismic time sections. The resulting depth-converted sections agreed favorably with nearby well data and did not vary erratically nor violate any of the tenets of the interpretational process.

The analyses of detailed vertical and horizontal velocity variations within units and across the Hosgri fault zone (discussed above) did not reveal differences between the more detailed velocity data and the basic "layer-cake" model that would result in significant distortions in the depth-converted sections of the montage. The depth-converted sections were created to provide a 1:1-scale interpretation of the seismic time sections within the accuracy that can be imposed by the available data quality and density. They provide additional insight into the thicknesses and dips of units, and the down-dip geometry and observable depth extent of fault strands. However, the interpretations of factors such as location and dip of the fault plane beneath that observed on the seismic sections, and the earthquake potential of any given fault, are based upon data sets other than the velocity model and associated depth conversions.

REFERENCES

Hatton, L., Larner, K., and Gibson, B., 1981, Migration of seismic data from inhomogeneous media: Geophysics, v. 46, no. 5, p. 751-767.

Table LP Q2-2

MIGPACK VELOCITY ANALYSIS
Line GSI 87

Equivalent PG&E Layer Cake Velocity Zone	Western Velocity (mps)[1]	Eastern Velocity (mps)	Average Velocity (mps)	Curve Type[2]
Seawater	1500	1500	1500	Linear
Post Mid-Pliocene	1575	1875	1714	Linear
Mid-Pliocene/Top Miocene	2182	2182	2182	Linear
Post Top Miocene (Thin layer)	1775	2150	1907	Quadratic[3]
Top Miocene/Top Monterey	1775	2075	1917	Linear
Top Monterey/Opal Ct/ Quartz Diagenitic Front	2525	2250	2378	Linear
Lower Monterey	2800	2975	2866	Linear
Basement[4]	3800	3800	3800	Linear

NOTES:

[1]Velocities are from analyses of horizons on both the western and eastern sides of the Hosgri fault zone.

[2]"Curve type" describes the form of a curve that best fits the horizontal variation within the layer.

[3]For a non-linear variation, the average may be greater than, or less than, the end values.

[4]Basement velocities are established from seismic refraction and sonic log data.

Table LP Q2-3

MIGPACK VELOCITY ANALYSIS
LINE GSI 100

Equivalent PG&E Layer Cake Velocity Zone	Western Velocity mps[1]	Eastern Velocity mps	Average Velocity mps	Curve Type[2]
Seawater	1500	1500	1500	Linear
Post Mid-Pliocene	1648	1648	1648	Linear
Mid-Pliocene/Top Miocene	1824	1824	1824	Linear
Post Top Miocene (Thin Layer)	1975	2500	2224	Linear
Top Miocene/Top Monterey	2200	2200	2200	Linear
Top Monterey/Opal Ct/ Quartz Diagenitic Front	2650	2350	2341	Quadratic[3]
Lower Monterey/Post Basement	2950	2725	2551	Quadratic[3]
Pre Top Monterey/Post Basement Sedimentary and Volcanic Rocks (Thin Layer)	3900	3175	3453	Linear
Basement[4]	3800	3800	3800	Linear

NOTES:

[1]Velocities are from analyses of horizons on both the western and eastern sides of the Hosgri fault zone.

[2]"Curve type" describes the form of a curve that best fits the horizontal variation within the layer.

[3]For a non-linear variation, the average may be greater than, or less than, the end values.

[4]Basement velocities are established from seismic refraction and sonic log data.

Faye, J.-P., and Jeannot, J.-P., 1986, Prestack migration velocities from focusing depth analyses: SEG expanded abstracts.

Pacific Gas and Electric Company, 1988, Final report of the Diablo Canyon Long Term Seismic Program: U. S. Nuclear Regulatory Commission, Docket Nos. 50-275 and 50-323.

QUESTION LP 3

Because new processing has been applied to the seismic reflection lines in the montages, show side-by-side the uninterpreted, reprocessed time sections for GSI lines 85, 86, 101, 103, and 106 and the same uninterpreted lines as they were processed for the LTSP final report. For reference, also display, at the same horizontal and vertical scales the time sections of the original 1980 processing by GeoCenter, Houston. For line GSI 103, which was not shown on the montage, make the comparison with line PG&E 3, which was shown.

The GSI, Nekton, Western, and other data sets purchased by PG&E in 1985 and 1986 were collected in the period from the mid-1970s to the early 1980s. The data were processed by various companies within a year after they were collected, and that was the processing received by PG&E at the time of purchase. Since the advent of digital processing of seismic data, the processing methodology has continued to improve. PG&E reprocessed selected lines in 1986 and 1987 to assess the improvements in image quality that could result from refinements in the processing techniques developed in the early to mid-1980s.

The common-depth-point seismic reflection data sets used in the Long Term Seismic Program are identified in the Table 2-3 of the Final Report (PG&E, 1988) and in the March 1990 Response to Question GSG 1, Attachment GSG Q1-A, Table GSG Q1-A.3. Reprocessing of the data is briefly described in the Final Report (Page 2-10, PG&E, 1988), and additional information on the reprocessing is provided in Section 3.2.2 of Attachment GSG Q1-A. The specific data sets that were reprocessed, in whole or in part, by PG&E are listed in Table LP Q3-1.

Table LP Q3-1

PG&E COMMON-DEPTH-POINT SEISMIC DATA PROCESSING

Acquisition Contractor	Year Shot	Total Kilometers Purchased by PG&E	Year Reprocessed by PG&E	Total Kilometers Reprocessed by PG&E
Aquatronics	1976	479	---	---
Comap Alaska	1986	500	1990	8.2
Digicon	1986	290	1989	290.0
GSI	1980	1296	1987 1989	216.0 25.0
Nekton 45	1983	154	1987	78.5
Western Geophysical	1974-1982	470	1987	117.0

Proprietary Data Notice: The response to this question contains seismic reflection records that are proprietary to the geophysical contractors or oil companies that originally collected the data. These data are shown on Figures LP Q3-2 through LP Q3-11. The distribution of these data is controlled and subject to the written permission of PG&E and the provisions of 10CFR 2.790. Therefore, copies of Figures LP Q3-2 through LP Q3-11 are not included with all copies of the Response to Question LP 3.

Table LP Q3-2 lists the typical processing sequence used for 1986 and 1987 PG&E contracted processing work, including the reprocessing of the GSI lines. These tables are from Attachment GSG Q1-A (Tables GSG Q1-A.4 and Q1-A.5, respectively) and are included in this response for ease of reference.

The GSI lines referred to in this question were originally processed by GeoCenter, Inc. in 1980 for Ogle Petroleum. These processed records were purchased by PG&E in 1986. Selected portions of this data set were reprocessed by PG&E in 1986 and 1987. Thus these reprocessed records were available and used along with the original records processed by GeoCenter in the analysis of offshore structures presented in the Final Report (PG&E, 1988).

We have prepared figures that show, side-by-side, the original processed record sections and the reprocessed sections from Seisdata Services, Inc. The figures were prepared for the five requested GSI lines, as well as for four additional GSI lines and one line from the Nekton-45 data set. Figure LP Q3-1 shows the locations of the seismic lines. The reprocessing comparisons are presented as Figures LP Q3-2 through Q3-11. Each figure shows the original processed sections on the left side and the reprocessed sections on the right side. Structure sections (also referred to as AGC sections or stacked sections) are shown on top, migrated sections on the bottom of the panels. The horizontal distance scale of all GSI sections is approximately 1:48,000, the same scale as that used for the montage sections provided with Attachment GSG-1A. The horizontal scale of the original Nekton record is 1:12,600, and the reprocessed sections are at 1:24,000. The vertical scale is two-way travel time, and is the same as that used in the montage sections. Therefore, the GSI sections presented in the figures can be compared directly with the migrated time sections and interpreted migrated time sections in the montage display.

The reprocessing sequence is outlined in Table LP Q3-2, and summary data for the reprocessed lines are presented in Table LP Q3-3. Five lines in addition to those requested were included to provide a broader geographic range to the data set, to show the effects of the reprocessing on the various structural features within the Hosgri fault zone, and to provide a basis for comparing the reprocessing results between two overlapping lines from two data sets.

A figure has been prepared for GSI line 103, comparing the original version with the reprocessed version of the same line, rather than line PG&E 3, as was requested. This figure also can be compared with the figure for Nekton-45 line 202, which is the line closest to GSI line 103, shown on the montage of the Point Sal area. These two lines are within 0.25 kilometers of each other over their 8-kilometer overlap distance. Because they illustrate the same structural features within the Hosgri fault zone, we did not include GSI line 103 on the Point Sal reach montage. PG&E line 3 is shown as section T-T′ on both the the Point Sal reach and San Luis Obispo Bay reach sections of the montage. However, the distance between GSI line 103 and PG&E line 3 is generally 2.5 kilometers or greater, and the data collection, data processing, and playback parameters for PG&E line 3 were significantly different from those for GSI line 103.

OBJECTIVES AND PROCEDURES OF THE REPROCESSING

Selected geophysical data were reprocessed primarily to improve the imaging of seismic events related to the Hosgri fault zone. Thus, reprocessing was concentrated on those parts of the lines that crossed the fault zone. In particular, we sought improvements in identifying the vertical extent and dip of the individual strands, quantifying dips of the reflectors within the fault zone, and defining stratigraphic units used in assessing the timing of the structural events.

Table LP Q3-2

TYPICAL DATA PROCESSING SEQUENCE FOR 1986 TO 1987 PG&E-CONTRACTED WORK

1. Demultiplex.
2. Gain recovery.
3. Deconvolution: spiking or predictive with time variant gates.
4. Bandwidth filter.
5. Sort: common-depth-point gathers and add water depth statics.
6. Vector multi-prestack: water bottom and long period multiple attenuator (proprietary to Seisdata Services, Inc.).
7. Velocity analysis every ½ mile or less along the line as structural complexity demands.
8. Normal moveout.
9. Trace muting.
10. Common-depth-point stack.
11. Time variant filter.
12. Automatic-gain-control (AGC): 250 to 500 ms gate depending on data type.
13. Noise rejection filter (NRF): enhances primary energy and attenuates severe steeply dipping diffracted energy with near water velocity. The NRF is similar to a 2-D FK filter.
14. Remove water depth statics applied in Step 5.
15. Wave equation migration: frequency domain operator using a smoothed root-mean-square (RMS) stacking velocity field converted to an average velocity via Dix's equation.
16. Film display of Steps 12, 13 and 15.

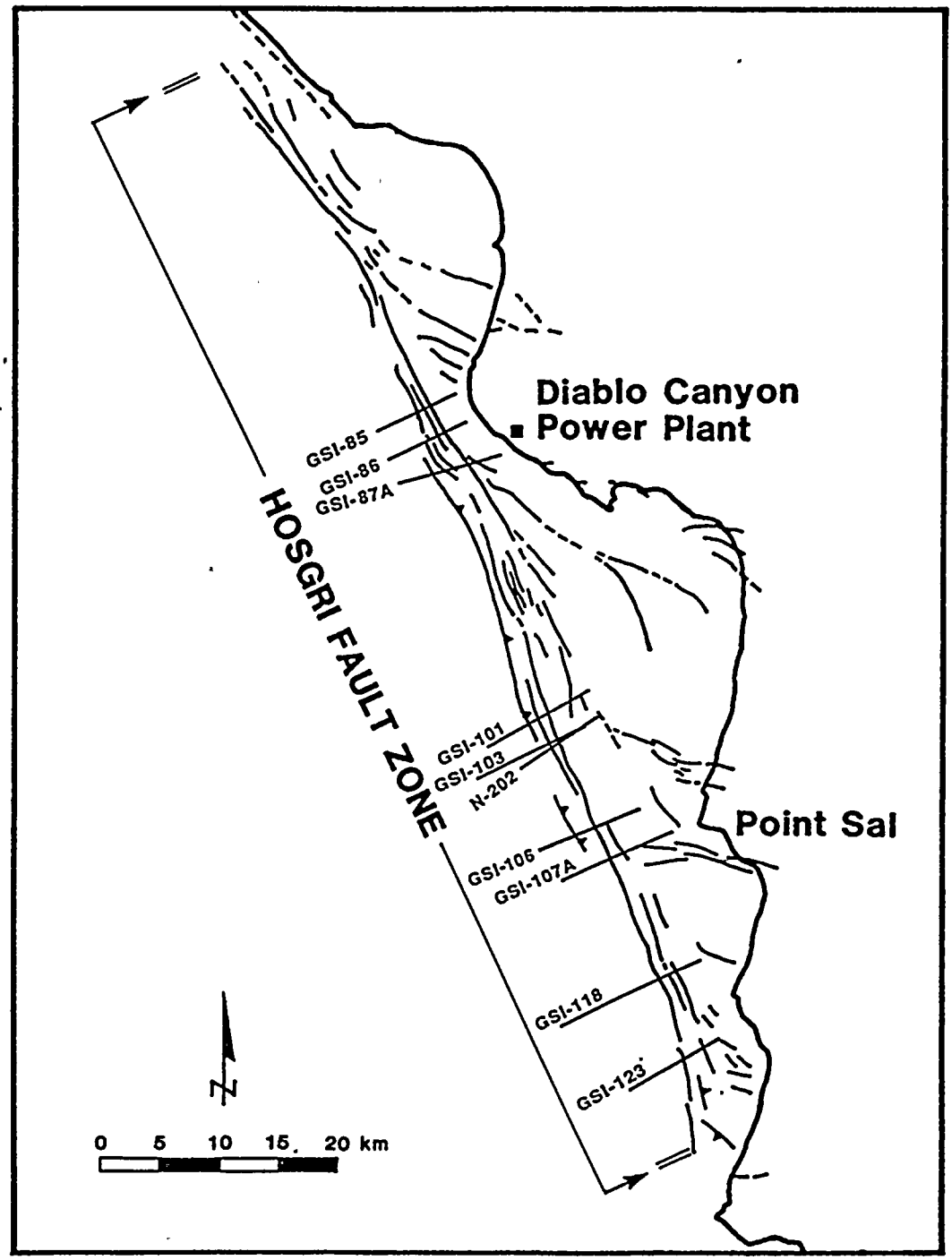

Figure LP Q3-1

Index map showing the approximate locations of the 10 seismic reflection survey lines used for comparing the results of original contractor processing with reprocessing performed under PG&E's direction.

Table LP Q3-3

SEISMIC LINES ILLUSTRATED FOR REPROCESSING COMPARISONS

Line Number	Figure Number	Montage Line and Reach	Original Processing Shot Points[1]	Reprocessing by Seisdata, Inc.	
				Shot Point	Length
GSI-85	LP Q3-2	K-K' San Luis/Pismo	50-724[2]	303-722	(11 km)
GSI-86	LP Q3-3	M-M' San Luis/Pismo	50-676	293-675	(10 km)
GSI-87A	LP Q3-4	N-N' San Luis/Pismo	50-533	53-533	(13 km)
GSI-101	LP Q3-5	U-U' Point Sal	50-516	53-516	(12 km)
GSI-103	LP Q3-6	Not shown. Point Sal	50-1350	824-1350	(14 km)
GSI-106	LP Q3-7	X-X' Point Sal	50-1356	803-1356	(14 km)
GSI-107A	LP Q3-8	Y-Y' Point Sal	676-1138	676-1137	(11 km)
GSI-118	LP Q3-9	BB-BB' Southern	50-892	53-892	(22 km)
GSI-123	LP Q3-10	DD-DD' Southern	50-699	274-700	(11 km)
N-202	LP Q3-11	V-V' Point Sal	137-98[3]	99-137	(12 km)

NOTES:

[1]Only the reprocessed parts of the original seismic sections are shown in the figures. The complete lines from the original processing were submitted in January 1989.

[2]GSI lines were originally processed by GeoCenter, Inc.

[3]Nekton lines were originally processed by Nekton, Inc.

The original field data tape from one GSI line was sent to eight seismic processing contractors for test processing. Six contractors reprocessed the line and submitted results for evaluation. A panel of outside consultants[1] reviewed the results and selected Seisdata Services Inc. (now Seismic Processors, Inc.) as the contractor, based on the quality of their submittal. Throughout the reprocessing effort, PG&E consultants worked closely with Seisdata Services to monitor quality and various intermediate products such as the velocity analyses. The reprocessing of selected lines was completed by mid-1987, although a few lines were revised after that date. Thus, these data were available for reference during the preparation of the Final Report (PG&E, 1988).

As part of PG&E's continuing outside peer review process, copies of the original and reprocessed seismic records were sent to Dr. Norman S. Neidell, an internationally recognized signal processing consultant from Houston, Texas. He reviewed the results of the reprocessing in detail, and his comments on specific lines are incorporated into the detailed evaluation comments presented below.

CRITERIA FOR EVALUATION

The evaluation of two or more processing sequences when they are applied to the same seismic data set is linked to the interpretative objectives of the study -- that is, the imaging of the geologic features significant to the specific investigation. In fact, no element of viewing seismic results is independent of the study objectives. Because of the continued improvement in digital processing techniques, there is also a time factor that must be taken into consideration when comparing results from two processing sequences. Since the advent of digital signal processing and its application to seismic reflection data, the processing technology has improved significantly. The processing results being evaluated within the framework of this question were based on the technology available from processing contractors in the early 1980s versus that available in 1986 and 1987. It is also important to recognize that certain processing procedures, which may emphasize particular attributes on a portion of a seismic record, will inevitably have other consequences, possibly in a negative sense, elsewhere on the same record or on records from adjacent lines. Optimum processing results are not achieved by applying a uniform set of parameters across an entire data set. This is especially true in areas of complex geology such as along the Hosgri fault zone.

The prime interpretive objective for the reprocessing of data in the offshore Santa Maria Basin was enhancement of the imaging of the Hosgri fault zone. Thus, we concentrated on reprocessing those parts of the seismic lines that crossed the fault zone. In some instances, parts of those lines that extended westward across the Santa Maria Basin were not reprocessed. In the following paragraphs we discuss the specific criteria and attributes that were used in our evaluation of the reprocessing results.

The evaluation of steeply dipping structural features will have a high degree of uncertainty because such features are poorly imaged or not imaged at all by standard seismic surveys. The presence and position of very steeply dipping boundaries are, in fact, usually inferred from those contrasts in the subsurface that are more readily imaged and are interrupted or displaced. In contrast, low-angle features (for example, thrust faults, shallowly dipping sedimentary units, and horizontal phase change boundaries), are among the elements that are well imaged on seismic records with traditional processing.

[1]The panel included three members of the Long Term Seismic Program Consulting Board: Clarence Allen, Bruce Bolt, and Cole McClure, as well as several technical advisors: Jan Rietman, a consulting geophysicist, and Robert Clayton and Donald Helmberger from the California Institute of Technology.

It then follows that one goal of the reprocessing is correct imaging of reflector elements that enable us to recognize both the steeply dipping as well as low-angle elements of the Hosgri fault zone. Continuous contrasts that show minor vertical separation or horizontal interruption, changes in background patterns or seismic character, vertical patterns of disruption, amplitude anomalies, and localized structural geometries are all important imaging goals. Detailed imaging of sequence stratigraphy and related interpretational attributes is also important, as it helps to establish structural axes and timing of deformation. Thus, attention to small detail contained in the higher frequency content of the seismic data is clearly warranted.

Along the same lines of logic, the identification of structural elements at the greatest depths possible is essential for discerning the down-dip geometry of the various elements. Such deep data are only present in the lower frequency content of the records. Due to scattering of energy from tightly folded structures in the upper section, such deeper events may not be well imaged. Short, continuous, low-frequency events seen at depth may be the partial seismic image of valid geologic information; however, they may also be artifacts of the data processing. Processing steps such as migration and frequency domain filters with amplitude enhancement can artificially smooth and increase the apparent coherence of adjacent low-frequency pulses in an otherwise incoherent part of the section. These effects appear on both the early 1980 processing and the 1986-1987 reprocessing.

East of the Hosgri fault zone, many lines show a region lacking layered structure. Although parts of the seismic records contain only dipping noise trains and nondescriptive events, the pattern is sufficiently consistent and distinctive to have interpretive and, therefore, imaging significance. The seismic imaging elsewhere on the sections is sufficiently definitive to establish that the pattern is real; if layers or some more regular character were present, they would have been imaged. The observed patterns result from geologic processes that destroyed any original "layers" to the extent they can no longer be approximated by dipping planer surfaces having the dimension of the Fresnel zone, which, even in the upper one second of record section can have a dimension of 100 meters or more.

One of the key elements to be noted on all sections is the frequency with which velocity analyses have been applied along the line. Assuming that the analyses are correct, an increase in the number of analyses will result in a corresponding increase in image quality. The validity of the velocity control can, in part, be established by noting the effectiveness with which multiple reflections are suppressed and the "sharpness" of the images produced by the subsequent migration.

The migration process attempts to achieve two goals. First, it attempts to place reflection events in their correct spatial position by removing the effects of inherent assumptions of the "vertical plotting" present in the structure sections. That is, to compensate for the incorrect assumption that all reflections originated from a point in the subsurface halfway between the source and receiver. The correctness of event migration and positioning is best confirmed by nonseismic data such as well-ties. Second, the migration process seeks to undo the averaging over the Fresnel zone and provide more distinct and spatially independent subsurface data. This degree of focusing is related to the quality of the velocity field and may be readily evaluated. If, after migration, diffraction events remain uncollapsed or are overmigrated (become concave rather than convex as on the structure sections), the velocities are incorrect. However, where the migration has eliminated such features, the correctness of the velocity field is confirmed.

EVALUATION OF THE REPROCESSING RESULTS

Our review of the reprocessing results showed, in general, major improvements in the following areas:

1. Suppression of multiple energy.
2. Improved imaging of stratigraphic relationships and unconformities.
3. Improved accuracy in imaging of folded structures.
4. Improved definition of fault strands through more accurate location of event terminations.
5. More accurate spatial positioning of data through improved migration.
6. Improved imaging of deeper events (2.0- to 4.0-second range).

These general observations are discussed further with regard to the individual seismic lines shown on Figures LP Q3-2 to LP Q3-11. The figures are discussed in the order presented in Table LP Q3-3. Elements of the Hosgri fault zone and their improved imaging resulting from the reprocessing are addressed in greater detail in the discussions for the first few seismic lines. The basic imaging improvements are present on most of the reprocessed lines, so subsequent references and discussions are generally shorter.

Line GSI 85, Figure LP Q3-2

This line is also illustrated as profile K-K' on the panels for the San Luis/Pismo reach of the montage. The Hosgri fault zone is between shot points 480 and 600. Elements of the fault zone and associated deformation that are more clearly shown on the reprocessed migrated section are: termination of steep dips on the west side (shot points 490 to 520, 0.6 to 0.9 seconds); onset of conflicting dip direction on the east side; tightly folded, closely spaced, conformable parallel beds (shot points 575 to 630, 0.2 to 1 seconds); and bed terminations (shot points 575 to 590, 0.4 to 1.5 seconds, and shot points 490 to 560, 1.2 to 1.7 seconds). The original processing migrated section shows very few of these features.

A comparison of the structure sections shows that the reprocessed record has used twice as many velocity analyses. This additional velocity control, coupled with a superior treatment of the seismic waveform, has resulted in a seismic section having broader band-width (in particular, higher frequency content -- note the thinner and better-resolved peaks on the reprocessed section), better signal-to-noise characteristics, and reduced diffraction content.

The improved signal content is seen both as a gain in definition of the reflectors against random noise, as in the case of the reflections at about 1.4 seconds around shot points 420 to 490, as well as in reduced multiple content. Dipping water-bottom multiples are far more pronounced on the original processing sections, for example below shot points 340 to 500, than they are on the more recent processing.

Reduced diffraction content is also quite evident. Note the signal content in the more or less linear portions of the diffraction "tails" seen in the deeper parts of the section. These signatures originate from features near the water bottom and represent low seismic velocities. The application of a good velocity

field in the reprocessing results in a superior migrated seismic section. The reprocessed section also incorporates an additional signal enhancement technique (Step 13, Table LP Q3-2, noise reduction filter), which even further improves the migrated seismic section.

Between shot points 460 to 520, from 0.5 to 2.0 seconds, the stacked and migrated data on both processing sequences display cross-over of reflections. These arise primarily from "tight" folding at depth and from oblique ray paths arising from out-of-plane sources. Although these are very prominent in the original structure section, they are most effectively corrected by migrating the data and using other operations in the reprocessing sequence, such as removal of the multiple of the water bottom and noise rejection filtering. Hence, the interpretive images are significantly improved.

Previously, we commented on the use of the quality of migrated images as a means to evaluate the underlying velocity field. The original migrated section for Line GSI 85 shows clear overmigration artifacts. This is best illustrated by the "bulls-eye" at shot point 535 at a time of 0.5 seconds. Hence, the apparent dips, the dimensions of anticlines, and other elements that depend on the validity of the migration operation are in error. The reprocessed section shows no comparable overmigration effects within the Hosgri fault zone.

The reprocessed data also demonstrate additional elements of structure at depth. Flat or slightly dipping elements east of shot point 570 appear from 1.2 to 3.0 seconds in the migrated reprocessed section. These elements do not appear on the original processed sections and are not multiples arising from overlying events.

Line GSI 86, Figure LP Q3-3

This line appears as profile M-M′ on the panels for the San Luis/Pismo reach of the montage. The Hosgri fault zone is between shot points 560 and 670. The attributes are similar to those described for Line GSI 85.

The near-surface traces of the Hosgri fault zone contribute to an abundance of diffracted energy that masks primary reflection energy and otherwise coherent events that we see subsequently as a result of reprocessing. In fact, the original processed structure section is dominated by the strength of the diffractions, as can be seen at shot points 550 to 600 from 0.2 to 1.8 seconds. The situation is improved but still severe in the restacked data.

The original processed migration section does not correct the diffractions as effectively as the reprocessing. Only subhorizontal "swaths" of possible reflection energy may be observed in the vicinity of shot points 500 to 650 from 1.0 to 2.5 seconds. Also, the original processed migration section has not corrected imaged reflections from 1.8 to 2.4 seconds at shot points 550 to 650. A rather convincing set ("swath") of reflections on the original processing are evident from the reprocessing to be nongeologic images, and possibly subject to incorrect interpretations.

As a result of reprocessing, the structure section demonstrates a better signal-to-noise level so that the reflections appear to be quite coherent and distinguishable from the more scattered noise. This is well illustrated at shot points 530 to 630 from 1.3 to 2.1 seconds, where deeper elements of the Hosgri fault zone may be observed. As a further distinction, the reprocessed migrated section demonstrates that these reflections are not continuous across the area where they had been previously imaged as such, but that

they are distinct in the area of shot points 550 to 620 and discontinuous, possibly due to faulting, from the reflections imaged to the east at shot points 620 to 670 from 1.7 to 2.6 seconds.

Within the Hosgri fault zone on the reprocessed record, the imaging is very good. The character of the closely spaced conformable beds showing tight curvature is clear. Below shot point 655, the completed crest of an anticline is visible at about 0.45 seconds. Such observations are not possible from the indistinct images on the original migrated section.

Line GSI 87A, Figure LP Q3-4

This line appears as profile N-N′ on the panels for the San Luis/Pismo and San Luis Obispo Bay reaches of the montage. The Hosgri fault zone is between shot points 400 to 520.

The general comments stated above concerning the improved velocity data, better water-bottom multiple removal, and higher frequency content of the reprocessed data sections also apply to line GSI 87A. The reprocessed migrated data, when compared to the original migration, clearly show evidence of overmigration in the original processing (around shot point 450 above 0.5 second), as well as clear improvements in detailed imaging of the reprocessed section. For shot points 420 through 450 and between 0.4 and 1.5 seconds, the reprocessed results have increased clarity and resolution. The original migration shows incorrect dips and unresolved character. In the original sections, reflections have been masked by diffraction patterns that have not been adequately treated by the migration. It is apparent that the new processing has a more accurate velocity field.

One of the most significant improvements for Line GSI 87A is the well-imaged, faulted anticline whose crest occurs at shot point 455 around 0.5 second. Both the east- and west-dipping limbs are imaged. Although there is some evidence for the dips in the reprocessed structure section, the original data allow no comparable interpretation in either the structure or migration sections.

Line GSI 101, Figure LP Q3-5

This line also appears as profile U-U′ on the panels for the Point Sal reach of the montage. Structural elements of the Hosgri fault zone are between shot points 350 and 500.

The reprocessing again incorporates more than two times the number of velocity analyses as the original processing, has reduced water-bottom multiples, and shows a higher frequency content. The original processing contains significant noise that has been subsequently reduced by applying a noise rejection filter, thus improving the imaging of the reprocessed migrated section. This is especially evident in the shot point range of 250 to 450 below 1.75 seconds.

Details of the Purisima structure at shot points 140 to 280 are much more evident in the reprocessed migrated section down to a time of 2.5 seconds. The improvement in primary signal content also gives some evidence for fault displacement of reflections around shot point 390, from 1.0 to 2.5 seconds. This is seen in terms of more clearly imaged dips, bed terminations, and generally improved signal content. Similar signal-to-noise improvements near shot points 480 and 500 combine with improvements in the migration process to demonstrate a clearer picture of an east trace of the Hosgri fault zone at shot points 480 to 500 from 0.5 to 1.0 second.

The diffractions apparently related to the gas around shot point 390 appear to persist almost to the sea bottom. Such a localized zone of gas, in terms of lateral extent, is usually associated with leakage along a fault. This is further discussed in the Response to Question LP 4 of this submittal. At this location, the time range and spatially limited nature of the gas are apparently not sufficient to cause observable velocity affects on the seismic section.

There is a well-developed half-anticline signature between shot points 360 and 390 in the range of 0.5 to 1.0 second. There also appears to be a buried anticlinal structure below it and to the west. The geometry of these structures does not extend into the shallow section. These structural details may only be observed in the reprocessed migrated section. Such information about the internal structure beneath the unconformity is important to understanding the style and timing of deformation associated with the Hosgri fault zone.

Line GSI 103, Eastern Part, Figure LP Q3-6

Line GSI 103 is not illustrated on a montage panel because two nearby lines, Nekton 202 and PG&E 3, were presented to illustrate alternate data sets and to specifically address the earlier published data (Crouch and others, 1984). Across the Hosgri fault zone, lines GSI 103 and Nekton 202 overlap for approximately 8 kilometers. Within this overlap they are generally within .25 kilometer of one another. Line Nekton 202 is also shown on Figure LP Q3-11.

Structural elements of the Hosgri fault zone are between shot points 1150 and 1280. The previous comments regarding frequency of velocity analyses, water-bottom multiple suppression, frequency content and improved signal-to-noise ratio, both shallow and deep, also apply to this line. Improved signal content is evident both over the Hosgri fault zone (shot points 1200 to 1280) and within the Purisima structure to the west (shot points 100 to 1080).

The termination of numerous reflection events, both flat-lying and east-dipping, is evident in the shot point range of 1200 to 1250, 0.4 to 1.4 seconds, on the reprocessed section but not on the original processing. The narrow, fault-associated gas zone at shot point 1210 is better defined on the reprocessed section (see discussion of line GSI 101). The migration used in the reprocessing was more successful in collapsing these diffractions. Also, the image of the minor displacement of the event at shot point 1265 at 0.5 second is much improved.

A strong event is evident at 3.1 seconds in both the original and reprocessed data between shot points 850 and 1020. However, the complexity of events above this reflector at 2.2 to 3 seconds is more evident on the reprocessed section.

Line GSI 106, Figure LP Q3-7

This line is shown as profile X-X′ on the panels for the Point Sal reach of the montage. Structural elements of the Hosgri fault zone are between shot points 1150 and 1250. Additional structural resolution is provided by the reprocessed data; the migration, in particular, supports the development of a broad faulted zone. One feature, in particular, that supports this improved resolution is the anticlinal structure seen between shot points 1150 and 1200 from 0.4 to 1.5 seconds. This structure is situated west of the west trace of the Hosgri fault zone. This anticlinal feature is not resolved by the original processed data, where it appears only as unfocused or overmigrated energy. Again, this is a clear indication of poor or

improperly constrained velocity analysis in the original processing. The reprocessed migrated data has clarified the image of this important interpretive element.

The Purisima structure (shot points 900 to 1100) is best resolved in terms of imaging the internal bedding on the reprocessed migrated data. Structural attitudes and apparent distance of separation between the Hosgri fault zone and the flanks of the Purisima structure are more clearly documented by the reprocessed data in the area of shot points 1050 to 1150 from 0.5 to 2.5 seconds. This separation is further resolved to the extent that roughly an additional 50 percent can be added to the distance between the flanks of the structures based on the newer migration.

Reprocessing the data has clarified the deformed structures and enabled move detailed observations to be made. For example, the character of deformation associated with the Hosgri fault zone to the north appears to be changing on this line at shallower depths. On the east side, folding appears shallower in the section on this profile, and the westward-dipping events are more widely spaced, broader, or of lower central frequency than the event sequences seen on lines to the north.

Line GSI 107A, Figure LP Q3-8

This line is illustrated as profile Y-Y′ on the panels for the Point Sal reach of the montage. The Hosgri fault zone is between shot points 930 and 1030.

In the original structure section, both the Purisima structure and the Hosgri fault zone are expressed by intense diffraction patterns. This had a detrimental effect on the quality of the resulting migration.

The reprocessing effort resulted in a better structure section, principally because of improvements in the stacking process and in the velocity field. Such results can be seen by general increases in the visible signal-to-noise ratio and suppressed diffraction signatures (note shot points 1000 to 1100, from 1.0 to 4.0 seconds, and also in other areas of the line at similar depths/times). The resulting migration of the improved reflection signal content substantially resolves the additional structural elements formed within the Hosgri fault zone. Anticlinal structure within the Hosgri fault zone is resolved clearly between shot points 950 and 1010 from 0.2 to 0.9 seconds. Event terminations hinted at by the original processing between shot points 950 and 1100 from 2.0 to 3.0 seconds, are resolved into more coherent reflectors.

Line GSI 118, Figure LP Q3-9

This line is also illustrated as profile BB-BB′ on the panels for the Southern reach of the montage. It crosses the Lompoc structure (shot points 250 to 400), the Purisima structure (shot points 450 to 690) and the Hosgri fault zone (shot points 720 to 800). The more complex nature of the deformation within the Hosgri fault zone, when compared with the other two structures, is more apparent on the reprocessed, migrated section than on the original migrated section.

The reflection signal level is increased on the reprocessed data relative to the background noise levels in the time range from 0.3 to 3.0 seconds. Near-surface event continuity better resolves the numerous anticlinal features, particularly in the time range of 0.3 to 1.3 seconds. Also, the reprocessed migration section shows the several traces of the Hosgri fault zone with increased clarity by virtue of the alignment of several reflection terminations between 0.2 to 1.5 seconds beneath the Hosgri fault zone surface expression (shot points 730 to 800).

In the original processed data, the structure section reveals numerous diffractions within the Hosgri fault zone. The real reflection events tend to blend with the diffractions, making the two types of events indistinguishable. The reprocessed stacked data tends to resolve the reflections, but makes quite obvious the need for migration. Once migrated, the expression of these reflections enables one to better delineate traces of the Hosgri fault zone, as well as the basement surface and possible low-angle detachments beneath the Lompoc and Purisima structures.

At reflection times between 2.0 to 4.5 seconds, short segments of intrabasement coherent events are enhanced between shot points 450 and 850. In the original processed sections, these events are absent or undifferentiated from the prevailing noise.

Line GSI 123, Figure LP Q3-10

This line is illustrated as profile DD-DD' on the panels for the Southern reach of the montage. The reprocessed portion of the line begins over a minor fold on the eastern flank of the Lompoc structure (shot point 280 to 330) and extends eastward across the Hosgri fault zone (shot point 580-660).

The reprocessed structure section illustrates considerable improvement in signal-to-noise ratio over the original structure section. Reflection terminations within the Hosgri fault zone distinguish the fault traces better because of this increased signal level, which is further improved via the subsequent migration. The clearly observed offset of reflections beneath shot points 590, 600, 620, and 650 from 0.3 to 2.0 seconds indicates the resulting improvements in interpretability of the records.

Nested, or conformably folded, synclines below shot point 360 are seen with far greater clarity on the reprocessed migration. Also, well-defined events from 2.2 to 2.6 seconds west of shot point 520 appear much more coherent in the reprocessed data. Given only the original sections the interpretations would, at best, represent approximate correlations, owing to the noise levels and multiples that mask events. Reprocessing has clearly increased the quality of the imaging.

Line N 202, Figure LP Q3-11

Although not specifically requested by the question, we have included an example of the reprocessing as it was applied to another data set, the Nekton-45 survey from the Point Sal area.

Line N 202 is shown as profile V-V' on the panels for the Point Sal reach of the montage. As previously discussed, it is within .25 kilometer of Line GSI 103 (Figure LP Q3-6) over most of its length. The original line crosses the Purisima structure, the Hosgri fault zone (shot points 115 to 122), and the Casmalia fault zone. A slightly different format was used for this figure because the original processing was plotted with a horizontal exaggeration, making the records very long, even when reduced to the scale shown on Figure LP Q3-11. The reprocessed records were produced at the same horizontal time scales as the other survey records used in the PG&E analysis.

Line N 202 was originally processed by Nekton, Inc., not GeoCenter, Inc., who originally processed the GSI seismic lines. Additionally, the seismic energy source used to acquire the data were water-guns, not the air-gun arrays used in acquiring most of the other lines. As such, a direct comparison with Line GSI 103 yields some differences related to source energy levels and frequency content. For instance, the time/depth limit for discernible reflection energy is only about 2.8 seconds on this Nekton line, whereas counterpart Line GSI 103 gives approximately 4.0 seconds of resolvable data.

East of the Hosgri fault zone, the original migrated record contains good quality reflected energy from 0.0 to 0.7 second. Below 0.7 second, the data appear to be noncoherent. In the reprocessed migration section, data in the same vicinity (shot points 106 to 113) yield coherent energy to 1.5 seconds and, to a lesser extent, below that. The improvement in signal-to-noise appears to be the major contribution in imaging the tight folding beneath the unconformity. A notable improvement is also indicated at depth, where conformable dip and reflection continuity is enhanced, especially at shot points 110 to 117 from 0.9 to 1.7 seconds. Within this range of shot points, the clear unconformity below about 0.5 seconds, separating parallel beds in the upper section from tightly folded beds below, is of interpretive importance in documenting the timing of deformation.

Another advantage of reprocessing is a compressed horizontal reference scale that more nearly matches the format of the other (GSI) lines. Although this is merely a plotting function, it adds to the overall comparative evaluation, particularly in ties to the interpretation of other seismic lines. The compressed scale emphasizes geologic continuities without requiring the viewer to stand at some great distance from the section, and this in itself is a considerable advantage.

The reprocessed structure section demonstrates considerably improved, primary reflected signal content, and the diffractions, though present, are not so pervasive as in the original sections. This improvement can be attributed to a better application of velocity analysis, which is especially important on this record because of the complex near-surface geology. The reprocessed migration section also does a better job of imaging the west-dipping reflections beneath the Hosgri fault zone.

If the imaging problems had not been corrected by reprocessing, the differences in imaging between the two data sets might well be attributed to acquisition differences. Recall that a water-gun source, rather than an air-gun array, was used and there were also receiver group differences. It is clear that reprocessing the Nekton data yielded results compatible with the upper portions of the GSI data, despite the differences in field practice.

REFERENCES

Crouch, J., Bachman, S., and Shay, J., 1984, Post-Miocene compressional tectonics along the central California margin; in Crouch, J., and Bachman, S., eds., Tectonics and Sedimentation along the California Margin: Pacific Section, Society of Economic Paleontologists and Mineralogists, vol. 38, p. 37-54.

Pacific Gas and Electric Company, 1988, Final Report of the Diablo Canyon Long Term Seismic Program: U. S. Nuclear Regulatory Commission Docket Nos. 50-275 and 50-323.

OVERSIZE DOCUMENT PAGE PULLED

SEE APERTURE CARDS

NUMBER OF OVERSIZE PAGES FILMED ON APERTURE CARDS 1

APERTURE CARD/HARD COPY AVAILABLE FROM

RECORDS AND REPORTS MANAGEMENT BRANCH

QUESTION LP 4

Gas-charged sediment appears to be present on many seismic reflection lines shown in the montages. Evaluate the effect of gas-charged sediment on the interpretations shown for the Hosgri fault zone. Particularly address the hypothesis that the area interpreted by PG&E as the vertical Hosgri fault is a gas-charged zone and not a fault.

Gas-charged sediment and accumulations of gas in the subsea sedimentary rocks of the offshore Santa Maria Basin have been observed and documented in the seismic reflection survey records and interpretations since exploration of the offshore basin began in the 1960s. The association of gas-charged sediments with large anticlinal trends and fault traces is one of the geologic aspects of the basin that encouraged extensive exploration of the area.

The presence of gas-charged sediments in the eastern offshore Santa Maria Basin was documented by PG&E during preparation of the Diablo Canyon Final Safety Analysis Report in 1973 and 1974. Such zones were mapped as part of the interpretation of the PG&E-sponsored high-resolution surveys conducted by BBN and Aquatronics in the mid-1970s. Mapping of the gas zones continued through the 1970s and 1980s as a result of data collected during petroleum exploration surveys in the basin, subsequent high-resolution geohazard surveys of the OCS lease blocks and potential platform sites and pipeline routes, and regional geohazard surveys sponsored by the U. S. Geological Survey, Minerals Management Service, and the California State Lands Commission. Composite maps of the zones of gas-charged sediments, shallow gas-charged reflectors, and discontinuous zones of gas accumulation in the basin have been periodically released in environmental impact reports and U. S. Geological Survey Open-File reports since the mid-1970s. The latest regional map of gas zones in the offshore Santa Maria Basin is Sheet 4A, Geologic Map of the South-Central California Continental Margin (McCulloch, 1989), which is part of the California Continental Margin Geologic Map Series.

Figure LP Q4-1 shows the mapped occurrences of gas in the shallow sedimentary rocks along the Hosgri fault zone and the adjacent eastern part of the offshore Santa Maria Basin. It is derived both from mapping by PG&E and from published sources.

To address the possible affect of gas-charged sediment on the geologic interpretations of the Hosgri fault zone, we first discuss several topics that relate to the distribution and identification of gas-charged sediment in the eastern offshore Santa Maria Basin. These topics include the source and modes of emplacement of gas in the shallow sedimentary section, the effects of gas-charged sediment on seismic records, for example, the seismic signature of the gas zone, and the mapped gas zone in the eastern offshore Santa Maria Basin and along the Hosgri fault zone. Following the discussion of these issues, we address the hypothesis that the area interpreted by PG&E as the vertical Hosgri fault zone is instead a gas-charged zone and not a fault. We conclude that the vertical Hosgri fault zone exists and that, in some areas, the fault traces are conduits for the upward migration of gas.

SOURCES AND MODES OF EMPLACEMENT OF GAS

Natural gas occurs in shallow sediment as a result of two processes: *in situ* biodegradation of recently buried organic material, and the upward migration of thermogenic gas from deeper sedimentary rocks. Both types of gas occurrences are present in the offshore Santa Maria Basin. In addition, the gas may

exist in either the bubble (gaseous) phase or in a dissolved phase. Concentrations can range up to 15 to 20 percent by volume, or perhaps even higher in a narrow conduit, such as a fault zone.

Gas from *in situ* biodegradation in shallow sediments generally extends over a broad area, unless the area of last sediment deposition was spatially limited by geologic features such as buried channels, levees, fault scarps, and so forth. It may be distributed from depths of several hundred feet up to the sea floor, or be confined to discreet horizontal layers. The apparent onset of the zone (based on observations on seismic reflection records) may be either gradual or abrupt.

Thermogenic gas is generated in deeply buried sedimentary rocks. The gas migrates up-section because it has a lower density than either the surrounding rock material or the other interstitial pore fluids. Within the sedimentary rocks, the migration path may be through zones of pervasive microscopic or macroscopic fracture systems, along leaky bedding planes or unconformities, or through narrow sheet-like conduits formed within the gouge or breccia associated with fault zones. Many migration paths are undoubtedly a combination of these features, and thus the gas may occur in a broadly distributed area or in a highly concentrated zone. The gas will migrate upward until it encounters an impermeable boundary or seal, where it is trapped. Traps may occur anywhere within the sedimentary section. In some areas, a combination of geologic conduits and/or a lack of an effective sealing horizon allows gas to reach the sea floor and escape into the water column.

THE SEISMIC SIGNATURE OF GAS-CHARGED SEDIMENT AND SEDIMENTARY ROCKS

The presence of gas in sediment or rock may affect the imaging of those units on seismic reflection records. Gas alters the density and elastic properties of the rock, and thus the acoustic impedance of the sediment or rock unit. In addition, shallow gas may scatter or absorb high-frequency components of the seismic energy and therefore reduce or eliminate coherent reflections from within or beneath the gas zone. The observed effects of the gas depends on a number of factors including, but not necessarily limited to, the nature of the gas occurrence, ranging from a narrow conduit to a broad area, the concentration of the gas in the pore fluids, the depth to the gas zone, the frequency content of the seismic source signal, and the data collection and processing parameters of the seismic system.

The effect of gas on a seismic record can range from nil to a total destruction of all subsurface data (termed a "wipeout'). Other common effects, all of which occur in the offshore Santa Maria Basin seismic records, are an increase in reflection amplitude ("bright spots"), sags in reflector surfaces ("velocity pull-down"), near-surface diffraction patterns, and water-column anomalies. These effects are observed in both the high-resolution analog records and the common-depth-point exploration data from the offshore Santa Maria Basin. Because of the differences in source energy and signal frequency content, "wipeouts" and water-column anomalies are most likely to occur on high-resolution records, whereas "bright spots" and "velocity pull-down" effects from deeper gas accumulations are more common on the lower-frequency-response, common-depth-point records.

None of the effects of gas on seismic records mentioned above are unique to gas; similar effects may result from other causes. For example, near-vertical diffraction patterns can result from bed terminations along a near-vertical fault. Illustrations of several of the different seismic signatures from gas-charged sediment and sedimentary rocks associated with the Hosgri fault zone and other structures in the offshore Santa Maria Basin are presented and discussed in the next section.

SHALLOW GAS-CHARGED SEDIMENT ZONES MAPPED IN THE EASTERN OFFSHORE SANTA MARIA BASIN

Figure LP Q4-1 shows the distribution of shallow gas-charged sediment and sedimentary rocks in the eastern offshore Santa Maria Basin. The map base is the regional Structural Trends Map of the Hosgri Fault Zone submitted in Response to Question GSG 1 in March 1990. It is a 1:96,000-scale compilation of the structural trends maps prepared for the individual reaches of the Hosgri fault zone. Gas zones along the traces of the Hosgri fault zone were mapped by PG&E based on the high-resolution and common-depth-point seismic reflection data sets. The gas zones west of the Hosgri fault zone in the offshore Santa Maria Basin were compiled from Map 4A of the California Continental Margin Map Series (McCulloch, 1989).

Within the region shown on Figure LP Q4-1, McCulloch (1989) mapped four types of gas zones, depending on their geophysical signature on seismic records: (1) areas of acoustic anomalies possibly indicating trapped shallow gas; (2) zones having continuous gas-charged reflectors; (3) zones having discontinuous gas-charged reflectors; and (4) discontinuous accumulations of gas observed on individual seismic profiles. These four types of gas zones are shown on Figure LP Q4-1, in the locations mapped by McCulloch.

In addition, we mapped the distribution of gas zones along each trace the Hosgri fault zone (Figure LP Q4-1). Where there is evidence for gas, the solid portion of the line representing the fault trace is replaced by a series of asterisks. This figure shows the distribution of the gas-charged zones along the Hosgri fault zone in more detail than does the regional map of McCulloch (1989). Table LP Q4-1 summarizes the data for the traces, indicating the length of each fault trace and the length along which there is evidence of shallow gas-charged sediment or a gas conduit. The gas zone is also expressed as a percent of the total fault trace length. Many of the fault traces show little or no evidence of associated gas-charged zones, especially in the Southern reach and the more easterly fault traces in the San Luis Obispo Bay area. From Point Sal northward to southern Morro Bay, the westerly fault traces have gas anomalies along sections that vary from 30 to 90 percent of the trace length. However, as shown on Table LP Q4-1, gas anomalies are mapped along only 26 percent of the fault zone when, the total length of all fault traces is considered as the basis for comparison. If the total length of only the main trace of the Hosgri fault zone is used, then 39 percent of the zone has gas anomalies. (Refer to Section 3.6.4 of Attachment GSG Q1-A, submitted in March 1990, for a discussion of the criteria for designating the main trace.)

Figure LP Q4-2 (line Nekton-202, V-V′ on the panels for the Point Sal reach of the montage) illustrates the seismic signature of a gas zone associated with the Purisima anticlinal structure. The gas is thermogenic and has migrated along fracture systems within the rock to form a broad diffuse aura over the top of the anticline. The aura is seen between shot points 128 and 136 in the time range of 0.5 to 1.25 seconds. The gas migrated above the structure into the more porous and permeable sandy and silty sediments, decreasing the compressional wave velocities in these layers with respect to the intervening shale layers. A local increase in reflection coefficient is created, which results in a region of higher-amplitude reflections in the gas-charged area. The swale in the horizons between shotpoints 129 and 131 in the time range of 0.7 to 1.0 seconds likely is the result of a velocity pull-down effect. Immediately to the west of shotpoint 118, Figure LP Q4-2 also illustrates the typical "gas bubble" type of anomaly associated with the west trace of the Hosgri fault zone in this reach. The anomaly is partially obscured by a splice in the record, and Figure LP Q4-3 is a better image.

Table LP Q4-1

LENGTH OF HOSGRI FAULT ZONE TRACES SHOWING "GAS BUBBLE" TYPE ANOMALIES ON SEISMIC REFLECTION RECORDS

Reach	Trace	Trace Length (km)	Gas Zone Length (km)	% Gas Zone
Northern	*Northern - NE	9	0	0
	*Northern - Central	14	4	29
	*Northern - SW	6	0	0
San Luis/ Pismo	West	13	4	31
	*East	21	10	48
	East #2	7	0	0
San Luis Obispo Bay	*West	24	21	88
	East #3	14	2	14
	East #4	9	0	0
Point Sal	*West	14	10	71
Southern	*West	27	0	0
	East #5 + #6	10	0	0
	East #7	13	0	0
	East #3, #9, #10	17	0	0
TOTAL FOR ALL TRACES		198[1]	51	26
TOTAL FOR MAIN(*) TRACES[2]		115[1]	45	39

NOTES:

[1]Sums of lengths of all traces and main traces exceed the overall length of the Hosgri fault zone because traces overlap.

[2]The criteria for identifying one or more traces as the "main trace" (marked with an *) are discussed in Section 3.6.4 of Attachment GSG Q1-A, March 1990.

PROPRIETARY DATA

Figure LP Q4-2

Nekton line 202 illustrating the appearance of gas-charged sediments on the seismic reflection record. Note the aura of increased reflection amplitudes above the Purisima structure (shot points 128 to 136, 0.5 to 1.25 seconds) and the swale (velocity pull-down) beneath shot point 130 (0.6 to 0.9 seconds). The narrow zone of "gas bubble" diffraction patterns associated with the west trace of the Hosgri fault zone is partially obscured by a splice on the record at shot point 118.

PROPRIETARY DATA

Figure LP Q4-3

GSI line 97 from the San Luis Obispo Bay reach illustrates the vertical pattern of narrow, high-amplitude, diffraction cones that are associated with the west trace of the Hosgri fault zone in this area. The diffraction patterns are interpreted as arising from gas migrating upward along a near-vertical fault plane.

Figure LP Q4-3 is a portion of line GSI-97 shown on the panels for the San Luis Obispo Bay reach montage as profile R-R′. A vertical pattern of short, steeply dipping, high-amplitude diffraction cones exists at shot point 1335, rising toward the sea floor from a time of about 0.8 seconds. This type of pattern has been cited as evidence of "gas bubbles." The pattern is evident on many of the common-depth-point seismic records shown on the Point Sal and San Luis Obispo Bay reaches of the montage, especially along the west trace of the Hosgri fault zone (for example, profiles X-X′ through Q-Q′, from south to north). Because these records are migrated sections, the diffraction patterns should have been collapsed by the migration process, unless either (1) there is a very local and rapid velocity change that is not adequately treated by the migration process or, (2) the diffractions are from "out of plane" sources. As previously mentioned, bedding terminations, as well as gas, in a narrow, near-vertical zone can be responsible for such a pattern. Other lines of evidence are required to make a distinction between possible sources. Based on the evidence discussed below, we interpret this pattern to be the result of gas migration along a near-vertical, near-surface fault plane that appears on the seismic records as a narrow column of data drop-out and diffraction cones.

Evidence for the disruption and distortion of the shallow sediment horizons within this area is documented in the tables and on Figures H-62 through H-82 of Section 13 of Attachment Q43-1, submitted in January 1989. Figure LP Q4-4 is a copy of Figure H-63a from that attachment. Diffraction cones are evident on the west trace and intermediate trace no. 1. Changes in bedding plane dips and vertical positions of the horizons in the zones between the several traces are also evident. Pervasive evidence of this nature supports the conclusion that there are steeply dipping fault planes and that the gas is migrating upward locally along the fault planes. Detailed observations and comments about similar features seen on the GSI common-depth-point lines are presented in Response to Question LP 3 and in Figures LP Q3-2 through LP Q3-11, comparing processing results.

Figure LP Q4-5 presents another detailed view of the sedimentary units in the immediate vicinity of the "vertical" west trace of the Hosgri fault zone. This is a near full-scale copy of a part of Comap line 117 where it crosses the west trace approximately 8 kilometers southwest of the Diablo Canyon Power Plant. Comap line 117 is shown as profile P-P′ on the San Luis Obispo Bay reach montage. The west trace occurs between shot points 23 and 24 (marked with an arrow). This common-depth-point record provides a more detailed image of the sediment horizons within the upper 1 second of section than do data from the GSI survey lines because of the higher frequency content of the seismic source, and a shorter cable with close group spacing. Although some of the apparent distortion of reflectors directly beneath shot point 24 (in the upper 1 second of section) may be caused by gas-related velocity pull-down, there are other observations that cannot be attributed to the effects of gas. These include:

- The relatively abrupt change in dip of reflectors that occurs across the fault trace,
- The apparent change in vertical separation of reflectors within the fault zone from west-side-down to east-side-down from 600 milliseconds up to 200 milliseconds,
- The abrupt and alternating changes in thickness of the sedimentary units across the fault zone,
- The eastward-dipping reflector that terminates at the unconformity at shot point 19 (at 750 milliseconds), changes dip, and is disrupted at shot point 24 (at 850 milliseconds), and

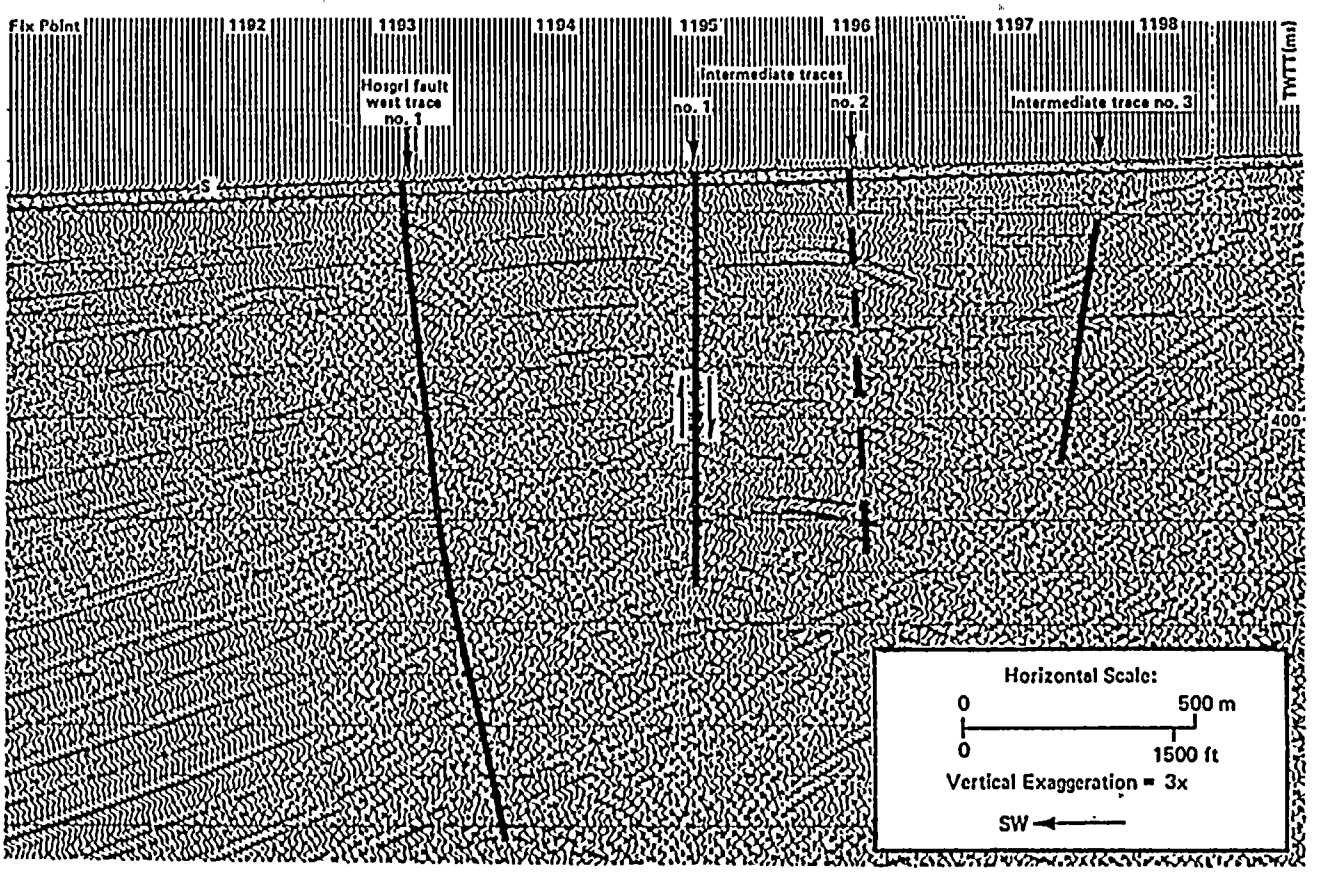

Figure LP Q4-4

Fairfield line 180, Fairflex sleeve, common-depth-point record from the vicinity of montage profile Q-Q' in the San Luis Obispo Bay reach. Diffraction cones suggest gas is migrating upward along the two western traces at this location. Note the changes in bedding plane dips.

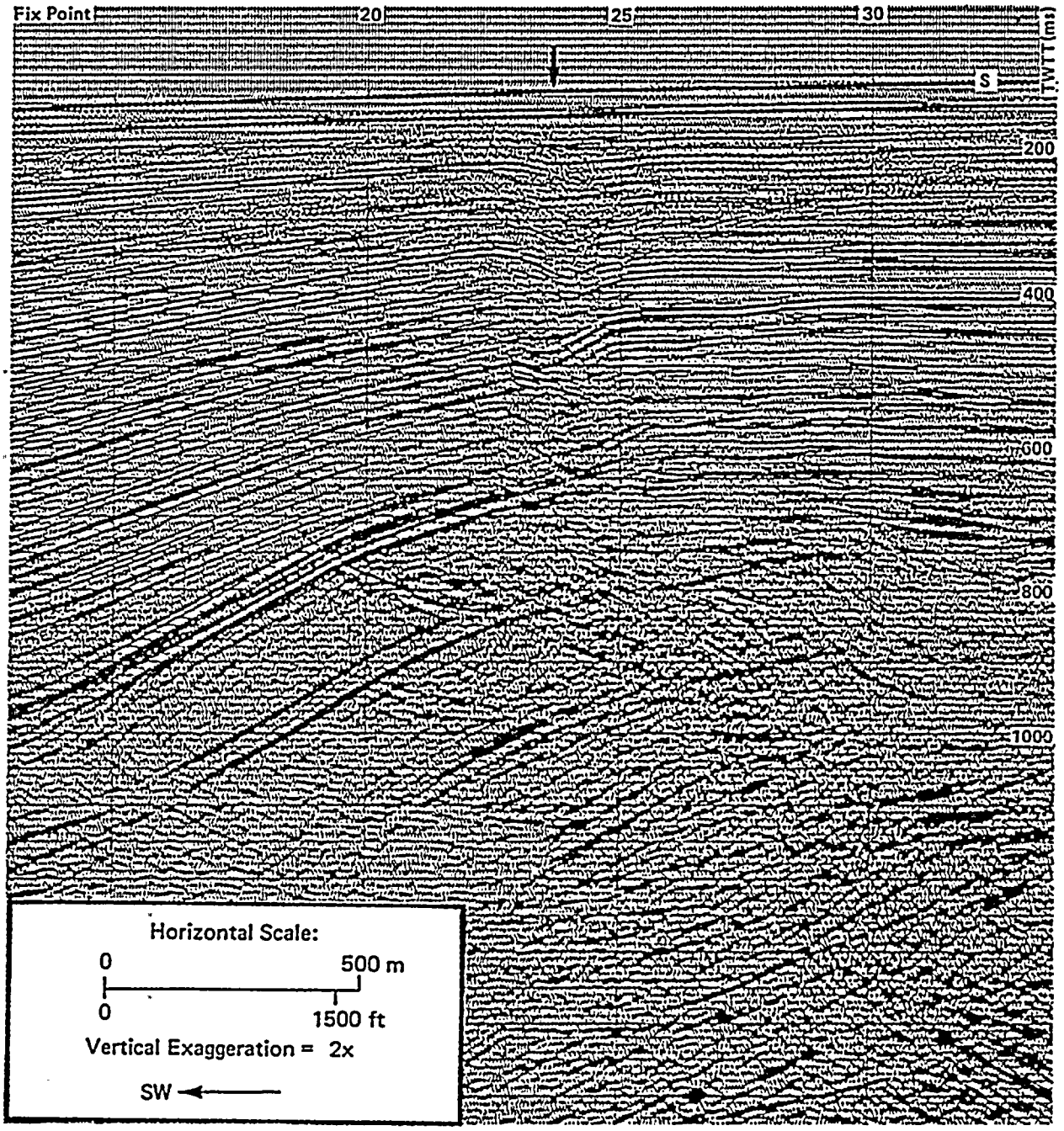

Figure LP Q4-5

A part of Comap line 117 (profile P-P′ on San Luis Obispo montage) showing detail of the sediment section within the upper 800 milliseconds. Gas may be responsible for "pull-down" effects beneath shot points 23 to 24. However, note abrupt changes in dips, apparent alternating up/down relationships, changes in thickness of units, and disruption of eastward-dipping reflector (shot point 19 at 750 milliseconds, shot point 24 at 850 milliseconds) -- deformation that cannot be caused by gas. Arrow indicates west trace of the Hosgri fault zone.

- "Gas-related" diffraction cones are not observed on either high-resolution or common-depth-point records along other parts of the same vertical traces or other traces of the Hosgri fault zones (Figures LP Q4-2, 3, and 4).

The map of shallow gas zones in the offshore Santa Maria Basin (Figure LP Q4-1), and the illustrations of seismic records (Figures LP Q4-2 through LP Q4-5) show three basic types of gas zones in the offshore Santa Maria Basin:

(1) The broad zone(s) of acoustic anomalies as mapped by McCulloch (1989). These are interpreted as possibly indicating trapped, shallow (biogenic) gas or shallow discontinuous gas-charged reflectors.

(2) Deeper, diffuse zones or "auras" (including "bright spots") of gas-charged sedimentary section over anticlinal structures (Figure LP Q4-2). These zones are interpreted to result from the upward migration of thermogenic gas through extensive micro and macro fracture zones associated with the structural deformation.

(3) Narrow, near-vertical (as seen in the upper 1 second of seismic records), linear zones of diffraction cones. These zones are interpreted to represent the upward migration of thermogenic gas through the permeable gouge and breccia zones of fault traces (Figures LP Q4-3 and LP Q4-4).

EVALUATION OF THE HYPOTHESIS: "THE AREA INTERPRETED BY PG&E AS THE VERTICAL HOSGRI FAULT IS A GAS-CHARGED ZONE AND NOT A FAULT"

This hypothesis must be evaluated considering the observations noted on the figures discussed in the preceding section, as well as considering other lines of evidence, both direct and indirect. This evidence includes:

- Relationships indicative of gas are observed only along 26 percent of the vertical trace of the Hosgri fault zone mapped by PG&E when all fault traces are considered, or 39 percent when only the main fault trace is considered (Figure LP Q4-1, Table LP Q4-1). Thus, gas-related anomalies were not the determining factor in defining the Hosgri fault zone.

- Pervasive evidence of localized deformation along the vertical traces of the Hosgri fault zone cannot be explained as gas-related anomalies. This evidence is seen not only on the high-resolution records (Figure LP Q4-4 and the Tabulation of Observations, PG&E, 1988), but also on the common-depth-point records (Figure LP Q4-4, Figures LP Q3-2 through LP Q3-11, and the montage panels).

- A distinct difference exists between the diffuse gas-related anomalies over fractured anticlinal structures (for example, the Purisima, Figure LP Q4-2) and those resulting from upward migration of gas through a narrow fault zone (Figures LP Q4-3 and LP Q4-4).

- Linear trends of gas anomalies occur along trend with vertical traces of the Hosgri that show no evidence of gas. This association is best illustrated by comparing Figure LP Q4-1 with the interpreted sections of the montage.

Thus our interpretation is: where gas is present along the vertical traces of the Hosgri fault zone, it uses the fault zone as a conduit for upward migration. Gas is not the sole criterion for interpreting of the vertical traces of the Hosgri fault zone. Criteria for identifying vertical to near-vertical traces of fault zones are discussed in Response to Question LP 3 and in Section 3.5.3 of the Response to Question GSG 1, March 1990.

The response to this question is limited to the discussion of the occurrences of and seismic response to shallow gas in the offshore Santa Maria Basin, and the relationship of such gas occurrences to the vertical traces of the Hosgri fault zone. There are numerous other lines of evidence that bear on the existence, down-dip geometry, and style of deformation of the Hosgri fault zone; for example, changes in structural trends across the zone, distribution of microseismicity, and regional tectonics, as discussed in the Final Report (PG&E, 1988), and in response to other questions.

REFERENCES

McCulloch, D., 1989, Geologic map of the south-central California continental margin; in Greene, G., and Kennedy, M., eds., California Continental Margin Geologic Map Series: Sheet 4A, California Division of Mines and Geology, Sacramento.

Pacific Gas and Electric Company, 1988, Final report of the Diablo Canyon Long Term Seismic Program: U. S. Nuclear Regulatory Commission, Docket Nos. 50-275 and 50-323.

QUESTION LP 5

During the discussion of the question of the possibility of strike slip motion on a non-vertical fault at the meeting it was noted that, there is at least one example, the Xieshi He fault zone in China, of a moderately dipping fault which accommodated reverse displacement in early Quaternary time and has more recently been reactivated as a strike-slip fault. Are there many cases of moderately dipping active strike-slip faults? Is there any evidence for this type of history for the Hosgri fault? What impact would this have on the resultant source characterization and ground motion for Diablo Canyon? (Dipping strike-slip faults have been previously identified as causes of high ground motion.)

Question LP 5 addresses the issue of moderately dipping strike-slip faults and whether this style of faulting might occur along the Hosgri fault zone near Diablo Canyon. Because source parameters of large earthquakes, such as focal mechanisms, are diagnostic of the style of faulting along a fault zone, we have addressed the question by examining a data base of worldwide earthquakes. We have also used associated seismicity data, such as the pattern of aftershocks, to evaluate the dip of the fault at seismogenic depths. We first examine components of slip and orientations of fault planes for continental earthquakes worldwide. We use this data base to evaluate the occurrence of moderately dipping strike-slip faults in the historical record. Second, we discuss the orientation and nature of displacement on the Haiyuan[1] (Xieshi He) fault. Third, we consider the issue of whether or not the Hosgri fault zone may have inherited a preexisting moderate dip from a previous period of tectonic activity.

SENSE OF SLIP AND DIP OF HISTORICAL EARTHQUAKES

To address the issue of moderately dipping strike-slip faults, we compiled a data base of earthquakes for which information is available on the components of slip, as represented by the rake angle and the dip of the fault plane. As presented in the Response to Question SSC 2, March 1990, published definitions of sense of slip are typically based on the components of strike slip and dip slip. The components of slip are directly related to the rake angle, because the ratio of strike slip to dip slip is equal to the cotangent of the rake angle (Bonilla and Buchanon, 1970). The concept of "rake" (also referred to as pitch) comes from structural geology whereby lines on a fault surface (for example, slickensides) are measured within the plane of a fault to discern the direction of relative slip along the surface. By definition, rake is the angle between the horizontal and the direction of slip, measured in the fault surface. Using this definition, Bonilla and Buchanon (1970) as well as Slemmons (1977) define strike-slip faults as those having rakes of 0 to 30 degrees, and oblique-slip faults as those having rakes of 30 to 60 degrees. The relative components of strike slip and dip slip are specified by a rake ranging from 0 to 90 degrees. However, if one is interested in defining the direction of slip (for example, left or right slip, reverse or normal dip-slip), then the rake must be specified with respect to 360 degrees. By convention, fault-slip events with a reverse component have positive rakes from 0 to 180 degrees, and fault-slip events with a normal component have negative rakes from 0 to -180 degrees. Furthermore, fault-slip events with a left-lateral component of slip have rakes whose absolute value is less than 90 degrees, and fault-slip events with a right-lateral component of slip have rakes whose absolute value is greater than 90 degrees.

[1]The "Xieshi He" fault is known in the literature as the Haiyuan fault (D. B. Slemmons, personal communication).

To address the question of nonvertical strike-slip faults, we reviewed published focal mechanisms for 160 earthquakes worldwide to evaluate fault dip and rake. The best constrained mechanism for each earthquake is listed in Table LP Q5-1. Focal mechanisms determined by waveform inversion (P and SH) are generally better constrained than P-wave first-motion solutions, thus the former are generally preferred. Because we are only interested in the relative components of strike slip and normal or reverse slip, and not the left/right direction of slip, we normalized all rake angles from these focal mechanisms into a measure from -90 to 90 degrees. Figure LP Q5-1 is a plot of rake angle versus dip for the worldwide earthquakes examined in this analysis.

To focus on the earthquakes of most interest, we have provided additional information in Table LP Q5-2 for those earthquakes on strike-slip faults dipping less than 80 degrees. The orientation of the fault plane for each earthquake is described through a variety of techniques, including measurements of surface exposures of the fault, focal mechanism solutions, and the three-dimensional geometry of aftershocks. In addition, the horizontal and vertical components of slip (as measured at the site of the net maximum displacement) are provided for each earthquake having associated surface rupture. Note that a considerable degree of variability may exist in the source parameters for any given earthquake; however, the focal mechanisms and the aftershock sequence typically indicate similar orientations for the fault plane. The rake derived from long-period focal mechanisms is considered to be representative of the overall source process of the earthquake, in contrast to single-point estimates of surface slip that may be affected by changes in surface fault geometry or surface geology. In general, to characterize the slip type and fault dip for the earthquakes in Table LP Q5-2, we gave the greatest credibility to estimates of rake and dip based on focal mechanisms derived from waveform inversion. We then examined estimates of fault dip based on the geometry of the aftershock sequence and on surface exposures of the fault plane as a check on the dip derived from focal mechanisms.

Figure LP Q5-1 clearly shows that the rake angle derived from earthquake focal mechanisms increases with decreasing dip of the fault plane. Strike-slip earthquakes typically occur on steeply dipping faults, dip-slip earthquakes occur on more shallowly dipping faults. The data indicate that the occurrence of strike-slip earthquakes on moderately dipping faults (dips of 70 degrees or less) is uncommon. Specifically, only 14 percent (10 of 71) of the strike-slip earthquakes appear to have occurred on faults that dip less than 70 degrees, and only 6 percent (4 of 71) on faults that dip less than 60 degrees (Figure LP Q5-1). In the following section, we further examine the 10 strike-slip earthquakes that appear to have occurred on faults dipping less than 70 degrees. In particular, we have evaluated the applicability of these earthquakes to the tectonic setting of coastal central California and have assessed the quality of the data used to constrain the focal mechanisms and fault geometry. We also examine two moderately dipping oblique-slip earthquakes that have a significant strike-slip component.

Strike-Slip Earthquakes Potentially Associated with Faults Dipping Less Than 70 Degrees

From the data base of focal mechanisms provided in Table LP Q5-1, 10 earthquakes may have occurred on moderately dipping strike-slip faults. Of these 10 earthquakes, 5 occurred in tectonic settings characterized by crustal extension or transtension, as opposed to the transpressional tectonic setting of south-central coast California. Four of these earthquakes (Texas, 8/16/31; Nevada, 12/16/54; India, 12/10/67; and California, 7/21/86) have a significant component of normal slip (rake less than or equal to -20 degrees; Table LP Q5-2). The planes (strike, dip, rake of 104, 48, -170 degrees for plane 1, and 7, 83, -136 degrees for plane 2) of the focal mechanism for the Virginia City, Montana, earthquake (11/23/47) were selected on the basis of the results of waveform inversion of body waves (Table LP Q5-2; Doser, 1989a). The strike of the Madison fault, on which the earthquake is thought to have occurred,

Table LP Q5-1

EARTHQUAKE FOCAL MECHANISMS

LOCATION	EARTHQUAKE	DATE	M_W	STRIKE[1] (°)	DIP[1] (°)	RAKE[1] (°)	METHOD[2]	R90[3] (°)	REFERENCES
USA, Nevada	Pleasant Valley	10/02/15	7.2	194	44	-61	2	-61	Doser, 1988
China	Haiyuan	12/20/20	8.0	115	90	0	2	0	Deng and others, 1984
USA, Montana	Clarkston	06/28/25	6.6	250	56	-38	2	-38	Doser, 1989a
Japan	North Izu	11/25/30	6.9	0	90	12	1	12	Abe, 1978
China	Fuyun	08/10/31	7.9	160	80	180	2	0	Molnar and Deng, 1984
USA, Texas	Valentine	08/16/31	6.3	23	54	-155	2	-25	Doser, 1987a
Japan	Saitama	09/21/31	6.5	196	80	0	1	0	Abe, 1974
USA, Nevada	Cedar Mountain	12/20/32	6.8	352	80	180	1	0	Doser and Smith, 1989
USA, Calif.	Long Beach	03/11/33	6.4	315	82	-165	2	-15	Woodward-Clyde, 1979
Nepal	Bihar	01/15/34	7.9	291	34	64	2	64	Wallace and others, 1989
USA, Nevada	Excelsior Mtns	01/30/34	6.1	248	40	-91	2	-89	Doser, 1988
USA, Utah	Hansel Valley	03/12/34	6.6	40	87	-11	2	-11	Doser and Smith, 1989
USA, Montana	Helena	10/19/35	6.2	260	74	167	2	13	Doser and Smith, 1989
Canada	Timiskaming	11/01/35	6.3	50	50	90	2	90	EPRI, 1986
Turkey	Erzihcan	12/26/39	7.8	108	86	151	1	29	Kadinsky-Cade and Barka (in press)
USA, Calif.	Imperial Valley	05/19/40	7.1	140	90	180	1	0	Trifunac and Brune, 1970
Peru	Ancash	11/10/46	6.8	135	30	-90	1	-90	Doser, 1987b
USA, Calif.	Manix, Mohave D.	04/10/47	6.6	65	85	8	2	8	Doser, 1990
USA, Montana	Virginia City	11/23/47	6.1	104	48	-170	2	-10	Doser, 1989a
USA, Calif.	Kern County	07/21/52	7.2	73	67	61	2	61	Wallace, 1988
Turkey	Canakkale	03/18/53	7.2	59	76	174	1	6	McKenzie, 1972
USA, Calif.	Arroyo Salada	03/19/54	6.3	307	85	175	2	5	Doser, 1989b
USA, Nevada	Rainbow Mtn	07/06/54	6.2	336	80	-140	2	-40	Doser, 1986
USA, Nevada	Rainbow Mtn	08/24/54	6.6	355	50	-145	2	-35	Doser, 1986

Table LP Q5-1 (continued)

LOCATION	EARTHQUAKE	DATE	M_W	STRIKE[1] (°)	DIP[1] (°)	RAKE[1] (°)	METHOD[2]	R90[3] (°)	REFERENCES
USA, Nevada	Dixie Valley	12/16/54	6.9	0	60	-90	2	-90	Doser, 1986
USA, Nevada	Fairview Peak	12/16/54	7.2	350	60	-160	2	-20	Doser, 1986
Mexico	San Miguel	02/09/56	6.6	303	87	180	2	0	Gonzalez-Ruiz and others, 1987
Mongolia	Gobi-Altai	12/04/57	8.1	103	53	32	1	32	Okal, 1976
USA, Alaska	Lituya Bay	07/10/58	7.8	335	72	172	1	8	Stauder, 1960
USA, Montana	Hebgen Lake	08/18/59	7.3	95	42	-90	2	-90	Doser and Smith, 1989
Japan	Kita-Mino	08/19/61	6.8	200	60	81	1	81	Kaminuma and Goto, 1970
USA, Utah	Cache Valley	08/30/62	5.6	201	49	-108	2	-72	Doser and Smith, 1989
Iran	Ipak	09/19/62	7.4	283	80	66	1	66	Petrescu and Purcaru, 1964
Japan	Wakasa-Bay	03/26/63	6.3	54	68	158	1	22	Abe, 1974
Canada	Baffin Island	09/04/63	6.1	98	66	-103	2	-77	Liu and Kanamori, 1980
Taiwan	(southwest)	01/18/64	6.4	15	50	100	2	80	Pezzopane and Wesnousky, 1989
Japan	Niigata	06/16/64	7.6	210	50	116	2	64	Mori and Boyd, 1985
USA, Alaska	Alaska	04/16/65	6.0	305	66	-85	2	-85	Liu and Kanamori, 1980
China	Xingtai	03/07/66	6.6	208	89	-178	2	-2	Chung and Cipar, 1983
Zaire	Congo	03/20/66	6.8	45	45	-82	2	-82	Wagner and Langston, 1988
China	Xingtai	03/22/66	6.3	208	82	-178	1	-2	Chung and Cipar, 1983
China	Xingtai	03/22/66	6.8	26	73	-169	2	-11	Chung and Cipar, 1983
China	X ingtai	03/26/66	6.1	30	74	-157	1	-23	Chung and Cipar, 1983
USA, Calif.	Parkfield	06/28/66	6.3	317	90	180	2	0	Tsai and Aki, 1969
Mexico	El Golfo	08/07/66	6.5	140	85	-177	2	-3	Ebel and others, 1978
Turkey	Varto	08/19/66	6.8	304	64	163	1	17	Jackson and McKenzie, 1988

Table LP Q5-1 (continued)

LOCATION	EARTHQUAKE	DATE	M_W	STRIKE[1] (°)	DIP[1] (°)	RAKE[1] (°)	METHOD[2]	R90[3] (°)	REFERENCES
USA, Calif.	Truckee	09/12/66	6.0	43	76	-11	2	-11	Wallace and others, 1981a
Mongolia	Mogod	01/05/67	7.0	12	80	180	1	0	Huang and Chen, 1986
Turkey	Mudurna Valley	07/22/67	7.3	93	90	180	1	0	Eyidogan, 1988
India	Koyna	12/10/67	6.5	16	67	-29	2	-29	Langston, 1976
USA, Calif.	Borrego Mountain	04/09/68	6.6	315	81	-178	1	-2	Burdick and Mellman, 1976
Iran	Dasht-e-Bayaz	08/31/68	7.2	251	80	6	1	6	McKenzie, 1972
Australia	Meckering	10/14/68	6.6	351	29	73	2	73	Fredrich and others, 1988
Turkey	Alaschir Valley	03/28/69	6.8	281	34	-90	1	-90	Jackson and McKenzie, 1988
Ethiopia	Serdo	03/29/69	6.2	328	82	-16	2	-16	Kebede and others, 1989
Ethiopia	Serdo	04/05/69	6.1	327	69	-45	2	-45	Wagner and Langston, 1988
USA, Calif.	Coyote Mountain	04/28/69	5.7	140	80	-143	1	-37	Thatcher and Hamilton, 1973
Japan	Gifu	09/09/69	6.3	330	90	180	1	0	Mikumo, 1973
South Africa	Ceres	09/29/69	6.3	133	80	-2	2	-2	EPRI, 1986
Peru	Huaytapallana	10/01/69	6.6	315	68	80	1	80	Suarez and others, 1983
China	Tonghai	01/04/70	7.3	116	86	180	1	0	Zhou and others, 1983a
Australia	Lake Mackay	03/24/70	6.1	161	45	80	2	80	Fredrich and others, 1988
Turkey	Gediz	03/28/70	7.1	308	35	-90	1	-90	Eyidogan and Jackson, 1985
Japan	Akita	10/16/70	6.1	171	46	118	1	62	Mikumo, 1974
USA, Calif.	San Fernando	02/09/71	6.7	290	53	76	2	76	Langston, 1978
Turkey	Bingol	05/22/71	6.7[4]	232	86	8	1	8	Jackson and McKenzie, 1988
Iran	Qir-Karzin	04/10/72	6.8	137	51	90	1	90	Chandra, 1984
USA, Alaska	Sitka	07/30/72	7.7	347	78	180	1	0	Schell and Ruff, 1989

Table LP Q5-1 (continued)

LOCATION	EARTHQUAKE	DATE	M_W	STRIKE[1] (°)	DIP[1] (°)	RAKE[1] (°)	METHOD[2]	R90[3] (°)	REFERENCES
Australia	Simpson Desert	08/28/72	6.0	55	60	90	2	90	Fredrich and others, 1988
China	Luhuo	02/06/73	7.5	305	87	1	2	1	Zhou and others, 1983a
USA, Calif.	Point Mugu	02/21/73	5.7	249	49	75	2	75	Ellsworth and others, 1973
China	Tibet	07/14/73	6.9	177	51	-81	1	-81	Singh and Gupta, 1979
Japan	Izu-Oki	05/08/74	6.5	307	80	162	1	18	Abe, 1978
Russia	Tadzhikestan	08/11/74	7.1	53	51	53	2	53	Ni and Fan, 1989
India	Kinnaur	01/19/75	6.8	180	63	-90	1	-90	Banghar, 1983
China	Haicheng	02/04/75	7.0	285	78	-14	2	-14	Stewart and others, 1976
Iran	Sarkhun	03/07/75	6.1[4]	70	65	90	1	90	Chandra, 1984
USA, Idaho	Pocatello Valley	03/28/75	6.1	200	38	-70	2	-70	Doser and Smith, 1989
Japan	Oita Prefecture	04/21/75	6.2	305	88	30	1	30	Hatanaka and Shimazaki, 1988
USA, Wyoming	Yellowstone	06/30/75	5.9	302	71	-129	1	-51	Doser and Smith, 1989
USA, Calif.	Oroville	08/01/75	6.1	180	65	-70	2	-70	Langston and Butler, 1976
Turkey	Lice	09/06/75	6.6	250	54	40	2	40	Eyidogan, pers. comm.
Guatemala	Motagua	02/04/76	7.6	75	90	5	2	5	Young and others, 1989
Russia	Uzbekistan	04/08/76	6.8	291	48	100	2	80	Kristy and others, 1980
Italy	Friuli	05/06/76	6.4	76	75	80	2	80	Cipar, 1980
Russia	Uzbekistan	05/17/76	6.8	227	36	108	2	72	Kristy and others, 1980
China	Yunnan	05/29/76	6.3	20	86	-14	1	-14	Okal and Stewart, 1981
China	Tangshan	07/27/76	7.5	214	80	167	2	13	Nabelek and others, 1987
Japan	Kawazu	08/17/76	5.5	304	82	173	1	7	Abe, 1978
China	Songpan, Huya	08/17/76	6.7	165	63	40	2	40	Jones and others, 1984

Table LP Q5-1 (continued)

LOCATION	EARTHQUAKE	DATE	M_W	STRIKE[1] (°)	DIP[1] (°)	RAKE[1] (°)	METHOD[2]	R90[3] (°)	REFERENCES
China	Songpan, Huya	08/21/76	6.4	215	60	90	2	90	Jones and others, 1984
China	Songpan, Huya	08/23/76	6.6	165	65	40	2	40	Jones and others, 1984
Turkey	Caldiran	11/24/76	7.2	107	78	-176	1	-4	Toksoz and others, 1978
Mexico	Mesa de Andrade	12/07/76	5.6	330	90	180	1	0	Nava and Brune, 1983
Iran	Khurgu	03/21/77	6.7	78	54	90	2	90	Jackson and McKenzie, 1988
Iran	Khurgu	04/01/77	6.0	78	54	90	1	90	Jackson and McKenzie, 1988
Iran	Naghan	04/06/77	6.0	95	45	90	1	90	Jackson and McKenzie, 1988
Argentina	Caucete	11/23/77	7.5	178	35	90	2	90	Kadinsky-Cade and others, 1985
Iran	Bob-Tangol	12/19/77	5.6	328	58	165	1	15	Berberian and others, 1979
Japan	Izu-Oshima	01/14/78	6.7	270	85	-172	2	-8	Shimazaki and Somerville, 1979
Greece	Thessaloniki	06/20/78	6.4	284	55	-59	2	-59	Barker and Langston, 1981
USA, Calif.	Santa Barbara	08/13/78	5.9	295	30	50	2	50	Wallace and others, 1981b
Germany	Swabian Jura	09/03/78	5.2	200	75	13	1	13	Haessler and others, 1980
Iran	Tabas-e-Golshan	09/16/78	7.4	330	30	79	2	79	Niazi and Kanamori, 1981
USA, Calif.	Homestead Valley	03/15/79	5.5	176	80	174	1	6	Hutton and others, 1980
Yugoslavia	Montenegro	04/15/79	7.0	322	15	90	1	90	Boore and others, 1981
Australia	Cadoux	06/02/79	6.1	171	34	98	2	82	Fredrich and others, 1988
USA, Calif.	Coyote Lake	08/06/79	5.9	336	80	176	2	4	Liu and Helmberger, 1983
Italy	Umbria (Norca)	09/19/79	5.8	315	70	-142	1	-38	Deschamps and others, 1984

Table LP Q5-1 (continued)

LOCATION	EARTHQUAKE	DATE	M_W	STRIKE[1] (°)	DIP[1] (°)	RAKE[1] (°)	METHOD[2]	R90[3] (°)	REFERENCES
USA, Calif.	El Centro	10/15/79	6.5	323	90	180	2	0	Hartzell and Heaton, 1983
Iran	Ghaenat	11/14/79	6.6	13	90	180	2	0	Niazi and Kanamori, 1981
Iran	Ghaenat	11/27/79	7.2	73	90	0	2	0	Niazi and Kanamore, 1981
USA, Calif.	Greenville	01/24/80	5.8	167	85	-160	1	-20	Bolt and others, 1981
USA, Calif.	Mammoth Lakes	05/25/80	6.3	12	50	-35	2	-35	Given and others, 1982
Mexico	Mexicali Valley	06/09/80	6.4	138	90	180	1	0	Anderson and Simons, 1981
Japan	Izu-Hanto-Toho	06/29/80	6.4	350	89	8	1	8	Ishida, 1984
Algeria	El Asnam	10/10/80	7.1	220	46	72	2	72	Nabelek, 1985
Italy	South Apennines	11/23/80	6.9	317	59	-85	2	-85	Deschamps and King, 1984
China	Daofu	01/23/81	6.7	321	90	0	2	0	Zhou and others, 1983b
Greece	Corinth	02/24/81	6.6	285	40	-70	2	-70	Kim and others, 1984
Greece	Corinth	02/25/81	6.3	250	42	-80	2	-80	Kim and others, 1984
Greece	Corinth	03/04/81	6.2	67	47	-85	2	-85	Kim and others, 1984
Iran	Gowk	06/11/81	6.6	270	80	140	1	40	Jackson and McKenzie, 1984
Iran	Gowk	07/28/81	7.2	127	52	102	1	78	Jackson and McKenzie, 1984
Canada	Miramichi	01/09/82	5.6	175	54	85	2	85	Yan and Alexander, 1990
North Yemen	Dhamer	12/13/82	6.3	340	60	-60	2	-60	Choy and Kind, 1987
USA, Calif.	Coalinga	05/02/83	6.4	157	32	125	2	55	Hartzell and Heaton, 1983
USA, Idaho	Borah Peak	10/28/83	6.9	155	50	-65	2	-65	Doser and Smith, 1989
Turkey	Erzurum-Kars	10/30/83	6.7	220	77	13	1	13	Person, 1984

Table LP Q5-1 (continued)

LOCATION	EARTHQUAKE	DATE	M_w	STRIKE[1] (°)	DIP[1] (°)	RAKE[1] (°)	METHOD[2]	R90[3] (°)	REFERENCES
West Africa	Guinea	12/22/83	6.4	75	60	-138	2	-42	Jensen and others, 1989
Russia	Gazli	03/19/84	7.0	210	40	83	2	83	Eyidogan and others, 1985
USA, Calif.	Morgan Hill	04/24/84	6.2	328	90	180	2	0	Hartzell and Heaton, 1986
Italy	Lazio-Abruzzo	05/07/84	6.0	123	48	-96	1	-84	Westaway and others, 1989
USA, Calif.	Round Valley	11/23/84	5.8	208	87	10	2	10	Barker and Wallace, 1986
Argentina	Mendoza	01/26/85	5.9	185	37	98	1	82	INPRES, 1985
New Guinea	New Britan	05/10/85	7.2	100	80	0	1	0	Mori and others, 1987
USA, Calif.	Kettleman Hills	08/04/85	6.1	142	12	109	2	71	Ekstrom and others, 1990
Canada	Nahanni	10/05/85	6.6	175	34	90	2	90	Wetmiller and others, 1988
Algeria	Constantine	10/27/85	5.9	240	80	0	1	0	Bounif and others, 1987
Canada	Nahanni	12/23/85	6.8	183	23	115	2	65	Choy and Boatwright, 1988
Australia	Marryat Creek	03/30/86	5.8	148	35	80	2	80	Fredrich and others, 1988
Taiwan	Hualien	05/20/86	6.3	35	60	90	1	90	Chen and Wang, 1986
USA, Calif.	N. Palm Springs	07/08/86	6.1	283	41	147	2	33	Pacheco and Nabelek, 1988
USA, Calif.	Oceanside	07/13/86	5.8	313	48	109	2	71	Pacheco and Nabelek, 1988
USA, Calif.	Chalfant Valley	07/21/86	6.2	142	48	-160	2	-20	Pacheco and Nabelek, 1988
Italy	Kalamata	09/13/86	5.9	204	45	-77	2	-77	Lyon-Caen and others, 1988
Taiwan	Hualien	11/14/86	7.4	38	58	90	1	90	Hwang and Kanamori, 1989
New Zealand	Edgecumbe	03/02/87	6.5	225	45	-110	1	-70	Anderson and others, 1990
USA, Calif.	Whittier Narrows	10/01/87	6.0	280	40	98	2	82	Bent and Helmberger, 1989

Table LP Q5-1 (continued)

LOCATION	EARTHQUAKE	DATE	M_W	STRIKE[1] (°)	DIP[1] (°)	RAKE[1] (°)	METHOD[2]	R90[3] (°)	REFERENCES
USA, Calif.	Elmore Ranch	11/24/87	6.2	45	90	0	2	0	Bent and others, 1989
USA, Calif.	Superstition H.	11/24/87	6.6	315	80	175	2	5	Bent and others, 1989
Australia	Tennant Creek	01/22/88	6.3	100	35	90	2	90	Choy and Bowman, 1990
Australia	Tennant Creek	01/22/88	6.4	290	70	120	2	60	Choy and Bowman, 1990
Australia	Tennant Creek	01/22/88	6.6	100	45	80	2	80	Choy and Bowman, 1990
Canada	Nahanni	03/25/88	6.3	178	51	103	2	77	Wetmiller and others, 1989
China	Lancang-Gengma	11/06/88	7.1	153	87	-171	2	-9	Holt and Wallace, 1989
Canada	Saguenay	11/25/88	5.9	320	65	78	2	78	Somerville and others, 1989
USSR	Armenia	12/07/88	6.8	299	64	151	2	29	Pacheco and others, 1989
USA, Calif.	Loma Prieta	10/17/89	7.0	128	70	138	2	42	Kanamori and Satake, 1990
USA, Calif.	Upland	02/28/90	5.5	212	60	-6	2	-6	Dreger and Helmberger, 1990

NOTES:

[1]After convention of Aki and Richards (1980)

[2]Focal mechanism method of solution: 1 = P-wave first motion; 2 = Waveform inversion

[3]Normalized rake (-90 to 90 degrees)

[4]M_s

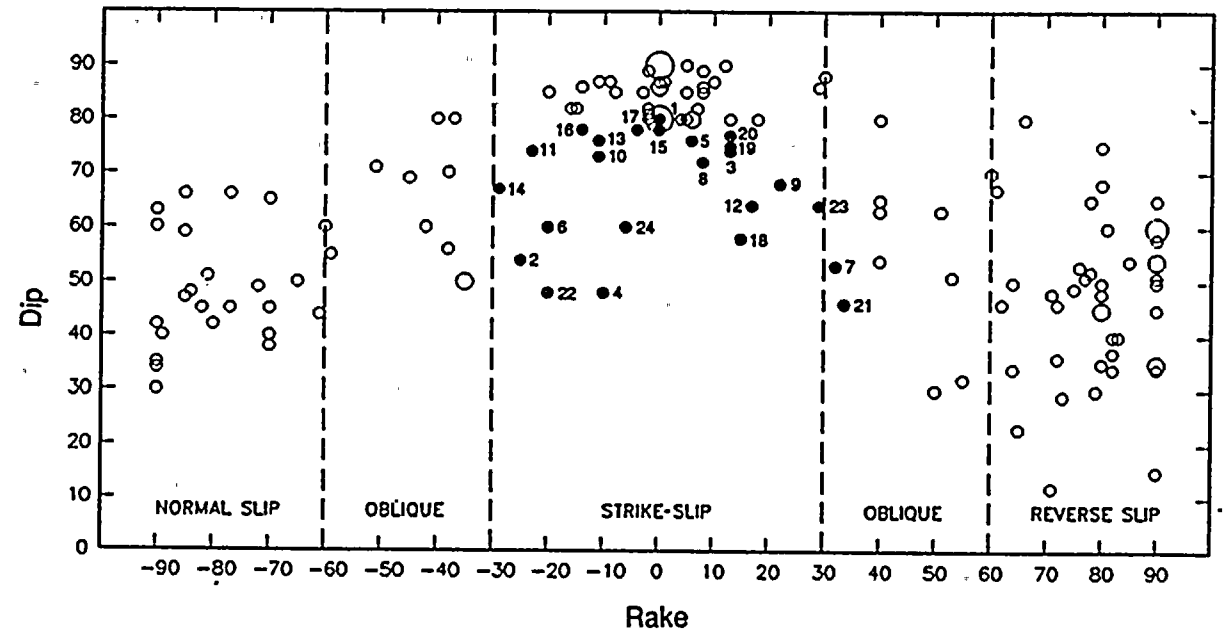

Figure LP Q5-1

Plot of fault dip and rake for earthquakes given in Table LP Q5-1. Values are best-supported estimates; rakes have been normalized to values between 0 and 90 degrees.

Table LP Q5-2

NONVERTICAL (DIP LESS THAN 80 DEGREES) STRIKE-SLIP EARTHQUAKES

Earthquake (*)[1]	Date	Magnitude		Orientation of Fault Plane									Maximum Coseismic Surface Slip[3] (m)		References[5]	Comments
				Focal Mechanism[3]					Aftershocks[3]		Surface Exposures[3]					
		M_s	M_w	S	D	R	R90	Method[4]	S	D	S	D	Horizontal	Vertical		
Haiyuan, China	12/20/20	8.7	8.0	115°	90°	0°	0°	3			115°	30° to 80°	10	<1	Deng and others, 1984 Deng and others, 1986 Zhang and others, 1987	Recorded Love waves are consistent with 90° dip and 0° rake, or with 45° dip and 45° rake. Vertical dip preferred on basis of nearly pure strike-slip displacement at surface.
Fuyun, China (1)	8/10/31	7.9	7.9	160°	80°	180°	0°	3			340°	70°	14.6	<17	Deng and Zhang, 1984 Molnar and Deng, 1984	Focal mechanism strike constrained to strike of surface rupture.
Valentine, Texas (2)	8/16/31	6.4	6.3	291° 10° 23°	70° 45° 54°	-159° -160° -155°	-21° -20° -25°	1 1 2							Doser, 1987a Doser and Smith, 1989 Dumas and others, 1980	P-wave focal mechanisms not well constrained.
Helena, Montana (3)	10/19/35	6.25	6.2	260°	74°	167°	13°	2	145°	60°					Doser, 1989a Doser and Smith, 1989 Freidline and others, 1976	Aftershock plane determined from microseismicity recorded in 1973. Focal mechanism dips NE, microseismicity dips SW.
Virginia City, Montana (4)	11/23/47	6.25	6.1	104°	48°	-170°	-10°	2							Doser, 1989a	Selection of fault planes based only on results of waveform inversion. Earthquake may have occurred on north-trending, subvertical normal fault.
Canakkale, Turkey (5)	3/18/53	7.2	7.2	059°	76°	174°	6°	1			53°	−90°	4.3	small (<17)	Ambraseys, 1970 Ambraseys and Zatopek, 1969 McKenzie, 1972	Small vertical displacement.

Table LP Q5-2 (continued)

Earthquake (*)[1]	Date	Magnitude		Orientation of Fault Plane									Maximum Coseismic Surface Slip[2] (m)		References[5]	Comments
				Focal Mechanism[3]					Aftershocks[3]		Surface Exposures[3]					
		M_s	M_w	S	D	R	R90	Method[4]	S	D	S	D	Horizontal	Vertical		
Fairview Peak, Nevada (6)	12/16/54	7.2	7.2	350° 350° 010°	60° 60° 60°	-150° -160° -150°	-30° -20° -30°	1 2 3	349°	62°	10°	65° to 90°	3.6	3.2	Doser, 1986 Doser and Smith, 1989 Slemmons, 1984 Snay and others, 1985 Stauder and Ryall, 1967	Aftershock orientation based on 1965 microseismicity study. Geodetic modeling indicates two rupture planes - Surface: 012°, 63°; Buried: 347°, 59°
Gobi-Altai, Mongolia (7)	12/4/57	7.9	8.1	103°	53°	32°	32°	1	~100° to 110°		~280° to 290°	40° to 70°	8.9	3.1	Forensov and Solonenko, 1965 Okal, 1976	3:1 horizontal:vertical slip ratio for coseismic displacement on Bogdo fault (main rupture). Surface exposures dip NE and focal mechanism dips SW?
Lituya Bay, Alaska (8)	7/10/58	7.9	7.8	335°	72°	172°	8°	1	325°	>80° ?	322°	78° to 81°	6.5	1.0	Ben-Menachem and Toksoz, 1963 Stauder, 1960 Sykes, 1971 Tocher, 1960	Steeply dipping (vertical?) aftershock zone.
Wakasa Bay, Japan (9)	3/26/63	6.9	6.3	054°	68°	158°	22°	1							Abe, 1974	Occurred offshore in Wakasa Bay.
Xingtai, China (10)	3/22/66	7.2	6.8	026°	73°	-169°	-11°	2	35°						Chung and Cipar, 1983 He and Ting, 1978	Four large strike-slip earthquakes occurred on steeply dipping faults. Focal mechanism for 3/26 event is poorly constrained.
(11)	3/26/66	6.2	6.1	030°	74°	-157°	-23°	1	35°							

Table LP Q5-2 (continued)

Earthquake (*)[1]	Date	Magnitude		Orientation of Fault Plane									Maximum Coseismic Surface Slip[3] (m)		References[4]	Comments
				Focal Mechanism[3]					Aftershocks[3]		Surface Exposures[3]					
		M_s	M_w	S	D	R	R90	Method[4]	S	D	S	D	Horizontal	Vertical		
Varto, Turkey (12)	8/19/66	6.8	6.8	304°	64°	163°	17°	1			~295°	>80° ?	0.3	small	Ambraseys and Zatopek, 1968 Jackson and McKenzie, 1984 Jackson and McKenzie, 1988 McKenzie, 1972 Wallace, 1968	Alternating sense of vertical displacement along fault; scarps up to 0.3 m high.
Truckee, California (13)	9/12/66	5.9	6.0	044° 043° 044°	80° 76° 80°	0° -11° 0°	0° -11° 0°	1 2 2	44°	90°	30°		0	0	Burdick, 1977 Kachadoorian and others, 1967 Tsai and Aki, 1970 Wallace and others, 1981a	No tectonic surface faulting. There was ground cracking in alluvium.
Koyna, India (14)	12/10/67	6.5	6.5	016°	67°	-29°	-29°	2	~10° to 20°	?					Langston, 1976 Rastogi and Talwani, 1980	Reservoir-induced earthquake.
Sitka, Alaska (15)	7/30/72	7.6	7.7	347° 340° ~340°	78° 85° 73°	180° 175° 173°	0° 5° 7°	1 2 2	335°	>80°					Schell and Ruff, 1989 Perez and Jacob, 1980	Steeply dipping (vertical?) aftershock zone.
Haicheng, China (16)	2/4/75	7.4	7.0	288° 285°	78° 78°	-18° -14°	-18° -14°	1 2	290° to 297°	>80°	300°				Cipar, 1979 Geodetic Survey Brigade, 1978 Gu and others, 1976 Stewart and others, 1976 Wu and others, 1976	Surface fissuring.

Table LP Q5-2 (continued)

Earthquake (*)[1]	Date	Magnitude		Orientation of Fault Plane									Maximum Coseismic Surface Slip[2] (m)		References[4]	Comments
				Focal Mechanism[3]					Aftershocks[3]		Surface Exposures[3]					
		M_s	M_w	S	D	R	R90	Method[4]	S	D	S	D	Horizontal	Vertical		
Caldiran, Turkey (17)	11/24/76	7.3	7.2	107° 115°	78° 74°	176° 174°	4° 6°	1 1			115° to 135°	~90°	3.7	≤ 0.5	Gulkan and others, 1978 Jackson and McKenzie, 1984 Toksoz and others, 1977, 1978	Variable relative vertical displacement.
Bob-Tangol, Iran (18)	12/19/77	5.8	5.6	328° 322°	58° 60°	165° 169°	15° 11°	1 1	140°	≥65°	320°	70°	0.2	0	Berberian and others, 1979 Jackson and McKenzie, 1984 Zohoorian and others, 1981	Aftershock zone dips SW. P-wave solutions and surface exposures dip NE.
Swabian Jura, Germany (19)	9/3/78	5.3	5.2	200° 192°	75° 60°	13° 0°	13° 0°	1 1	13°	≥80°					Haessler and others, 1980 Turnovsky and Schneider, 1982	Aftershocks and focal mechanism solutions dip in opposite directions.
Erzurum-Kars, Turkey (20)	10/30/83	6.9	6.7	220° 218°	77° 70°	13° 10°	13° 10°	1 1	211°	75° (?)	195° to 215°		1.0	0.6	Barka and others, preprint Islami, 1986 Person, 1984	
North Palm Springs, California (21)	7/8/86	6.0	6.1	300° 283° 287° 287° 287°	45° 41° 46° 46° 46°	180° 147° 154° 150° 135°	0° 33° 26° 30° 45°	1 2 2 2 4	300°	50° to 60°	290°				Hartzell, 1989 Jones and others, 1986 Mendoza and Hartzell, 1988 Pacheco and Nabelek, 1988	Minor fracturing along Banning trace, San Andreas fault. Teleseismic P-waveform inversion indicates ≈ 2:1 SS:RV slip ratio for fault plane at 287° 46° 154°. Strong motion inversion indicates ≈ 1:1 SS:RV slip ratio for fault plane at 287° 46° 135°.

Table LP Q5-2 (continued)

Earthquake (*)[1]	Date	Magnitude		Orientation of Fault Plane									Maximum Coseismic Surface Slip[2] (m)		References[5]	Comments
				Focal Mechanism[3]					Aftershocks[3]		Surface Exposures[3]					
		M_s	M_w	S	D	R	R90	Method[4]	S	D	S	D	Horizontal	Vertical		
Chalfant Valley, California (22)	7/21/86	6.2	6.2	155° 139° 142°	60° 54° 48°	-180° -173° -160°	0° -7° -20°	1 2 2	154°	60° to 90°	175°		0.11	0	Cockerham and Corbett, 1987 Pacheco and Nabelek, 1988 Prescott and others, 1987	Displacement measured across zone of fractures. Geodetic modeling indicates rupture occurred on 2 planes: 1. 140°, 55°, 0.6 m horizontal slip 2. 140°, −90°, 0.8 m horizontal slip
Armenia, USSR (23)	12/7/88	6.8	6.8	300° 299° 307°	63° 64° 60°	100° 151° 159°	80° 29° 21°	2 2 3	310° and 277°	50° 50°	300°	50° to 80°	0.40	1.60	Cisternas and others, 1989 Haessler and others, 1989 Pacheco and others, 1989	Maximum displacement includes an additional 1.1 m of shortening. Broad band waveform inversion for 3 subevents are (S, D, R)[2]: 299° 45° 127° 309° 90° 150° 264° 69° 148°
Upland, California (24)	2/28/90	5.5	5.5	220° 212°	70° 60°	0° -6°	0° -6°	1 2	220°	>70°					Dreger and Helmberger, 1990 Hutton, K., pers. comm.	Fault length is less than 7 km; strike is perpendicular to structural grain (Dreger, pers. comm.).

[1]Numbers correspond to numbered data points on Figure LP Q5-1.
[2]Components of slip measured at site of net maximum displacement.
[3]S = Strike; D = Dip; R = Rake, after convention of Aki and Richards, 1980; R90 = Normalized rake (-90 to 90 degrees).
[4]Method of solution: 1 = P-wave first motion; 2 = Waveform inversion (P & SH); 3 = Waveform inversion (R & L); 4 = Strong-ground-motion inversion.
[5]References are listed in alphabetical order.

changes in the vicinity of the epicenter and is consistent with both nodal planes. The Madison fault is a normal fault, thus the earthquake may have occurred on a steeply dipping oblique-normal fault (plane 2), rather than on a moderately dipping strike-slip fault (plane 1). In addition, the earthquake occurred in the Northern Basin and Range province, a region clearly dominated by extensional tectonics. Because these five events occurred within extensional regimes, they are not considered to be relevant examples with respect to the current transpressional nature of central coastal California (McCulloch, 1987). The remaining five earthquakes are discussed below.

The focal mechanism for the Wakasa Bay, Japan, earthquake (3/26/63), as determined from P-wave first-motion and S-wave polarization data, indicates that the fault dips 68 degrees and has a rake of 22 degrees (Table LP Q5-2). Because this type of short period mechanism is not considered to be as reliable as long period mechanisms determined from waveform inversion of P and SH waves, the source parameters are more uncertain than for most other earthquakes in the data base. The tectonic setting of Wakasa Bay is characterized by oblique subduction. Strike-slip faulting occurs within the overriding continental crust of central Honshu, Japan. An actively subducting margin is not analogous to the contemporary tectonic setting of central coastal California.

The geometry and sense of slip associated with the Varto, Turkey, earthquake (8/19/66) is uncertain. Focal mechanism data and geologic data provide conflicting information. The focal mechanism was derived from P-wave first motions, and suggests that the earthquake had a reverse component of slip (rake of 17 degrees; Table LP Q5-2). However, surface displacements associated with the Varto earthquake are consistent with a nearly pure strike-slip sense of displacement. The upthrown block alternates along the strike of the fault, and the vertical component of slip is much smaller than the horizontal displacement. As a further complication, the focal mechanism of the largest aftershock (8/20/66) indicates faulting on a subvertical strike-slip fault, which is similar to the focal mechanisms of other earthquakes along the North Anatolian fault to the west of the triple junction between the Arabian, Turkish, and Eurasian plates (McKenzie, 1972). The epicenter of the main shock is located to the east of this triple junction. Other earthquakes east of the triple junction also have a reverse component of slip. In this region to the east of the triple junction, the continental Arabian plate is colliding with the continental Eurasian plate, forming a compressional continental collision zone (Cisternas and others, 1989), unlike the oceanic/continental transpressional margin of south-central coastal California.

Similarly, seismologic and geologic data for the Bob-Tangol, Iran, earthquake (12/19/77) provide conflicting information with regard to sense of slip and dip of the fault plane. The P-wave first-motion focal mechanism solution suggests that the fault dips about 58 degrees northeast and that it was a strike-slip earthquake having a small reverse component (rake of 15 degrees; Jackson and McKenzie, 1984). However, surface exposures of the fault dip steeply (approximately 70 degrees; Table LP Q5-2) to the northeast, and Berberian and others (1979) note that the earthquake reactivated an early Quaternary high-angle reverse fault (Kuhbanan fault). In addition, the aftershock sequence defines a plane that is subvertical to steeply southwestward dipping (more than 65 degrees; Zoohorian and others, 1979). The Bob-Tangol earthquake occurred within the Iranian plate to the east of the Zagros fold belt. Plate motion vectors for the Arabian and Iranian plates indicate that the Zagros region is an oblique continental collision zone (Jackson and McKenzie, 1984). The uncertainties in the available data regarding this event allow for interpretations of a strike-slip earthquake on a near-vertical fault or a high-angle to moderately dipping reactivated reverse fault.

The waveform inversion of broad-band teleseismic waves for the Armenia, USSR, earthquake (12/7/88) indicates that the earthquake had an extremely complicated rupture process. The focal mechanism for the earthquake as a single-source event has a rake of 29 degrees, but the rupture process is better defined by a source model with three subevents (Pacheco and others, 1989). Two of the subevents have oblique mechanisms and occurred on moderately dipping faults (dips of 45 and 69 degrees, and rakes of 53 and 32 degrees respectively); the third subevent also has an oblique mechanism and occurred on a vertical fault (90- degree dip and 30-degree rake; Table LP Q5-2). Thus, as the three subevent solution is considered to be more representative of the overall rupture process, we conclude that the Armenian earthquake resulted from oblique slip on both moderately dipping and steeply dipping faults. In addition, the components of surface slip at the site of the maximum net displacement indicate a 1:4 ratio of horizontal to vertical slip (0.4 meter right-lateral, 1.6 meters vertical; Table LP Q5-2). The Armenian earthquake occurred within the Lesser Caucasus Mountains, a region that is dominated by compressive tectonics resulting from the collision of the Arabian and Eurasian plates (Cisternas and others, 1989).

Seismologic and geologic data also provide conflicting information regarding the geometry of the fault that caused the Upland, California, earthquake (2/28/90). The focal mechanism solution from waveform analysis indicates that the fault plane has a dip of 60 degrees. However, the P-wave first-motion focal mechanism solution indicates a dip of 70 degrees, and the dip of the aftershock sequence is greater than 70 degrees, suggesting that the earthquake may have occurred on a more steeply dipping fault (Table LP Q5-2). Furthermore, the strike of the fault plane (northeast) is approximately perpendicular to the major compressional structures along the range-front, suggesting that the earthquake occurred on a relatively minor 7-kilometer-long tear fault between the two thrust faults (Dreger, personal communication). The Upland earthquake occurred along the southern edge of the Transverse Ranges, a part of the North American-Pacific plate margin that is dominated by compressional rather than transpressional tectonics.

Moderately Dipping Oblique-Slip Earthquakes

The Gobi Altai, Mongolia, earthquake (12/4/57) is classified as an oblique-slip earthquake (Figure LP Q5-1). It is discussed here because of its proximity to the strike-slip/oblique-slip boundary in Figure LP Q5-1, and because the available data regarding the orientation of the fault plane for the Gobi Altai earthquake are conflicting. The focal mechanism is derived from P-wave first motions and indicates that the earthquake occurred on a moderately dipping (to the southwest) oblique-slip fault (dip and rake of 53 and 32 degrees) Surface exposures of the fault dip at 40 to 70 degrees northeast, although the dip of the fault plane was observed only at three locations over a rupture length of more than 230 kilometers (Florensov and Solonenko, 1965). The components of slip at the site of the net maximum displacement (8.4 meters horizontal) and at other sites along the main fault trace indicate an approximate 3:1 horizontal to vertical slip ratio (Table LP Q5-2). The largest displacement (9.2 meters vertical), however, was observed on a reverse fault that strikes perpendicular to the main rupture. The largest horizontal and vertical displacements thus have an approximate 1:1.1 slip ratio, which supports an interpretation that the Gobi Altai earthquake resulted from oblique slip on a moderately dipping fault. In addition, the earthquake occurred in central Mongolia, a region characterized by northwest-southeast extension and northeast-southwest compression resulting from collision of the Indian plate into central Asia (Molnar and Deng, 1984).

The North Palm Springs, California, earthquake (7/8/86) is also classified as an oblique-slip earthquake (Figure LP Q5-1). It is discussed here because of its proximity to the strike-slip/oblique-slip boundary shown in Figure LP Q5-1. The earthquake apparently ruptured a short section of the Banning trace of

the San Andreas fault (Jones and others, 1986). Waveform inversion of teleseismic P-waves by Pacheco and Nabelek (1988) indicates that the rake is 147 degrees; this is similar to the rake of 150 degrees based on inversion of teleseismic P-waves for the components of slip by Mendoza and Hartzell (1988). In addition, Hartzell (1989) determined a rake of 135 degrees from inversion of strong ground motion records for the components of slip (Table LP Q5-2). The normalized rakes for these three solutions are 33, 30 and 45 degrees, respectively. Thus, the North Palm Springs earthquake is characterized as an oblique-slip earthquake that occurred on a moderately dipping (46 degrees) fault. The Banning trace of the San Andreas fault trends east to southeast and is located in the eastern Transverse Ranges (Jones and others, 1986). The restraining geometry along this reach of the fault is likely the cause of the oblique sense of slip.

Summary of Earthquake Data Base

The earthquake data base clearly shows that sense of slip (rake) is directly related to the dip of the fault. When the rakes and dips of all earthquakes based on focal mechanisms are considered, it is apparent that the occurrence of strike-slip earthquakes on moderately dipping faults is uncommon. Only 14 percent (10 of 71) of the earthquakes have focal mechanisms suggesting strike-slip faulting on faults dipping less than 70 degrees. Closer examination of each of these earthquakes in terms of the full suite of data (surface rupture, aftershock patterns, strong-ground-motion inversion, and Holocene deformation) shows that fewer still may be considered to be moderately dipping strike-slip earthquakes. Further, of these 10 earthquakes having focal mechanisms that suggest strike-slip faulting on moderately dipping faults, 5 occurred in extensional environments that are not considered analogous to the transpressional setting of the central coastal California environment. The available data for the Armenian earthquake indicate that this earthquake occurred on a moderately to steeply dipping oblique fault. For the remaining four earthquakes, data are limited and of poor quality, or the geologic data and focal mechanisms provide conflicting results. In particular, for three of these earthquakes, the geologic data or aftershock patterns indicate that the earthquake very likely occurred on a steeply dipping (greater than 70 degrees) strike-slip fault. Furthermore, all five events occurred in compressive tectonic settings that do not appear to be analogous to the transpressional tectonic setting of the Hosgri fault zone. We therefore conclude that strike-slip faulting on moderately dipping faults is very rare, and that there are no unequivocal examples in the data base of strike-slip earthquakes on moderately dipping faults (less than 70 degrees) in a tectonic setting analogous to that of central coastal California.

REACTIVATION OF REVERSE FAULTS IN CHINA

The Haiyuan fault zone is more than 1000 kilometers long and trends north-northwest to west-northwest through north-central China (Institute of Geomechanics, 1984). The eastern section of the Haiyuan fault zone ruptured during the 1920 Haiyuan earthquake (M_W 8.0), resulting in approximately 220 kilometers of surface faulting. The maximum horizontal displacement was 10 meters and the maximum vertical displacement apparently did not exceed 1 meter, suggesting that the earthquake resulted from nearly pure left slip (Table LP Q5-2; Deng and others, 1986). Measured dips along the surface trace range from approximately 30 degrees to subvertical. According to the interpretation of Deng and others (1986), the Haiyuan fault zone developed during the middle Pleistocene, when strike-slip faulting occurred at an acute angle to an existing series of subparallel Pliocene(?) and early Pleistocene reverse faults. More recent strike-slip faulting apparently broke through the reverse faults, forming steeply dipping (more than 60 degrees) segments that are connected by reactivated, shallowly dipping (30 to 60 degrees) segments of the existing reverse faults (Figure LP Q5-2). Rather than simply reactivating a preexisting, moderately dipping, Quaternary reverse fault, as implied in the question, the Haiyuan fault zone has reactivated

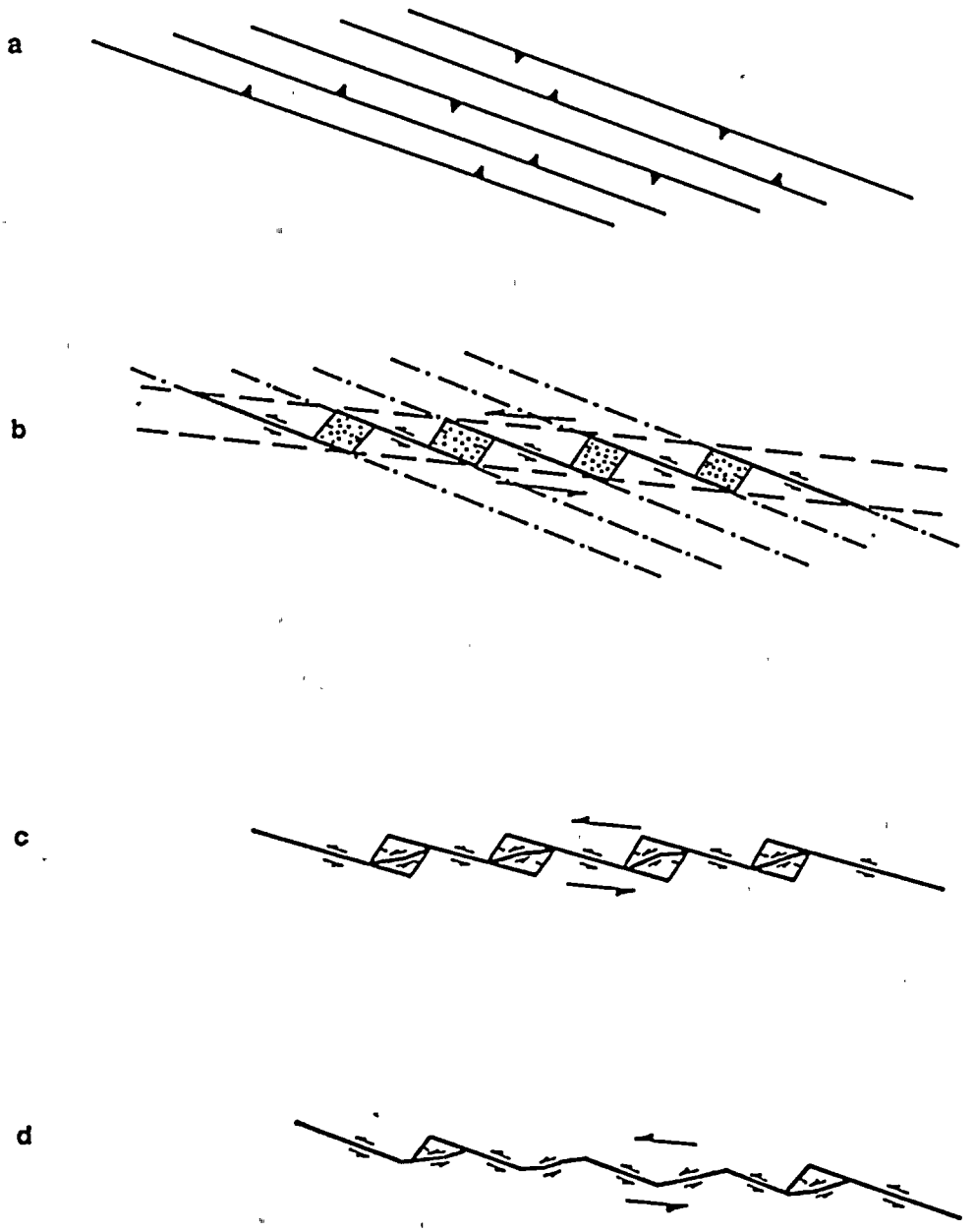

Figure LP Q5-2

Simple schematic evolution of the Haiyuan fault zone. (a) Lines indicate the average trends of thrust faults active before middle Pleistocene time. (b) Initiation of strike-slip faulting along a trend different from that of the thrust faults, during middle Pleistocene time. (c) Evolution of subparallel strike-slip faults, or shear fractures, and the formation of pull-apart basins during late Quaternary time. (d) Surface faulting during the Haiyuan earthquake. (Modified from Deng and others, 1986.)

segments of different reverse faults, forming a single trace that has alternating moderately dipping and steeply dipping segments.

Based on structural relationships portrayed on the geologic maps of China (Institute of Geomechanics, 1984), this relationship may exist for other large strike-slip fault zones in north-central China (D.B. Slemmons and Peizhan Zhang, personal communication). There is no information on these maps regarding the slip type, fault dip, or recency of faulting; thus we simply note that there may be other strike-slip fault zones in China that have reactivated segments of existing reverse faults. Extensive field studies of faults in China indicate, however, that there are no shallowly dipping (30 to 45 degrees) strike-slip faults exposed at the surface (Peizhan Zhang, personal communication from Deng Qidong).

INFLUENCE OF TECTONIC HISTORY ON THE GEOMETRY AND SENSE OF SLIP OF THE HOSGRI FAULT ZONE

Question LP 5 asks whether or not the tectonic history of the Hosgri fault zone may have imparted a dipping geometry that now, in the present strike-slip regime, would accommodate strike-slip displacement along a moderately dipping fault surface. The Hosgri fault zone has had a long history as a major strike-slip fault zone along the central California coast. The history of deformation encompasses a variety of tectonic settings and consequently has produced a complex pattern of faulting. Tectonic models for the region suggest that the inception of faulting along the Hosgri fault zone began in Oligocene to early Miocene time, when transcurrent relative motion between the Pacific and North American plates replaced oblique subduction along the plate boundary (Atwater and Molnar, 1973). Until middle Miocene time, the Hosgri fault zone acted as a high-angle, southwest-dipping, right-lateral fault, and had a significant component of down-on-the-west displacement (McCulloch, 1987). This Miocene episode of transtensional displacement changed to the contemporary transpressional tectonic regime in late Miocene to early Pliocene time. This transition in tectonic style along the Hosgri fault zone is roughly contemporaneous with a significant early Pliocene change in relative plate motion (Harbert and Cox, 1989; Cox and Engebretson, 1985), and with onset of opening of the Gulf of California.

Sense of slip on the Hosgri fault zone and evidence for steep dips along the fault zone are documented in the Final Report (PG&E, 1988) and in responses to several questions (GSG 1, Attachment GSG Q1-A, GSG 3, GSG 4, SSC 2, and SSC 4, March 1990). A consideration of the tectonic history of the Hosgri fault zone leads to the conclusion that the fault zone probably inherited a steep dip from its initial history as a transtensional strike-slip fault. If the transtensional geometry is imparted to the present fault zone, steep dips to the west should have been inherited. The degree to which the preexisting geometry of a fault zone is inherited or modified as changes in tectonic regimes occur is not very well known. Nevertheless, the prior history on the Hosgri fault zone would suggest that the fault is steeply dipping.

CONCLUSIONS

Question LP 5 raises the issue of strike-slip faulting along moderately dipping faults and whether this style of faulting might occur along the Hosgri fault zone. To examine the occurrence of dipping strike-slip faults, we have compiled an earthquake data base that focuses particularly on the geometry of coseismic faulting as well as the components of slip, as represented by the rake angle. The data clearly show that the sense of slip (rake) is related to the dip of the fault. The occurrence of strike-slip earthquakes on moderately dipping faults (less than 70 degrees) is uncommon in the historical record. When the focal mechanisms of all events are compared, only 14 percent (10 of 71) of the strike-slip earthquakes that we examined may have occurred on faults that dip less than 70 degrees; only 6 percent

(4 of 71) may have occurred on faults that dip less than 60 degrees. A closer review of these events in terms of all available data shows that fewer still may be considered moderately dipping strike-slip earthquakes. For several of the earthquakes, the focal mechanism solution conflicts with the sense of displacement and fault dip indicated by coseismic surface fault rupture, aftershock patterns, and observations of Holocene deformation. These data suggest that, in some cases, the strike-slip earthquakes in fact occurred on steeply dipping fault planes; in other cases, the earthquake is more accurately characterized as oblique when all the data are considered. In addition, many of the events occurred within extensional tectonic environments that are different from the transpressional tectonic setting of south-central California. We conclude that moderately dipping strike-slip faults are likely to be very rare. We have found no unequivocal case of moderately dipping strike-slip faults within a transpressional tectonic setting analogous to south-central coastal California.

The question also raises the issue of whether the tectonic history of the Hosgri fault zone might imply that it has inherited a dipping geometry that is now being reactivated in a strike-slip sense. The question cites the Haiyuan fault zone as an example of a formerly reverse fault zone that has been reactivated as a complex series of strike-slip and reverse fault segments. The tectonic history of the Hosgri fault zone is one of primarily strike-slip deformation, either transtensional or transpressional. There is no history of reverse slip on a moderately dipping fault plane similar to the Haiyuan fault. During Miocene time, the Hosgri fault zone experienced transtensional deformation on a vertical or steeply west dipping fault plane. We conclude that the tectonic history of the Hosgri fault zone would support the interpretation that the present-day Hosgri fault zone is vertical to steeply dipping. Multiple lines of evidence, given in the Final Report and in responses to questions, indicate that the Hosgri fault zone is steeply dipping within the contemporary tectonic environment. Because the conclusion of a steeply dipping Hosgri fault zone reached here is the same as that reached in characterizing the Hosgri fault zone as a seismic source in the Final Report, there is no impact on source characterization or ground motion estimates at the site.

REFERENCES

Abe, K., 1974, Fault parameters determined by near- and far-field data: The Wakasa Bay earthquake of March 26, 1963: Bulletin of the Seismological Society of America, v. 64, p. 1369-1382.

Abe, K., 1978, Dislocations, source dimensions and stresses associated with earthquakes in the Izu Peninsula, Japan: Journal of the Physics of the Earth, v. 26, p. 253-274.

Aki, K., and Richards, P., 1980, Quantitative Seismology; Theory and Practice: W. H. Freeman, San Francisco, p. 106.

Ambraseys, N. N., 1970, Some characteristic features of the Anatolian fault zone: Tectonophysics, v. 9, p. 143-165.

Ambraseys, N. N., and Zatopek, A., 1968, The Varto, Ustukran (Anatolia) earthquake of 19 August 1966, summary of a field report: Bulletin of the Seismological Society of America, v. 58, p. 47-102.

Anderson, H., Smith, E., and Robinson, R., 1990, Normal faulting in a back arc basin: seismological characteristics of the March 2, 1987, Edgecumbe, New Zealand, earthquake: Journal of Geophysical Research, v. 95, no. B4, p. 4709-4723.

Anderson, J. G., and Simmons, R. S., eds., 1981, The Mexicali Valley Earthquake of 9 June 1980, Earthquake Engineering Research Institute Newsletter #16.

Atwater, T., and Molnar, P., 1973, Relative motion of the Pacific and North American plates deduced from sea-floor spreading in the Atlantic, Indian, and South Pacific oceans; in Kovach, R. L., and Nur, A., (eds.), Proceedings, Conference on Tectonic Problems of the San Andreas Fault System: Stanford University Publications in Geological Sciences, v. 13, p. 136-148.

Banghar, A. R., 1983, Synthetic P-wave seismograms for the Kinnaur (Himachal Pradesh, India) earthquake of January 19, 1975: Physics of the Earth and Planetary Interiors, v. 32, p. 331-341.

Barka, A., Toksoz, M. N., Kadinsky-Cade, K., and Gulen, L., preprint, The segmentation, seismicity, and earthquake potential of the eastern part of the North Anatolian fault zone: in review, Journal of Geophysical Research.

Barker, J. S., and Langston, C. A., 1981, Inversion of teleseismic body waves for the moment tensor of the 1978 Thessaloniki, Greece, earthquake: Bulletin of the Seismological Society of America, v. 71, p. 1423-1444.

Barker, J. S., and Wallace, T. C., 1986, A note on the teleseismic body waves from the 23 November 1984 Round Valley, California, earthquake: Bulletin of the Seismological Society of America, v. 76, p. 883-888.

Ben-Menahem, A., and Toksoz, M. N., 1963, Source-mechanism from spectra of long-period seismic surface waves. 3. The Alaska earthquake of July 10, 1958: Bulletin of the Seismological Society of America, v. 53, no. 5, p. 905-919.

Bent, A., and Helmberger, D., 1989, Source complexity of the October 1, 1987, Whittier Narrows earthquake: Journal of Geophysical Research, v. 94, no. B7, p. 9548-9556.

Bent, A., Helmberger, D. V., Stead, R. J., and Ho-Liu, P., 1989, Waveform modeling of the November 1987 Superstition Hills earthquake: Bulletin of the Seismological Society of America, v. 79, no. 2, p. 500-514.

Berberian, M., Asudeh, I., and Arshadi, S., 1979, Surface rupture and mechanism of the Boh-Tangol (south-eastern Iran) earthquake of 19 December 1977: Earth and Planetary Letters, v. 42, p. 456-462.

Bolt, B. A., McEvilly, T. V., and Uhrhammer, R. A., 1981, The Livermore Valley, California, sequence of January 1980: Bulletin of the Seismological Society of America, v. 71, p. 451-463.

Bonilla, M. G., and Buchanon, J. M., 1970, Interim report on worldwide historic surface faulting: U. S. Geological Survey Open-file Report, 32 p.

Boore, M., Sims, J. D., Kanamori, H., and Harding, S., 1981, The Montenegro, Yugoslavia, earthquake of April 15, 1979: source orientation and strength: Physics of the Earth and Planetary Interiors, v. 27, p. 133-142.

Bounif, A., Haessler, H., and Meghraoui, M., 1987, The Constantine (north-east Algeria) earthquake of October 27, 1985: surface ruptures and aftershock study: Earth and Planetary Science Letters, v. 85, p. 451-460.

Burdick, L. J., 1977, Broad-band seismic studies of body waves: Ph.D. thesis, California Institute of Technology, Pasadena, 68 p.

Burdick, L. J., and Mellman, G. R., 1976, Inversion of the body waves from the Borrego Mountain earthquake to the source mechanism: Bulletin of the Seismological Society of America, v. 66, p. 1485-1499.

Chandra, U., 1984, Focal mechanism solutions for earthquakes in Iran: Physics of the Earth and Planetary Interiors, v. 34, p. 9-16.

Chen, K-C., and Wang, J-H., 1986, The May 20, 1986 Hualien, Taiwan, earthquake and its aftershocks: Bulletin of the Institute of Earth Sciences, Academia Sinica, v. 6., p. 1-13.

Choy, G. L., and Boatwright, J., 1988, Teleseismic and near-field analysis of the Nahanni earthquakes in the Northwest Territories, Canada: Bulletin of the Seismological Society of America, v. 78, no. 5, p. 1627-1652.

Choy, G. L., and Bowman, J. R., 1990, Rupture process of a multiple main shock sequence: analysis of teleseismic, local, and field observations of the Tennant Creek, Australia, earthquakes of January 22, 1988: Journal of Geophysical Research, v. 95, no. B5, p. 6867-6882.

Choy, G. L., and Kind, R., 1987, Rupture complexity of a moderate-sized (m_b 6.0) earthquake: broadband body-wave analysis of the North Yemen earthquake of 13 December 1982: Bulletin of the Seismological Society of America, v. 77, no. 1, p. 28-46.

Chung, W., and Cipar, J. J., 1983, Source modeling of the Hsingtai, China earthquakes of March 1966: Physics of the Earth and Planetary Interiors, v. 33, p. 111-125.

Cipar, J., 1979, Source processes of the Haicheng, China earthquake from observations of p and s waves: Bulletin of the Seismological Society of America, v. 69, p. 1903-1916.

Cipar, J., 1980, Teleseismic observations of the 1976 Friuli, Italy, earthquake sequence: Bulletin of the Seismological Society of America, v. 70, p. 963-983.

Cisternas, A., Philip, H., Bousquet, J. C., Cara, M., Deschamps, A., Dorbath, L., Dorbath, C., Haessler, H., Jimenez, E., Nercessian, A., Rivera, L., Romanowicz, B., Gvishiani, A., Shebalin, N. V., Aptekman, I., Arefiev, S., Borisov, B. A., Gorshkov, A., Graizer, V., Lander, A., Pletnev, K., Rogozhin, A. I., and Tatevossian, R., 1989, The Spitak (Armenia) earthquake of 7 December 1988: field observations, seismology, and tectonics: Nature, v. 339, p. 675-679.

Cockerham, R. S., and Corbett, E. J., 1987, The July 1986 Chalfant Valley, California, earthquake sequence: preliminary results: Bulletin of the Seismological Society of America, v. 77, p. 280-289.

Cox, A., and Engebretson, D., 1985, Change in motion of Pacific plate at 5 Myr BP: Nature, v. 313, p. 472-474.

Deng, Q., and Zhang, P., 1984, Research on the geometry of shear fracture zones: Journal of Geophysical Research, v. 89, p. 5699-5710.

Deng, Q., Sung, F., Zhu, S., Li, M., Wang, T., Zhang, W., Burchfiel, B. C., Molnar, P., and Zhang, P., 1984, Active faulting and tectonics of the southern Ningxia-Hui Autonomous Region: Journal of Geophysical Research, v. 89, p. 4427-4445.

Deng, Q., Chen, S., Song, F., Zhu, S., Wang, Y., Zhang, W., Jiao, D., Burchfiel, B. C., Molnar, P., Royden, L., and Zhang, P., 1986, Variations in the geometry and amount of slip on the Haiyuan (Nanxihaushan) fault zone, China, and the surface rupture of the 1920 Haiyuan earthquake; in Das, S., Boatwright, J., and Scholz, C., eds., Earthquake Source Mechanics, Geophysical Monograph 37: Maurice Ewing Volume 6, Washington, D.C., American Geophysical Union, p. 169-182.

Deschamps, A., and King, G. C. P., 1984, Aftershocks of the Campania-Lucania (Italy) earthquake of 23 November 1980: Bulletin of the Seismological Society of America, v. 74, no. 6, p. 2483-2517.

Deschamps, A., Iannaccone, G., and Scarpa, R., 1984, The Umbrian earthquake (Italy) of 19 September 1979: Annales Geophysicae, v. 2, no. 1, p. 29-36.

Doser, D. I., 1985, Source parameters and faulting processes of the 1959 Hebgen Lake, Montana, earthquake sequence: Journal of Geophysical Research, v. 90, no. B6, p. 4537-4555.

Doser, D. I., 1986, Earthquake processes in the Rainbow Mountain-Fairview Peak-Dixie Valley, Nevada Region 1954-1959: Journal of Geophysical Research, v. 91, p. 12,572-12,586.

Doser, D. I., 1987a, The 16 August 1931 Valentine, Texas earthquake: evidence for normal faulting in west Texas: Bulletin of the Seismological Society of America, v. 77, no. 6, p. 2005-2017.

Doser, D. I., 1987b, The Ancash, Peru, earthquake of 1946 November 10: evidence for low-angle normal faulting in the high Andes of northern Peru: Geophysical Journal of the Royal Astronomical Society of London, v. 91, p. 57-71.

Doser, D. I., 1987c, Modeling the Pnl waveforms of the Fairview Peak - Dixie Valley, Nevada, U.S.A., earthquake sequence (1954-1959): Physics of the Earth and Planetary Interiors, v. 48, p. 64-72.

Doser, D. I., 1988, Source parameters of earthquakes in the Nevada seismic zone, 1915-1943: Journal of Geophysical Research, v. 93, no. B12, p. 15,001-15,015.

Doser, D. I., 1989a, Source parameters of Montana earthquakes (1925-1964) and tectonic deformation in the northern Intermountain Seismic Belt: Bulletin of the Seismological Society of America, v. 79, no. 1, p. 31-50.

Doser, D. I., 1989b, A study of large (M > 6.0) historical earthquakes (1942, 1954) along the San Jacinto fault system, southern California (abs.): EOS Transactions, American Geophysical Union, v. 70, no. 43, p. 1209.

Doser, D. I., 1990, A re-examination of the 1947 Manix, California, earthquake sequence and comparison to other sequences within the Mojave block: Bulletin of the Seismological Society of America, v. 80, no. 2, p. 267-277.

Doser, D. I., and Smith, R. B., 1989, An assessment of source parameters of earthquakes in the Cordillera of the western United States: Bulletin of the Seismological Society of America, v. 79, no. 5, p. 1383-1409.

Dreger, D. S., and Helmberger, D. V., 1990, Source characteristics of the February 28, 1990 Upland sequence from broad-band modeling: EOS Transactions, American Geophysical Union, v. 71, no. 17, p. 552.

Dumas, D. B., Dorman, H. J., and Latham, G. V., 1980, A reevaluation of the August 16, 1931 Texas earthquake: Bulletin of the Seismological Society of America, v. 70, no. 4, p. 1171-1180.

Ebel, J. E., Burdick, L. J., and Stewart, G. S., 1978, The source mechanism of the August 7, 1966 El Golfo earthquake: Bulletin of the Seismological Society of America, v. 68, p. 1281-1292.

Ekstrom, G., Stein, R. S., Eaton, J. P., and Eberhart-Phillips, D., 1990, Seismicity and geometry of a 110-km-long blind fault, 1: the 1985 Kettleman Hills, California, earthquake: submitted to Journal of Geophysical Research, April 1990.

Ellsworth, W. L., Campbell, R. H., Hill, D. P., Page, R. A., Alewine, R. W., III, Hanks, T. C., Heaton, T. H., Hileman, J. A., Kanamori, H., Minster, B., and Whitcomb, J. H., 1973, Point Magu, California, earthquake of 21 February 1973 and its aftershocks: Science, v. 182, p. 1127-1129.

EPRI, 1986, Source-scaling relations of eastern North American earthquakes: Final Report, NP-4789.

Eyidogan, H., 1988, Rates of crustal deformation in western Turkey as deduced from major earthquakes: Tectonophysics, v. 148, p. 83-92.

Eyidogan, H., and Jackson, J., 1985, A seismological study of normal faulting in the Demirci, Alasehir and Gediz earthquakes of 1969-70 in western Turkey: implications for the nature and geometry of deformation in the continental crust: Geophysical Journal of the Royal Astronomical Society of London, v. 81, p. 569-607.

Eyidogan, H., Nabelek, J., and Toksoz, M. N., 1985, The Gazli, USSR, 19 March 1984 earthquake: The mechanism and tectonic implications: Bulletin of the Seismological Society of America, v. 75, p. 661-675.

Florensov, N. A., and Solonenko, V. P., (eds.), 1965, The Gobi-Altai earthquake: Academy of Sciences of the USSR, translated from Russian by the Israel Program for Scientific Translations, Jerusalem, 424 p.

Fredrich, J., McCaffrey, R., and Denham, D., 1988, Source parameters of seven large Australian earthquakes determined by body waveform inversion: Geophysical Journal, v. 95, p. 1-13.

Freidline, R. A., Smith, R. B., and Blackwell, D. D., 1976, Seismicity and contemporary tectonics of the Helena, Montana area: Bulletin of the Seismological Society of America, v. 66, no. 1, p. 81-95.

Geodetic Survey Brigade for Earthquake Research, National Seismological Bureau, 1978, Ground surface deformation of the Haicheng earthquake of magnitude 7.3: Chinese Geophysics, v. 1, p. 139-155.

Given, J. W., Wallace, T. C., and Kanamori, H., 1982, Teleseismic analysis of the 1980 Mammoth Lakes sequence: Bulletin of the Seismological Society of America, v. 72, p. 1093-1109.

Gonzalez-Ruiz, J. R., Rebollar, C. J., Soares, J., and McNalley, K. C., 1987, Seismological evidence of rupture patterns along the San Miguel fault (Peninsular Ranges, Baja California, Mexico) during February 9-15, 1956 (abs.): EOS Transactions, American Geophysical Union, v. 68, no. 44, p. 1348.

Gu, H-D., Chen, Y-T., Gao, X-L., and Zhao, Y., 1976, Focal mechansim of Haicheng, Liaoning Province, earthquake of February 4, 1975: Acta Geophysica Sinica, v. 19, no. 4, p. 270-285.

Gulkan, P., Gurpinar, A., Celebi, M., Arpat, E., and Gencoglu, S., 1978, Engineering report on the Muradiye-Caldiran, Turkey, earthquake of 24 November 1976: prepared for Committee on Natural Disasters, Commission on Sociotechnical Systems, National Research Council, 32 p.

Haessler, H., Cara, M., Jimenez, E., Cisternas, A., Deschmps, and Romanowicz, B., 1989, Rupture process of the Armenian earthquake from broad-band and very long period teleseismic records: EOS Transactions, American Geophysical Union, v. 70, no. 43, p. 1199.

Haessler, H., Hoang-Trong, P., Schick, R., Schneider, G., and Stroback, K., 1980, The September 3, 1978, Swabian Jura earthquake: Tectonophysics, v. 68, p. 1-14.

Harbert, W., and Cox, A., 1989, Late Neogene motion of the Pacific plate: Journal of Geophysical Research, v. 94, no. B3, p. 3052-3064.

Hartzell, S., 1989, Comparison of seismic waveform inversion results for the rupture history of a finite fault: Application to the 1986 North Plam Springs, California, earthquake: Journal of Geophysical Research, v. 94, no. B6, p. 7515-7534.

Hartzell, S. H., and Heaton, T. H., 1983, Inversion of strong ground motion and teleseismic waveform data for the fault rupture history of the 1979 Imperial Valley, California, earthquake: Bulletin of the Seismological Society of America, v. 73, p. 1553-1583.

Hartzell, S. H., and Heaton, T. H., 1986, Rupture history of the 1984 Morgan Hill, California, earthquake from the inversion of strong motion records: Bulletin of the Seismological Society of America, v. 76, p. 649-674.

Hatanaka, Y., and Shimazaki, K., 1988, Rupture process of the 1975 central Oita, Japan, earthquake: Journal of the Physics of the Earth, v. 36, p. 1-15.

He, Z., and Ting, X., 1978, The hypocentral distribution of the Xingtai earthquake series: tectonic stress field and the process of earthquake occurrences: Chinese Geophysics, v. 1, no. 1, p. 97-109.

Holt, W. E., and Wallace, T. C., 1989, Source parameters of three recent earthquakes in eastern India and Burma: implications for the style of deformation in the India-Eurasia collision zone (abs.): Seismological Research Letters, v. 60, no. 1, p. 26.

Huang, J., and Chen, W-P., 1986, Source mechanisms of the Mogod earthquake sequence of 1967 and the event of 1974 July 4 in Mongolia: Geophysical Journal of the Royal Astronomical Society of London, v. 84, p. 361-379.

Hutton, L. K., Johnson, C. E., Pechmann, J. C., Ebel, J. E., Given, J. W., Cole, D. M., and German, P. T., 1980, Epicentral locations for the Homestead Valley earthquake sequence, March 15, 1979: California Geology, v. 33, p. 110-114.

Hwang, L. J., and Kanamori, H., 1989, Teleseismic and strong-motion source spectra from two earthquakes in eastern Taiwan: Bulletin of the Seismological Society of America, v. 79, no. 4, p. 935-944.

INPRES, 1985, El Terremoto de Mendoza, Argentina, del 26 de Enero de 1985: Informe General, Instituto Nacional de Prevención Sesmìca, Argentina.

Institute of Geomechanics, 1984, Tectonic systems map of the People's Republic of China and adjacent sea area: Chinese Academy of Geological Sciences, Bejing, scale 1:2,500,000.

Ishida, M., 1984, Spatial-temporal variation of seismicity and spectrum of the 1980 earthquake swarm near the Izu Peninsula, Japan: Bulletin of the Seismological Society of America, v. 74, no. 1, p. 199-221.

Islami, A. A., 1986, Summary for Farsi Articles. Erzurum-Kars earthquake of 30 October 1983 Analysis: Journal of Earth and Space Physics, v. 15, nos. 1 & 2.

Jackson, J., and McKenzie, D., 1984, Active tectonics of the Alpine-Himalayan belt between western Turkey and Pakistan: Geophysical Journal of the Royal Astronomical Society of London, v. 77, p. 185-264.

Jackson, J., and McKenzie, D., 1988, The relationship between plate motions and seismic moment tensors and the rates of active deformation in the Mediterranean and Middle East: Geophysical Journal, v. 83, p. 45-73.

Jensen, B. L., Chung, W. Y., and Johnston, A. C., 1989, The Guinea, West Africa earthquake of 22 December 1983: source paramaters from teleseismic P- and S-waveforms (abs.): EOS Transactions, American Geophysical Union, v. 70, no. 15, p. 398.

Jones, L. M., Han, W., Hauksson, E., Jin, A., Zhang, Y., and Luo, Z., 1984, Focal mechanisms and aftershock locations of the Songpan earthquakes of August 1976 in Sichuan, China: Journal of Geophysical Research, v. 89, p. 7697-7707.

Jones, L. M., Hutton, L. K., Given, D. D., and Allen, C. R., 1986, The July 1986 North Palm Springs, California, earthquake: Bulletin of the Seismological Society of America, v. 76, p. 1830-1837.

Kachadoorian, R., Yerkes, R. F., and Waananen, A. O., 1967, Effects of the Truckee, California, earthquake of September 12, 1966: U.S. Geological Survey Circular 537, 14 p.

Kadinsky-Cade, K., and Barka, A. A., (in press), Effects of restraining bends on the rupture of strike-slip earthquakes.

Kadinsky-Cade, K., Reilinger, R., and Isacks, B., 1985, Surface deformation associated with the November 23, 1977, Caucete, Argentina, earthquake sequence: Journal of Geophysical Research, v. 90, no. B14, p. 12,691-12,700.

Kaminuma, K., and Goto, Y., 1970, On the observational studies of aftershocks in Japan: Bulletin of the Earthquake Research Institute, v. 48, p. 507-520.

Kanamori, H., and Satake, K., 1990, Broadband study of the 1989 Loma Prieta earthquake: Geophysical Research Letters, v. 17, no. 8, p. 1179-1182.

Kebede, F., Kim, W.-Y., and Kulhánek, O., 1989, Dynamic source parameters of the March-May 1969 Serdo earthquake sequence in Central Afar, Ethiopia, deduced from teleseismic body waves: Journal of Geophysical Research, no. 94, no. B5, p. 5603-5614.

Kim, W-Y., Kulhanek, O., and Meyer, K., 1984, Source processes of the 1981 Gulf of Corinth earthquake sequence from body-wave analysis: Bulletin of the Seismological Society of America, v. 74, no. 2, p. 459-477.

Kristy, M. J., Burdick, L. J., and Simpson, D. W., 1980, The focal mechanisms of the Gazli, USSR, earthquakes: Bulletin of the Seismological Society of America, v. 70, p. 1737-1750.

Langston, C. A., 1976, A body wave inversion of the Koyna, India, earthquake of December 10, 1967, and some implications for body wave focal mechanisms: Journal of Geophysical Research, v. 81, p. 2517-2529.

Langston, C. A., 1978, The February 9, 1971 San Fernando earthquake: A study of source finiteness in teleseismic body waves: Bulletin of the Seismological Society of America, v. 68, p. 1-29.

Langston, C. A., and Butler, R., 1976, Focal mechanism of the August 1, 1975, Oroville earthquake: Bulletin of the Seismological Society of America, v. 66, p. 1110-1120.

Lisowski, M., Prescott, W. H., Savage, J. C., and Johnston, M. J., 1990, Geodetic estimate of coseismic slip during the 1989 Loma Prieta, California, earthquake: submitted to Geological Research letters Special Issue.

Liu, H-L., and Helmberger, D. V., 1983, The near-source ground motion of the 6 August 1979 Coyote Lake, California, earthquake: Bulletin of the Seismological Society of America, v. 73, no. 1, p. 201-218.

Liu, H-L., and Kanamori, H., 1980, Determination of source parameters of mid-plate earthquakes from the waveforms of body waves: Bulletin of the Seismological Society of America, v. 70, p. 1989-2004.

Lyon-Caen, H., Armijo, R., Drakopoulos, J., Baskoutass, J., Delibassis, N., Gaulon, R., Kouskouna, V., Latoussakis, J., Makropoulos, K., Papadimitriou, P., Papanastassiou, D., and Pedotti, G., 1988, The 1986 Kalamata (South Peloponnesus) earthquake: detailed study of a normal fault, evidences for east-west extension in the Hellenic arc: Journal of Geophysical Research, v. 93, no. B12, p. 14,967-15,000.

McCulloch, D. S., 1987, Regional geology and hydrocarbon potential of offshore central California; in Scholl, D. W., Grantz, A., and Vedder, J., eds., Geology and Resource Potential of the Continental Margin of Western North America and Adjacent Ocean Basins, Beaufort Sea to Baja California: American Association of Petroleum Geologists, Circum Pacific Earth Science, v. 6, p. 353-401.

McKenzie, D., 1972, Active tectonics of the Mediterranean region: Geophysical Journal of the Royal Astronomical Society of London, v. 30, p. 109-185.

Mendoza, C., and Hartzell, S. H., 1988, Inversion for slip distribution using teleseismic P waveforms: North Palm Springs, Borah Peak, and Michoacan earthquakes: Bulletin of the Seismological Society of America, v. 78, p. 1092-1111.

Mikumo, T., 1973, Faulting mechanism of the Gifu earthquake of September 9, 1969, and some related problems: Journal of the Physics of the Earth, v. 21, p. 191-212.

Mikumo, T., 1974, Some considerations of the faulting mechanism of the southeastern Akita earthquake of October 16, 1970: Journal of the Physics of the Earth, v. 22, p. 87-108.

Molnar, P., and Deng Q., 1984, Faulting associated with large earthquakes and the average rate of deformation in central and eastern Asia: Journal of Geophysical Research, v. 89, p. 6203-6227.

Mori, J., and Boyd, T., 1985, Seismological evidence indicating rupture along an eastward dipping fault plane for the 1964 Niigata, Japan earthquake: Journal of the Physics of the Earth, v. 33, p. 227-240.

Mori, J., McKee, C., and Letz, H., 1987, The central New Britian earthquake of May 10, 1985: tensional stresses in the frontal arc: Physics of the Earth and Planetary Interiors, v. 48, p. 73-78.

Nabelek, J., 1985, Geometry and mechanism of faulting of the 1980 El Asnam, Algeria, earthquake from inversion of teleseismic body waves and comparison with field observations: Journal of Geophysical Research, v. 90, no. B14, p. 12,713-12,728.

Nabelek, J., 1990, Rupture process of the October 18, 1989 Loma Prieta earthquake from broadband teleseismic body waves (abs.): Seismological Research Letters, v. 61, no. 1, p. 46

Nabelek, J., Chen, W-P., and Ye, H., 1987, The Tangshan earthquake sequence its implications for the evolution of the north China Basin: Journal of Geophysical Research, v. 92, no. B12, p. 12,615-12,628.

Nava, F. A., and Brune, J. N., 1983, Source mechanism and surface wave excitation for two earthquakes in northern Baja California, Mexico: Geophysical Journal of the Royal Astronomical Society of London, v. 73, p. 738-763.

Ni, J. F., and Fan, G., 1989, Fault plane solutions of earthquakes and active tectonics of the Pamir-Karakorum region (abs.): EOS Transactions, American Geophysical Union, v. 70, no. 43, p. 1226.

Niazi, M., and Kanamori, H., 1981, Source parameters of 1978 Tabas and 1979 Quaint, Iran, earthquakes from long-period surface waves, Bulletin of the Seismological Society of America, v. 71, p. 1201-1213.

Okal, E. A., 1976, A surface-wave investigation of the rupture mechanism of the Gobi-Altai (December 4, 1957) earthquake: Physics of the Earth and Planetary Interiors, v. 12, p. 319-328.

Okal, E. A., and Stewart, L. M., 1981, A negative search for an ultra-slow component to the source of the Yunnan earthquakes of May 29, 1976: Physics of the Earth and Planetary Interiors, v. 26, p. 208-216.

Pacheco, J., and Nabelek, J., 1988, Source mechanisms of three moderate California earthquakes of July 1986: Bulletin of the Seismological Society of America, v. 78, no. 6, p. 1907-1929.

Pacheco, J. F., Estabrook, C. H., Simpson, D. W., and Nabelek, J. L., 1989, Teleseismic body wave analysis of the 1988 Armenian earthquake: Geophysical Research Letters, v. 16, no. 12, p. 1425-1428.

Pacific Gas and Electric Company, 1988, Final report of the Diablo Canyon Long Term Seismic Program: U. S. Nuclear Regulatory Commission Docket Nos. 50-275 and 50-323.

Perez, O. J., and Jacob, K. H., 1980, Tectonic model and seismic potential of the eastern Gulf of Alaska and Yakataga seismic gap: Journal of Geophysical Research, v. 85, p. 7132-7150.

Person, W. J., 1984, Seismological Notes - September-October: Bulletin of the Seismological Society of America, v. 74, no. 4, p. 1503-1507.

Petrescu, G., and Purcaru, G., 1964, The mechanism and stress pattern at the focus of the September 1, 1962, Buyin-Zara (Iran) earthquake: Annales de Geophysique, v. 20, no. 3, p. 242-247.

Pezzopane, S. K., and Wesnousky, S. G., 1989, Large earthquakes and crustal deformation near Taiwan: Journal of Geophysical Research, v. 94, no. B6, p. 7250-7264.

Prescott, W. H., Savage, J. C., and Lisowski, M., 1987, Crustal strain: U.S. Geological Survey, National Earthquake Hazards Reduction Program, Summaries of Technical Reports Volume XXV, Open-File Report 88-16, p. 274-281.

Rastogi, B. K., and Talwani, P., 1980, Relocation of Koyna earthquakes: Bulletin of the Seismological Society of America, v. 70, p. 1849-1868.

Schell, M. M., and Ruff, L. J., 1989, Rupture of a seismic gap in southeastern Alaska: the 1972 Sitka earthquake (M_S 7.6): Physics of the Earth and Planetary Interiors, v. 54, p. 241-257.

Shimazaki, K., and Somerville, P., 1979, Static and dynamic parameters of the Izu-Oshima, Japan earthquake of January 14, 1978: Bulletin of the Seismological Society of America, v. 69, p. 1343-1378.

Singh, D. D., and Gupta, H. K., 1979, Source mechanism and surface-wave attenuation studies for Tibet earthquake of July 14, 1973: Bulletin of the Seismological Society of America, v. 69, p. 737-750.

Slemmons, D. B, 1977, Faults and earthquake magnitude: U.S. Army Corps of Engineers, Waterways Experimental Station, Miscellaneous Papers S-73-1, Report 6, p. 1-129.

Slemmons, D. B., 1984, Dixie Valley - Fairview Peak earthquake areas: in Lintz, J., Jr. (ed.), Western Geological Excursions Volume 4, Guidebook for Selected Nevada Earthquake Areas, p. 418-420.

Snay, R. A., Cline, M. W., and Timmerman, E. L., 1985, Dislocation models for the 1954 earthquake sequence in Nevada: in Stein, R. S., and Bucknam, R. C. (eds.), Proceedings of Workshop XXVIII on the Borah Peak, Idaho, Earthquake, Volume A, National Earthquake Prediction and Hazards Program, U. S. Geological Survey Open-File Report 85-290, p. 531-555.

Somerville, P. G., McLaren, J. P., and Helmberger, D. V., 1989, Source parameters of the Saguenay, Quebec earthquake of November 25, 1988 estimated by waveform modeling: Seismological Research Letters, v. 60, no. 1, p. 18.

Stauder, W., 1960, The Alaska earthquake of July 10, 1958: seismic studies: Bulletin of the Seismological Society of America, v. 50, no. 2, p. 293-322.

Stauder, W., and Ryall, A. R., 1967, Spatial distribution and source mechanism of microearthquakes in central Nevada: Bulletin of the Seismological Society of America, v. 57, no. 6, p. 1317-1345.

Stewart, G. S., Butler, R., and Kanamori, H., 1976, Surface and body wave analyses for the Feb. 4, 1975 Haicheng and July 27, 1976 Tangshan chinese earthquakes (abs.) EOS, v. 57, no. 11, p. 953-954.

Suarez, G., Molnar, P., and Burchfiel, B. C., 1983, Seismicity, fault plane solutions, depth of faulting, and active tectonics of the Andes of Peru, Ecuador, and southern Colombia: Journal of Geophysical Research, v. 88, p. 10,403-10,428.

Sykes, L. R., 1971, Aftershock zones of great earthquakes, seismicity gaps, and earthquake prediction for Alaska and the Aleutians: Journal of Geophysical Research, v. 76, p. 8021-8041.

Thatcher, W., and Hamilton, R. M., 1973, Aftershocks and source characteristics of the 1969 Coyote Mountain earthquake, San Jacinto fault zone, California: Bulletin of the Seismological Society of America, v. 63, no. 3, p. 647-661.

Tocher, D., 1960, The Alaska earthquake of July 10, 1958: movement on the Fairweather fault and field investigation of southern epicentral region: Bulletin of the Seismological Society of America, v. 50, no. 2, p. 267-292.

Toksoz, M. N., Arpat, E., and Saroglu, R., 1977, East Anatolian earthquake of 24 November 1976: Nature, v. 270, p. 423-425.

Toksoz, M. N., Nabelek, J., and Arpat, E., 1978, Source properties of the 1976 earthquake in east Turkey: A comparison of field data and teleseismic results: Tectonophysics, v. 49, p. 189-198.

Trifunac, M. D., and Brune, J. N., 1970, Complexity of energy release during the Imperial Valley, California, earthquake of 1940: Bulletin of the Seismological Society of America, v. 60, no. 1, p. 137-160.

Tsai, Y., and Aki, K., 1969, Simultaneous determination of the seismic moment and attentuation of seismic surface waves: Bulletin of the Seismological Society of America, v. 59, p. 275-287.

Tsai, Y., and Aki, K., 1970, Source mechanism of the Truckee, California, earthquake of September 12, 1966: Bulletin of the Seismological Society of America, v. 60, p. 1199-1208.

Turnovsky, J., and Schneider, G., 1982, The seismotectonic character of the September 3, 1978, Swabian Jura earthquake series: Tectonophysics, v. 83, p. 151-162.

Wagner, G. S., and Langston, C. A., 1988, East African earthquake body wave inversion with implications for continental structure and deformation: Geophysical Journal, v. 94, p. 503-518.

Wallace, T. C., 1988, The seismic source process of the 1952 Kern County, California, earthquake: Seismological Research Letters, v. 59, no. 1, p. 20.

Wallace, T. C., Helmberger, D. V., and Mellman, G. R., 1981a, A technique for the inversion of regional data in source parameter studies: Journal of Geophysical Research, v. 86, no. B3, p. 1679-1685.

Wallace, T. C., Helmberger, D. V., and Ebel, J. E., 1981b, A broadband study of the 13 August 1978 Santa Barbara earthquake: Bulletin of the Seismological Society of America, v. 71, p. 1701-1718.

Wallace, T. C., Ni., J. F., and Holt, W. E., 1989, A source mechanism for the 15 January 1934 Bihar-Nepal earthquake (abs.): EOS Transactions, American Geophysical Union, v. 70, no. 43, p. 1226.

Westaway, R., Gawthorpe, R., and Tozzi, M., 1989, Seismological and field observations of the 1984 Lazio-Abruzzo earthquakes: implications for the active tectonics of Italy: Geophysical Journal, v. 98, p. 489-514.

Wetmiller, R. J., Horner, R. B., Hasegawa, H. S., North, R. G., Lamontagne, M., Weichert, D. H., and Evans, S. G., 1988, An analysis of the 1985 Nahanni earthquakes: Bulletin of the Seismological Society of America, v. 78, p. 590-616.

Wetmiller, R. J., Lamontagne, M., Hasegawa, H. S., Buchbinder, G. G. R., and Horner, R. B., 1989, The March 1988 M 6.0 Nahanni earthquake and its aftershocks (abs.): Seismological Research Letters, v. 60, no. 1, p. 28.

Woodward-Clyde Consultants, 1979, Report of the evaluation of maximum earthquake and site ground motion parameters associated with the offshore zone of deformation, San Onofre Nuclear Generating Station: report prepared for Southern California Edison, Rosemead, California.

Wu, K-T., Yue, M-S., Wu, H-Y., Cao, X-L., Chen, H-T., Huang, W-Q., Tian, K-Y., and Lu, S-D., 1976, Certain characteristics of Haicheng earthquake (M = 7.3) sequence: Acta Geophysica Sinica, v. 19, no. 2, p. 95-109.

Yan, B., and Alexander, S. S., 1990, Source mechanism study of the 1982 New Brunswick, Canada, earthquake sequence using combined surface-wave methods: Bulletin of the Seismological Society of America, v. 80, no. 2, p. 296-312.

Young, C. J., Lay, T., and Lynnes, C. S., 1989, Rupture of the 4 February 1976 Guatemalan earthquake: Bulletin of the Seismological Society of America, v. 79, no. 3, p. 670-689.

Zhang, W., Jiao, D., Zhang, P., Molnar, P., Burchfiel, B. C., and Deng, Q., 1987, Displacement along the Haiyuan Fault associated with the great 1920 Haiyuan, China, earthquake: Bulletin of the Seismological Society of America, v. 77, p. 117-131.

Zhou, H. L., Allen, C. R., and Kanamori, H., 1983a, Rupture complexity of the 1970 Tonghai and 1973 Luhuo earthquakes, China, from P-wave inversion relationship to surface faulting: Bulletin of the Seismological Society of America, v. 73, p. 1585-1597.

Zhou, H., Liu, H. L., and Kanamori, H., 1983b, Source processes of large earthquakes along the Xianshuihe fault in southwestern China: Bulletin of the Seismological Society of America, v. 73, p. 537-551.

Zohoorian Izadpanah, A. A., Mohajer-Ashjai, A., Salehi Rad, M. R., Taghizadeh, Gh. A., and Kabiri, A., 1981, Damage distribution and aftershock sequence of Zarand earthquake of 19 December 1977: Journal of Earth and Space Physics , v. 10, nos. 1 & 2, p. 25-42.

QUESTION LP 6

We were informed during the January meeting that the drilling log of an oil exploration well, which is located in the vicinity of the PG&E cross section T-T', has recently become available. The information contained in this log should be incorporated into the interpretation of the nearby seismic reflection lines. What is the impact of this information upon previous interpretations?

Question LP 6 requests that we provide information from an oil exploration well in the vicinity of section T-T' on the panels for the Point Sal reach montage, submitted in Response to Question GSG 1, March 1990, and to describe the implications of this information to our interpretation of the geophysical data in the area. At the January 1990 NRC meeting to review PG&E's geophysical data interpretations, it was noted that section T-T' (line PG&E-3) apparently did not incorporate information from well 397-1 drilled by Phillips Petroleum. We responded at the meeting that data from this well are available to PG&E and they would be incorporated into the final interpretations shown on the montage.

In this response, we review the available well data, how the data were interpreted by PG&E, and the use of the data in the project. It is important to note that we have used data from well 397-1 since 1987. These data have been referenced and incorporated into previous submittals to the NRC. The problem noted in the preliminary montage panels displayed at the January 1990 meeting was the result of an error in marking and coloring profile T-T'. The error was not reflected in the adjacent profiles, the Final Report (PG&E, 1988), nor the final montage panels.

DATA AVAILABLE FROM WELL 397-1

Well 397-1 is near the eastern edge of the Hosgri fault zone approximately 15.5 kilometers northwest of Point Sal (Figure LP Q6-1). It is the only offshore well east of the main trace of the Hosgri fault zone and is within 2 kilometers of seismic reflection survey lines from Seiscom Delta (line 6), the GSI-80 survey (lines 100 and 101), the Nekton-45 survey (lines 200, 229, 231, and 235), the CGI survey (lines 19 and 484), the Western Geophysical survey (line W-84), the PG&E Deep Crustal Survey (line 3), as well as a number of high-resolution survey lines. The well is also within 3.5 kilometers of well 397-2, which lies on the west side of the Hosgri fault zone. Therefore, it is a critical well for the interpretation of seismic data from this area, and for the correlation of rock units across the Hosgri fault zone.

The available data from well 397-1 consist of a number of well logs, some of which have been released to the public through the Minerals Management Service, and others that remain proprietary. These logs are listed, along with all other offshore well data available to the project, in Table GSG Q1-A.2 of Attachment GSG Q1-A to the Response to Question GSG 1, submitted in March 1990. The available logs for this well included the mud log, E-log, sonic log, density log, natural gamma log, and the dipmeter log. These data are uninterpreted logs. They are not released with marked interpretations, nor with marked correlations between the several logs or other wells in the vicinity. Paleontological data are proprietary and were not available from these two wells.

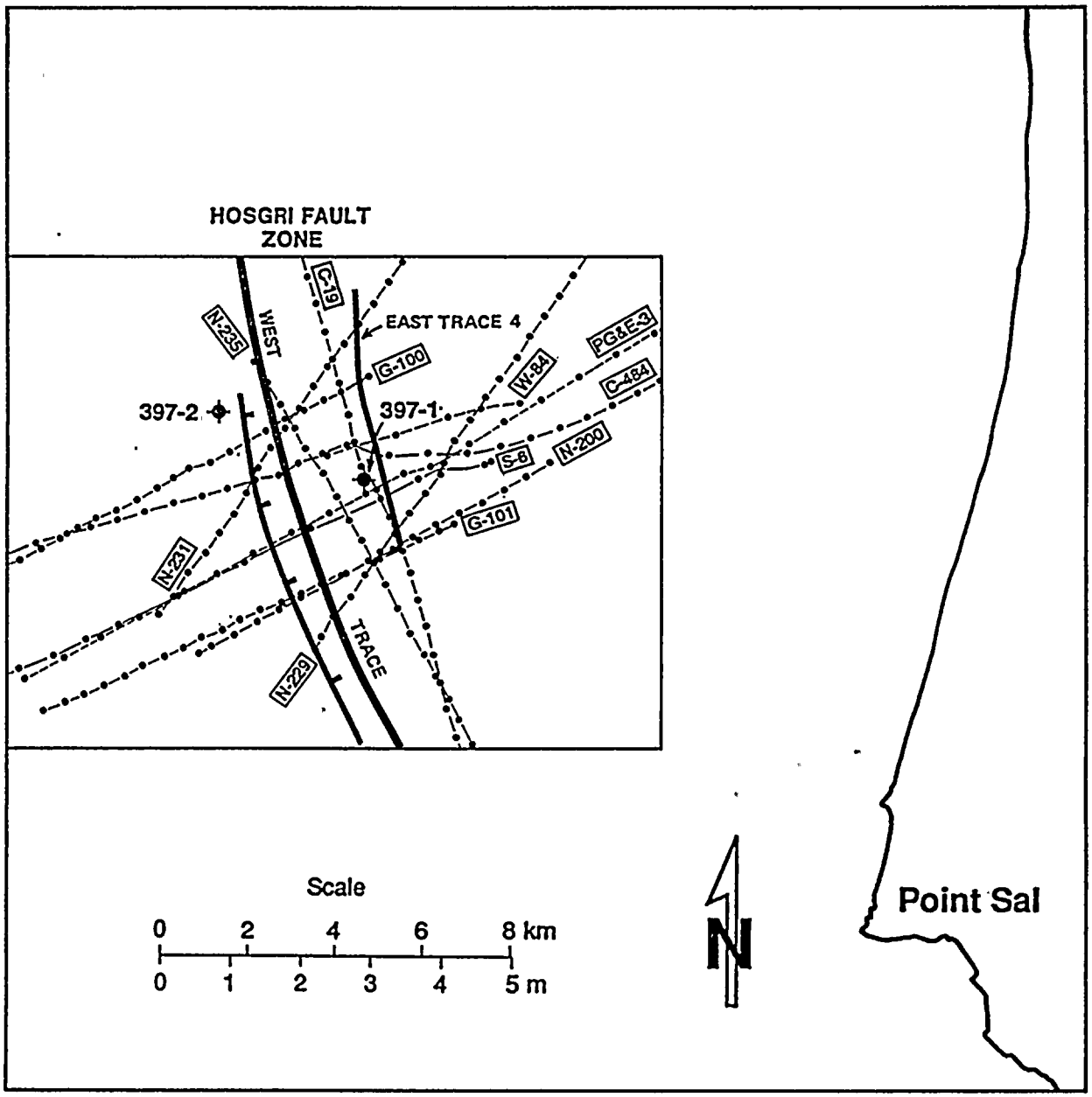

Figure LP Q6-1

Index map showing the location of Phillips offshore wells 397-1 and 397-2 with respect to nearby common-depth-point seismic reflection lines, the Hosgri fault zone traces, and Point Sal.

INTERPRETATION AND UTILIZATION OF THE WELL LOG DATA

PG&E's interpretation of the seismic reflection data from the offshore Santa Maria Basin was illustrated through a series of structural trend and structure contour maps, interpreted seismic reflection sections, and depth-converted profiles. These interpretations have been presented in a number of formats, including the Final Report (PG&E, 1988), responses to questions, and a montage. The recognition of unconformities on the seismic records has been used, in part, in the interpretation of the style and timing of the structural deformation observed in the offshore Santa Maria Basin.

Offshore well data provided the basis for the ties between the seismic reflection records and the rock units and intervening unconformities. Tables LP Q6-1, 2, and 3 provide the specific well log criteria and descriptions that were used to estimate the depths and reflection times of the three mapped unconformities in the vicinity of the Hosgri fault zone at locations of wells 397-1 and 397-2.

Data from well 397-1 have been available and used in our interpretation of the offshore geology since 1987, as documented below:

- Final Report (PG&E, 1988): The well is referenced in the Final Report and the location plotted on Plates 1 and 2 (top margin of Sheet 1 of 3), and on the interpreted and depth converted seismic sections of Seiscom Delta line 6 (Plate 7, Sheet 2).

- Data Audit: Data from well 397-1 were available for review at the November 1988 data audit and discussed in a presentation by Mr. Heck.

- Response to Questions, March 1989: Well locations were shown on the base maps for the D-Series Maps (scale 1:24,000) submitted in Response to Question Q43o. The data were used in the production of the structure contour and isotime maps produced in response to Question Q43y. This is one of the few areas where horizon contours could be extended across the Hosgri fault zone.

- Response to Questions, March 1990: The data available from well 397-1 are listed in Table GSG Q1-A.2, and were used in the interpreted sections presented on the final copies of the montage.

IMPACT ON PREVIOUS INTERPRETATIONS

Data from well 397-1 have been used throughout the program since 1987. As explained above, an error was made in one of the preliminary copies of the montage panels shown at the January 1990 meeting; it was limited to that specific illustration and did not affect previous submittals nor our interpretation of the offshore geology.

The well data were used in an integrated interpretation of the seismic reflection data. An interpreted copy of seismic line Seiscom Delta, line 6 is shown on Plate 7, Sheet 2, in the Final Report (PG&E, 1988). This line is approximately 250 meters south of well 397-1 at shot point 1305. The interpretation shows the basement contact to be at approximately 1.15 seconds, depth converted to 1050 meters. This is in good agreement with the well log, which places the basement contact at 1032 meters (Table LP Q6-2 and Figure LP Q2-1).

Table LP Q6-1

CRITERIA FOR IDENTIFYING KEY UNCONFORMABLE HORIZONS IN THE CENTRAL OFFSHORE SANTA MARIA BASIN NEAR THE HOSGRI FAULT

Base "Foxen" (late Pliocene)/Top "upper" Sisquoc (early Pliocene) Unconformity

The unconformity between the early and late Pliocene deposits is referred to as the mid-Pliocene unconformity. Well data show that the lithology changes from unconsolidated gray clay with occasional sand and dolomite of the late Pliocene "Foxen" above the unconformity, to massive diatomaceous claystone and siltstone with the common dolomite beds and occasional chert in the early Pliocene "upper" Sisquoc below the contact. Hydrocarbon shows are rare in the "Foxen" section, whereas gas shows and occasional oil shows are logged in the "upper" Sisquoc. Electric logging tools, including the dipmeter, are responsive to the lithologic changes, and normally can be used to define the contact. A seismic reflector that correlates with this unconformity can be mapped over large portions of the basin.

Base "upper" Sisquoc (early Pliocene)/Top "lower" Sisquoc (late Miocene) Unconformity

The unconformity between the early Pliocene and the late Miocene deposits is referred to as the top Miocene unconformity. The Miocene-age, "lower" Sisquoc claystone and siltstone are more consolidated than the early Pliocene "upper" Sisquoc beds. Dolomite and chert are more commonly found, as are stronger indications of hydrocarbons. Drill rates in the Miocene are significantly reduced. E-log and dipmeter characteristics are adequately reflective of the differences above and below the unconformity to define the contact.

In localities nearer the eastern source area, an increase in clastic coarseness at the base of the Pliocene "upper" Sisquoc marks the contact. However, on some prominent subsurface elevations, e.g., anticlinal folds, the early Pliocene section is missing. The contact is then formed of *late* Pliocene sediments resting on the Miocene beds. A strong seismic reflector that corresponds to this unconformity can be mapped basin-wide.

Basement (Franciscan) Unconformity

The basement is identified primarily by lithologic descriptions from drill cuttings and cores, indicating penetration of a metamorphic suite of rocks. In most wells, E-log responses also clearly define the basement contact. The contact is generally the source of a strong, relatively continuous reflector in the seismic data.

Table LP Q6-2

WELL LOG CRITERIA
Phillips P-0397 #1

Base "Foxen" (late Pliocene)/Top "upper" Sisquoc (early Pliocene) Unconformity, 328 meters.

The unconformity in this well is best defined by the lithology. The "Foxen" is a soft, sticky, gray clay with sand and silt streaks. Shell fragments and forams are common. The "upper" Sisquoc consists of clay and sandy siltstone. At the base is a sandy conglomerate. Electric log responses at the contact are unaffected or marginally affected by the transitional changes in lithology at the contact. The changes in caliper log response help define the more consolidated nature of the "upper" Sisquoc versus the "Foxen." Dipmeter quality above and below the contact is too poor to be definitive. In summary, in this well, E-log criteria do not clearly define this contact due in part to its shallow depth below the ocean floor (205 meters) and the logging depths which begin only 41 meters above the unconformity. A seismic reflector at 0.32 sec. on line Seiscom-6 (PG&E, 1988, Plate 7) is interpreted to represent this contact.

Base "upper" Sisquoc (early Pliocene)/Top "lower" Sisquoc (late Miocene) Unconformity, 429 meters.

The sandy conglomerate at the base of the "upper" Sisquoc defines the contact between these rock sequences. The "lower" Sisquoc is a gray to brown, firm siltstone with interbedded mudstone, claystone, dolomite and traces of chert. Trace visible oil shows begin at 457 meters. All the electric logging tools, including the dipmeter, recorded a change at the contact depth. A prominent seismic reflector at 0.44 second on line Seiscom Delta-6 (PG&E, 1988, Plate 7) is interpreted to represent the contact.

Basement (Franciscan) Unconformity, 1032 meters.

The basement rocks penetrated by P-0397 #1 are fractured, schistose metamorphic rocks, with asbestos fibers, talc and chlorite. Colors are varied (light- to dark-green, red, brown), luster is waxy. Some metaquartzite and chloritic clays are also described in the section. Franciscan basement was drilled from 1032 to 1118 meters (86 meters) but because of hole conditions, E-logs were run from a depth of 1062 meters, resulting in only 30 meters of logged basement section. In general the E-log responses do not clearly reflect the change from the overlying Obispo volcanic rocks to the metamorphic basement. A seismic reflector at 1.15 seconds on line Seiscom Delta-6 (PG&E, 1988, Plate 7) is interpreted to be the basement contact.

NOTES:

1. The sonic log for this well is presented as Figure LP Q2-1.

2. All depths are measured from Kelly bushing.

Table LP Q6-3

WELL LOG CRITERIA
Phillips P-0397 #2

Base "Foxen" (late Pliocene)/Top "upper" Sisquoc (early Pliocene) Unconformity, 750 meters.

The "Foxen" is a soft, sticky, gray clay with abundant shell fragments and microfossils. The "Upper" Sisquoc is a gray, diatomaceous and silty claystone with traces of dolomite. Background gas shows in the "upper" Sisquoc increase by a factor of approximately 10 over the "Foxen" interval. The gamma ray, density, resistivity, caliper, sonic and dipmeter logs all have changes of character that mark the contact in this well.

Base "upper" Sisquoc (early Pliocene)/Top "lower" Sisquoc (late Miocene) Unconformity, 963 meters.

Approximately 18 meters above the contact (945 meters), the diatomaceous claystone of the "upper" Sisquoc begins to drop out. Below the contact, the "lower" Sisquoc is a gray, firm to occasionally soft, silty claystone with chert and dolomite streaks. Gas shows are increased compared to the "upper" Sisquoc. First trace oil shows begin at 1250 meters and persist to base "lower" Sisquoc. The entire log suite, including the dipmeter, changes character below the contact. The drill rate is reduced below the contact from 60 to 90 meters/hour to approximately 30 meters/hour.

Basement (Franciscan) Unconformity, 2423 meters.

Lithology is described as schistose metamorphics with abundant chlorite, varied colors, waxy textures and calcite veins. The gamma ray response is reduced; the bulk density, neutron and photoelectric curves change character at the contact; however, the dipmeter is poor quality and the contact is not distinguishable on this record, because the dipmeter in the overlying section is also a poor quality log record.

NOTES:

1. The sonic log for this well is presented as Figure LP Q2-2.

2. All depths are measured from Kelly bushing.

The Top of "Basement" structure contour map, Plate Q43y-3 in the Response to Question 43y, also shows basement (on GSI-100 at shot point 480) at a shallow depth (1.10 seconds) in this area.

The final versions of the montage panels from line PG&E-3 (profile T-T′ on the San Luis Obispo Bay and Point Sal reaches) show the basement to be at 1.08 seconds, or approximately 1080 meters in the vicinity of shot point 370. Again, the interpretation of shallow basement is in agreement with the well data.

The data from well 397-1 regarding depth-to-basement have been incorporated into previous submittals and the latest interpretation. The relative depths and reflector times on the seismic records are in good agreement with the well data and with each other, and further substantiate the velocity model (Response to Question LP 2).

REFERENCES

Pacific Gas and Electric Company, 1988, Final report of the Diablo Canyon Long Term Seismic Program: U. S. Nuclear Regulatory Commission, Docket Nos. 50-275 and 50-323.

QUESTION LP 7

We have seen on various maps, cross sections, and montages, that to the east of the Hosgri fault zone compressional features such as the Los Osos fault, the Pecho fault, and the Casmalia fault have strikes which make angles of about 40 to 60 degrees with the strike of the Hosgri, indicating a northeast-southwest horizontal compression. West of the Hosgri the major compressional features (folds and thrust faults) have strikes that are parallel to the strike of the Hosgri, indicating an almost east-west horizontal compression. The focal mechanisms you presented for earthquakes in these two areas seem to be in agreement with this assessment. How do you explain these apparent differences in stress orientation over a relatively small region and what implications does it have for the source characteristics of Hosgri earthquakes?

Question LP 7 makes the observation that there is a change in the trend of regional compressive structures across the Hosgri fault zone. The question then requests an explanation of "...these apparent differences in stress orientation over a relatively small region...". In doing so, the question appears to assume that stress and strain are coaxial in south-central coastal California. As described in this response, this assumption may not be valid. South-central coastal California is underlain by highly deformed Franciscan Complex basement, and the preexisting structural fabric probably causes the stress and strain axes to diverge during progressive deformation.

Structural interpretations of offshore seismic reflection data (Response to Question GSG 1, March 1990) and onshore geologic mapping (Response to Question 43, March 1989; PG&E, 1988; Hall, 1973a, Hall, 1973b) indicate there is an abrupt change in the trend of late Cenozoic folds and reverse/thrust faults across the Hosgri fault zone (Figure LP Q7-1). East of the Hosgri fault zone, faults and folds within the Los Osos/Santa Maria domain trend oblique to the fault trace. West of the fault zone, within the southern offshore Santa Maria Basin, compressive structures trend approximately parallel to the fault zone.

The differing structural trends east and west of the Hosgri fault zone appear inconsistent for two reasons. First, the abrupt change in strike of folds and reverse/thrust faults across the relatively narrow Hosgri fault zone may suggest that the regional maximum horizontal stress direction also undergoes an abrupt change across the fault. This contradicts the concept that regional stress trajectories represent a continuous force field when at equilibrium, and do not change trend abruptly. Second, the structural trends on either side of the fault zone imply conflicting theories regarding the mechanical nature of strike-slip fault zones: the oblique, en echelon trend of compressive structures within the Los Osos/Santa Maria domain suggest a "wrench" style of deformation along a high-shear-strength strike-slip fault (Wilcox and others, 1973); whereas the fault-parallel trend of compressive structures within the offshore Santa Maria basin domain suggest a "strain partitioning" style of deformation along a low-shear-strength strike-slip fault (Zoback and others, 1987; Response to Question GSG 2; Lettis and Hanson, in review).

We resolve the apparent inconsistency in the observed structural trends and conflicting concepts of deformation style within strike-slip fault zones by interpreting that the Hosgri fault zone may be a low-shear-strength fault, with the regional maximum horizontal stress oriented at a high angle to the fault trace. We explain the oblique structural trends of the Los Osos/Santa Maria domain as the result of three processes: (1) non-coaxial stress and strain caused by preexisting structures within the Franciscan Complex basement; (2) local distortion of the regional stress field by increasingly elastic strains near the southern tip of the Hosgri fault zone; and (3) late Cenozoic clockwise rotation of the western Transverse

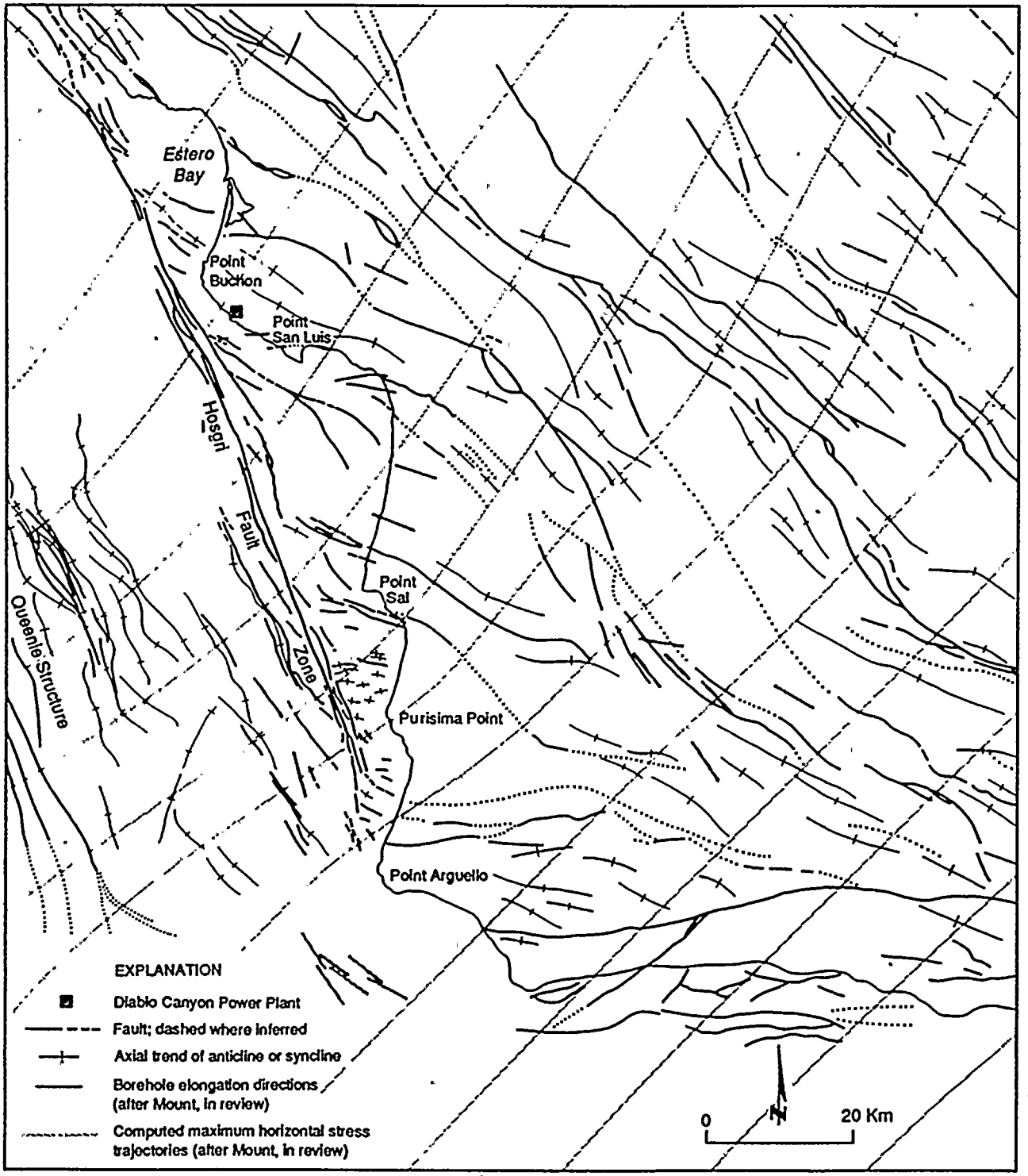

Figure LP Q7-1

Borehole breakout azimuths, structural trends, and predicted maximum horizontal stress trajectories in west-central California (predicted stress trajectories from Mount, in review).

Ranges causing northeast-southwest-directed compression of the Los Osos/Santa Maria domain.

Question LP 7 requests that we address the implications that the change in structural trends have on the source characteristics of the Hosgri fault zone. In this response, we show that our interpretations of the source characteristics of the Hosgri fault zone and the sense of slip in the fault zone are in agreement with these structural trends. Figure LP Q7-1 shows the interpreted stress trajectories assessed by Mount (in review). The stress trajectories for the maximum horizontal compressive stress are oriented at high angles to the main trace of the Hosgri fault zone, and slightly oblique to the structural trends on either side of the fault zone. It should be noted that there is little control for these trajectories west of the Hosgri fault zone. The stress trajectories shown in Figure LP Q7-1 are computed from borehole breakouts, and data from only three wells in the offshore Santa Maria Basin have been included. These, however are consistent with each other and with the earthquake focal mechanisms for the three events referred to in the question.

In addressing the orientation of crustal stresses in south-central coastal California and the relationship between strain and stress across the Hosgri fault zone, it is important to note that this is a topic of extensive ongoing research and multiple working hypotheses. The relationship of stress and strain across the Hosgri fault zone is not well documented. There is an observed pattern of contrasting crustal strain on either side of the Hosgri fault zone, but only a limited data set to constrain the pattern of stress in the region. In this response, we briefly outline the concepts of wrench tectonics and strain partitioning along strike-slip fault zones, give evidence demonstrating that the latter concept best fits observations of the Hosgri fault zone, and show how the ideal geometry of this "weak fault" concept has been altered by influence from the three tectonic factors listed above. These interpretations are consistent with our previous characterization of the Hosgri fault zone as a right-slip fault (PG&E, 1988; Response to Questions GSG 3, GSG 4, and SSC 2, March 1990).

TECTONIC MODELS

Wrench Tectonics

Sylvester (1988) suggests abandoning the term "wrench" in favor of the term "strike-slip." Sylvester (1988) argues that the term has been used to describe "... any and all strike-slip faults whether or not they are regional, vertical, or involve ... basement," contrary to the originally intended usage described by Moody and Hill (1956). We employ the term "wrench" here, not because of disagreement with Sylvester (1988), but rather for clarity when comparing contrasting concepts regarding the mechanics of strike-slip faults, and because our usage complies with that for which it was originally intended.

The concept of wrench tectonics in theory, experiment, and nature is outlined by Wilcox and others (1973). These authors show a strong correlation between stress and brittle failure as dictated by the Mohr-Coulomb theory of failure, results from clay-model experiments simulating strike-slip deformation, and natural examples of strike-slip fault zones around the world. Anderson's (1951) application of Mohr-Coulomb theory to geologic structures shows that strike-slip faults develop in stress fields where the maximum and minimum principal stresses are horizontal, and the intermediate principal stress is vertical. In this regional stress regime and within a homogeneous medium, strike-slip faults will be oriented at approximately 30 to 40 degrees to the maximum principal stress direction (Figure LP Q7-2).

Results from experimental modeling of basement-controlled, strike-slip faults by Tchalenko (1970), Wilcox and others (1973), and Naylor and others (1986) agree well with the theoretical predictions. In

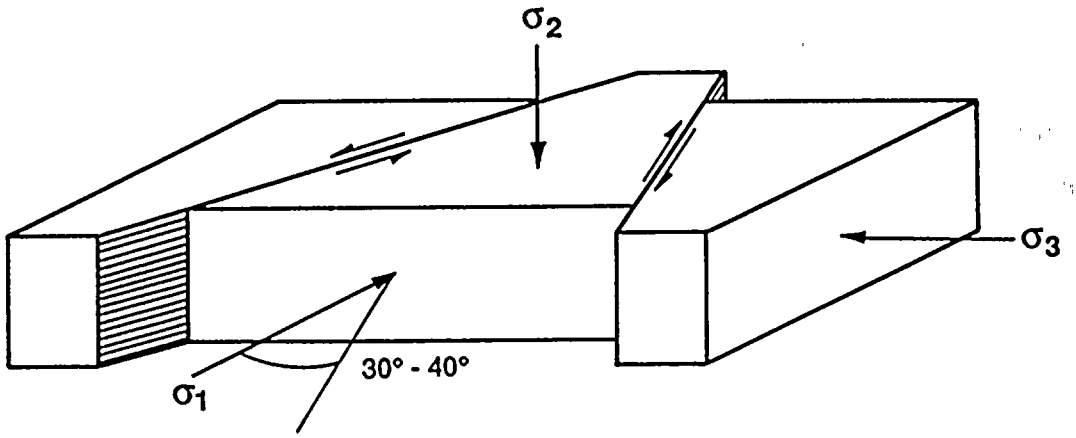

Figure LP Q7-2

Orientation of the principal stress axes during the development of a near-surface strike-slip fault (Anderson, 1951).

these experiments, a continuous layer of homogeneous, natural geologic material (sand or clay) representing sedimentary cover is placed over a pair of boards or plates representing basement and the two plates are moved parallel to each other, producing a shear couple in the overlying cover. During the initial stages of wrench deformation, en echelon, conjugate Reidel shears form at approximately 15 and 75 degrees to the wrench zone. With increasing shear strain on the basement fault, the antithetic R′ shears are suppressed, whereas the synthetic R shears increase in length and interconnect, eventually forming a throughgoing fault. Wilcox and others (1973) show that during the early stages of deformation, en echelon folds are formed at approximately 45 degrees to the wrench zone when the cover material responds ductilely and is able to detach from the underlying basement. The repeated occurrence of these and other secondary structures, such as P and X shears, with consistent geometric relationships to the main throughgoing fault suggest a simple two-dimensional model relating the trends of these structures to the maximum principal stress direction (Figure LP Q7-3).

Observations in wrench zones around the world (Wilcox and others, 1973; Harding, 1974; Naylor and others, 1986) indicate that the geometric relationships between the main fault trace and associated minor structures often agree well with the experimental data and therefore also with the simple shear model shown in Figure LP Q7-3. The wrench tectonic model was applied to the San Andreas fault in the mid-1970s and early 1980s by Harding (1976) and Zoback and Zoback (1980). This model suggests that the San Andreas fault formed in a high-drag environment associated with a strong, mechanically coupled fault where deformation occurs by distributed simple shear (Figure LP Q7-4a). Accordingly, they interpreted that the orientation of the maximum principal stress was 30 to 40 degrees to the fault, approximately north-south for the right-lateral San Andreas fault.

Strain Partitioning

Recent measurements of tectonic stress in central California, assessed from borehole breakout azimuths, earthquake focal mechanisms, and borehole hydraulic fracture, indicate that the maximum principal stress direction is oriented approximately northeast-southwest, nearly perpendicular to the San Andreas fault (Zoback and others, 1987; Mount and Suppe, 1987; Mount, in review). This stress orientation contrasts with the north-south orientation of maximum horizontal stress predicted by the wrench model of strike-slip deformation described above. These data are in close agreement with geologic data from detailed mapping and cross-section construction, and with geophysical data from seismic reflection profiles and earthquake focal mechanisms from within 50 to 100 kilometers of the central San Andreas fault that indicate contemporary fault-normal convergence (Mount and Suppe, 1987; Medwedeff, 1989; Namson and Davis, 1988; Stein, 1983). Preliminary concepts to explain the development of subparallel strike-slip, fold, and thrust-style structures within the same stress regime have been developed by several authors (Zoback and others, 1987; Mount and Suppe, 1987; Response to Question GSG 2, March 1990; Mount, in review) (Figure LP Q7-4b).

According to Zoback and others (1987) and Mount and Suppe (1987), the fault-normal orientation of the maximum principal stress direction in central California is caused by a "weak" San Andreas fault. As shown in Figure LP Q7-1, the stress trajectories of Mount (in review) are oriented more fault-normal within an approximately 70- to 90-kilometer-wide corridor centered on the San Andreas fault zone. The "weak" fault behaves as a free surface that is unable to support significant shear stress, and one of the principal stress axes must be oriented approximately normal to the fault in order to minimize the resolved shear stress on that surface. The weak nature of the San Andreas fault is supported by down-hole measurements of low heat-flow in the vicinity of the fault and by the very low shear stresses parallel to the fault measured from down-hole hydraulic fracturing experiments conducted near Cajon Pass (Zoback

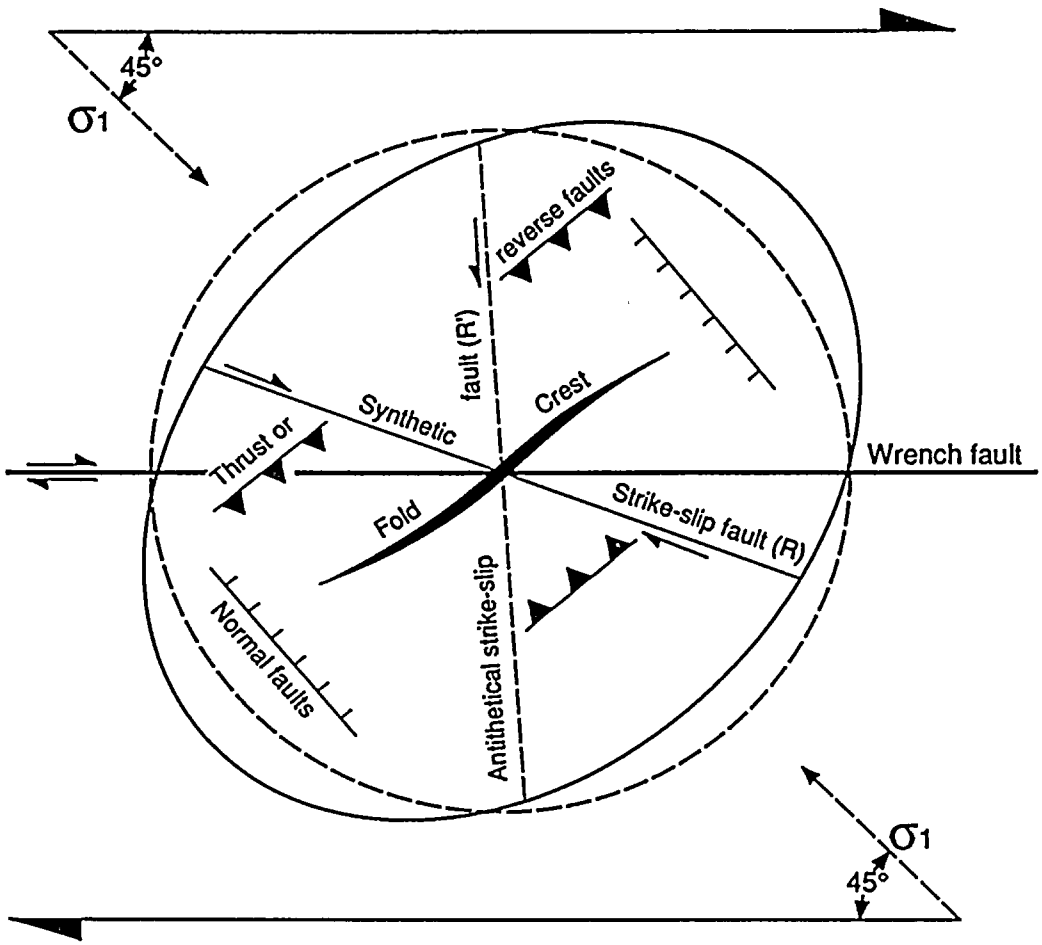

Figure LP Q7-3

Simple shear model showing the map-view relationships among secondary structures, the thoroughgoing main fault trace, and maximum principal stress direction in a right-lateral wrench zone (after Sylvester, 1988).

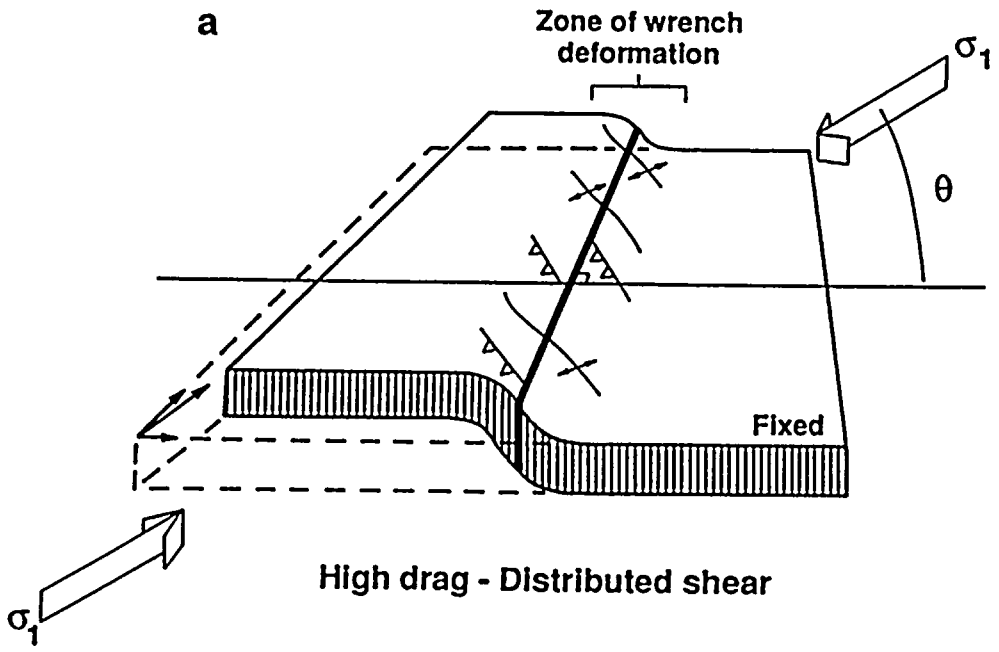

Figure LP Q7-4

(a) Deformation style predicted by the distributed shear, high-drag concepts of wrench tectonics, theta approximately 45 degrees. (b) Deformation style predicted for a decoupled, low shear strength strike-slip fault, theta at a high angle to the main fault (Mount and Suppe, 1987).

and others, 1987). Heat flow measurements taken in the vicinity of the central San Andreas fault do not indicate a positive anomaly, as would be expected from frictional faulting (Lachenbruch and Sass, 1980), implying very low shear stresses, on the order of 100 to 200 bars, for the fault surface (Brune and others, 1969).

We interpret the Hosgri fault zone to be a fundamentally weak fault, similar to the San Andreas fault. This hypothesis is supported by two lines of evidence: (1) the stress trajectory map for west-central California produced by Mount (in review) indicates that the maximum horizontal compressive stress is oriented at a high angle to the Hosgri fault zone (Figure LP Q7-1), producing a low magnitude of resolved shear stress parallel to the fault; and (2) compressive structures and nodal planes of compressive earthquake focal mechanisms in the offshore Santa Maria Basin trend parallel to the Hosgri fault zone, suggesting that the maximum horizontal stress is normal to the Hosgri fault zone (PG&E, 1988; Response to Question GSG 2).

Finite strains east of the Hosgri fault zone appear inconsistent with deformation around a weak fault, primarily due to the influence three tectonic factors: (1) preexisting structural fabric in the Franciscan Complex basement near the southern tip of the Hosgri fault; (2) elastic strains; and (3) compression of the southern Los Osos/Santa Maria domain zone by clockwise rotation of the western Transverse Ranges.

RELATION BETWEEN STRESS AND STRAIN NEAR THE HOSGRI FAULT ZONE

Noncoaxial Deformation

The assumption that stress and strain are coaxial is valid when it can be shown that the deforming rocks approximate the ideal rheological models employed in theoretical studies of rock deformation (Ramsay, 1967; Jaeger and Cook, 1979). These simple models assume that the deforming materials are homogeneous (all parts have the same composition) and isotropic (properties are the same in all directions).

Coaxial stress and strain, however, cannot be assumed for south-central California, where the basement is composed largely of the Franciscan Complex. Well-documented, widespread lithologic changes, regionally consistent pervasive shear fabric, and late Mesozoic to early Cenozoic thrust faults impart a strongly heterogeneous and anisotropic character to the Franciscan Complex (Hsu, 1969; Hall, 1973a, 1973b; Page, 1981). Structural trends related to these material properties are oriented approximately northwest-southeast in the Los Osos/Santa Maria domain, and approximately north-south in the offshore Santa Maria Basin (PG&E, 1988; Response to Question GSG 1; McCulloch, 1987). Preexisting structures in the Franciscan Complex basement can cause noncoaxial stress and strain by two mechanisms. First, preexisting faults and planes of weakness can be reactivated under compression when these planes are not oriented parallel to the planes of maximum shear stress with respect to the direction of maximum principal stress as predicted by Mohr-Coulomb theory of failure, resulting in noncoaxial deformation. Second, the presence of an anisotropy introduces an elastic symmetry to the deforming body, and when the axis of elastic symmetry is not parallel to the principal stress direction, the resulting deformation will be noncoaxial.

When considering the effects of elastic symmetry in the Franciscan Complex basement, one can ignore the heterogeneities produced by tabular or lenticular exotic lithologic inclusions. This is because the inclusions are elongate parallel to the dominant shear fabric (anisotropy), and are generally limited in length to tens of kilometers or less (Hall, 1973a, 1973b), whereas the anisotropy is pervasive over

hundreds of square kilometers. The effects of the anisotropy will therefore dominate the rheological response of the Franciscan Complex to regional differential stress.

Noncoaxial behavior resulting from the asymmetric orientation of an anisotropy in a linearly elastic material under compression is shown in Figure LP Q7-5. In anisotropic materials, each principal stress direction has its own associated modulus of elasticity, and therefore also its own stress/strain ratio (Jaeger and Cook, 1979). The symmetry to the angular change in the elastic modulus defines the elastic symmetry of the material. When the axes of elastic symmetry are parallel to the axes of principal stress, the resulting deformation is coaxial (Figure LP Q7-5a). When the axes of elastic symmetry are oblique to the axes of principal stress, the resulting deformation is noncoaxial (Figure LP Q7-5b). Note that in Figure LP Q7-5b) the principal strain axes rotate away from the principal stress axes and towards the axes of elastic symmetry. The noncoaxial behavior shown in Figure Q7-5b) is analogous to late Cenozoic deformation on either side of the Hosgri fault zone. The fabric anisotropy in the Franciscan Complex is oblique to the maximum horizontal stress in both the Los Osos/Santa Maria domain and in the offshore Santa Maria Basin. As a result, the strain axes are rotated clockwise in the offshore Santa Maria Basin and counterclockwise in the Los Osos/Santa Maria domain, away from the principal stress trajectories computed by Mount (in review) and towards the axes of elastic symmetry defined by the structural grain in the Franciscan complex basement (Figure LP Q7-1).

Similar effects are caused by the reactivation of preexisting planes of weakness in the Franciscan Complex basement. Experimental deformation of rocks containing preexisting planes of weakness (fractures, cleavages) indicates that these planes may be reactivated as faults when they are oblique to the planes of maximum shear stress predicted by Mohr-Coulomb theory of failure (see, for example, Donath, 1961). This effect is shown schematically by the simple Mohr-circle diagram in Figure LP Q7-6. The envelope of failure defined by the cohesive strength of intact rock is given by the line labelled "intact rock", and the angle of shear failure with respect to the maximum principal stress direction in intact rock is given by the angle theta, defined by the intersection of the Mohr circle with the envelope of failure. The envelope of failure for weak rock (faults, planes of weakness, and so forth) intersects the Mohr circle at two points. The reactivated planes of weakness can therefore theoretically be oriented anywhere between the angles theta′ and theta″ with respect to the maximum principal stress direction. This explains how preexisting faults and planes of weakness in Franciscan basement can be oblique to the maximum horizontal stress direction shown in Figure LP Q7-1. An example of fault reactivation beneath the Queenie fold in the offshore Santa Maria Basin is described by Clark and others (in press). These authors conclude that the Queenie fold developed by late Cenozoic inversion of an underlying normal fault in Franciscan Complex basement.

Distortion of the Regional Stress Field by Elastic Strain

Elastic strains associated with the southern tip of the Hosgri fault zone influence the orientation of the stress field on a local scale. The build-up of elastic strain at the end of a fault is a necessary consequence of decreasing slip on the fault surface toward the fault tip. A simple theoretical model of this effect is given by Anderson (1951). In this model, he uses Griffith failure criterion and Mohr-Coulomb theory of brittle failure to model the values and orientations of principal stresses along a fault of finite length after displacement has taken place. According to his model, stresses are relieved in the central portion of the fault, but are increased towards the tips of the fault in the form of elastic strain energy, causing the maximum and minimum horizontal stress axes to rotate to become approximately parallel and normal to the fault plane. An illustration of this effect is shown in Figure LP Q7-7a.

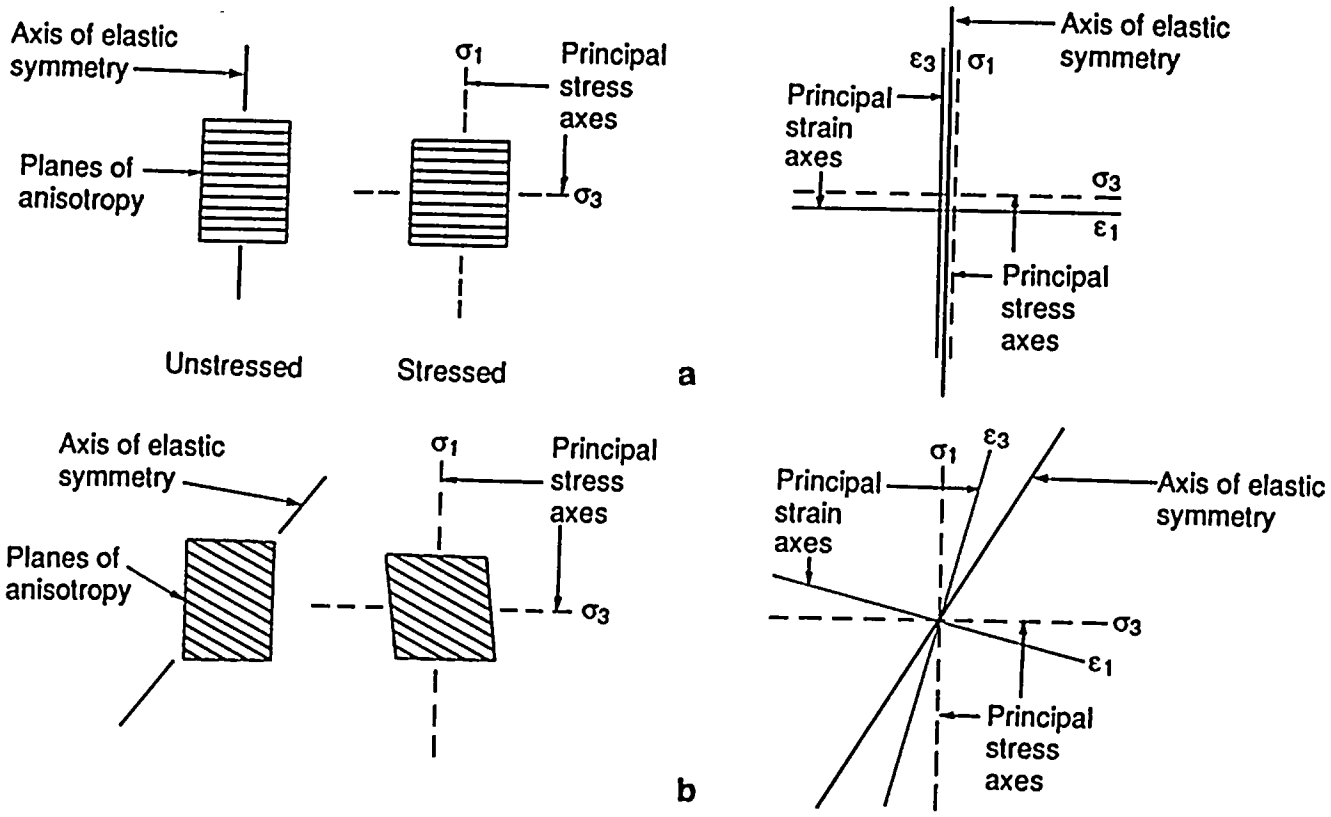

Figure LP Q7-5

Relation of principal axes of stress and strain and axes of elastic symmetry in an anisotropic, linearly elastic material under compression. Actual angle between stress and strain axes after deformation depends upon the compliances and stiffness of the material (Means, 1976).

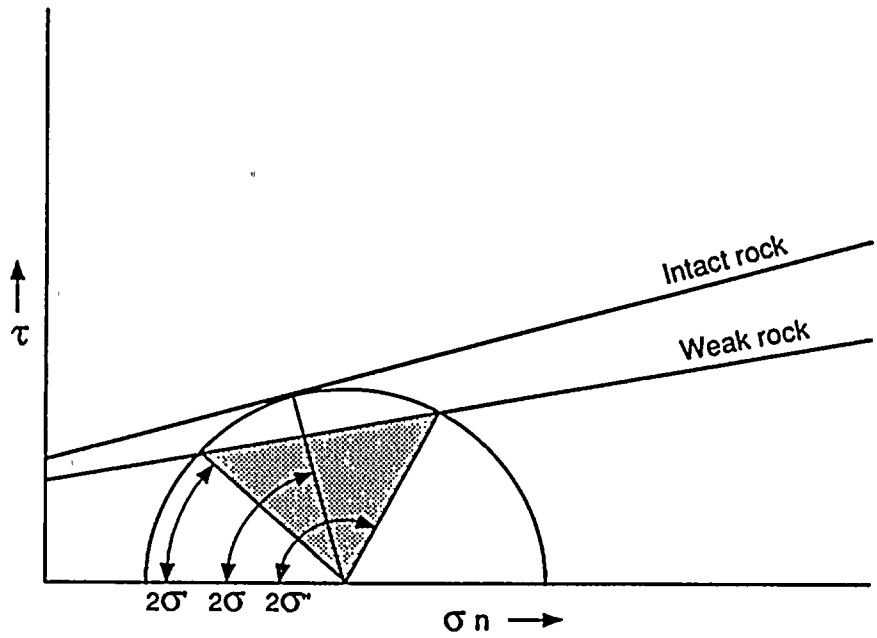

Figure LP Q7-6

Mohr diagram illustrating the orientation range (shaded region) over which reactivation takes place in preference to nucleation of a new shear fracture in the surrounding intact rock (after Etheridge, 1986).

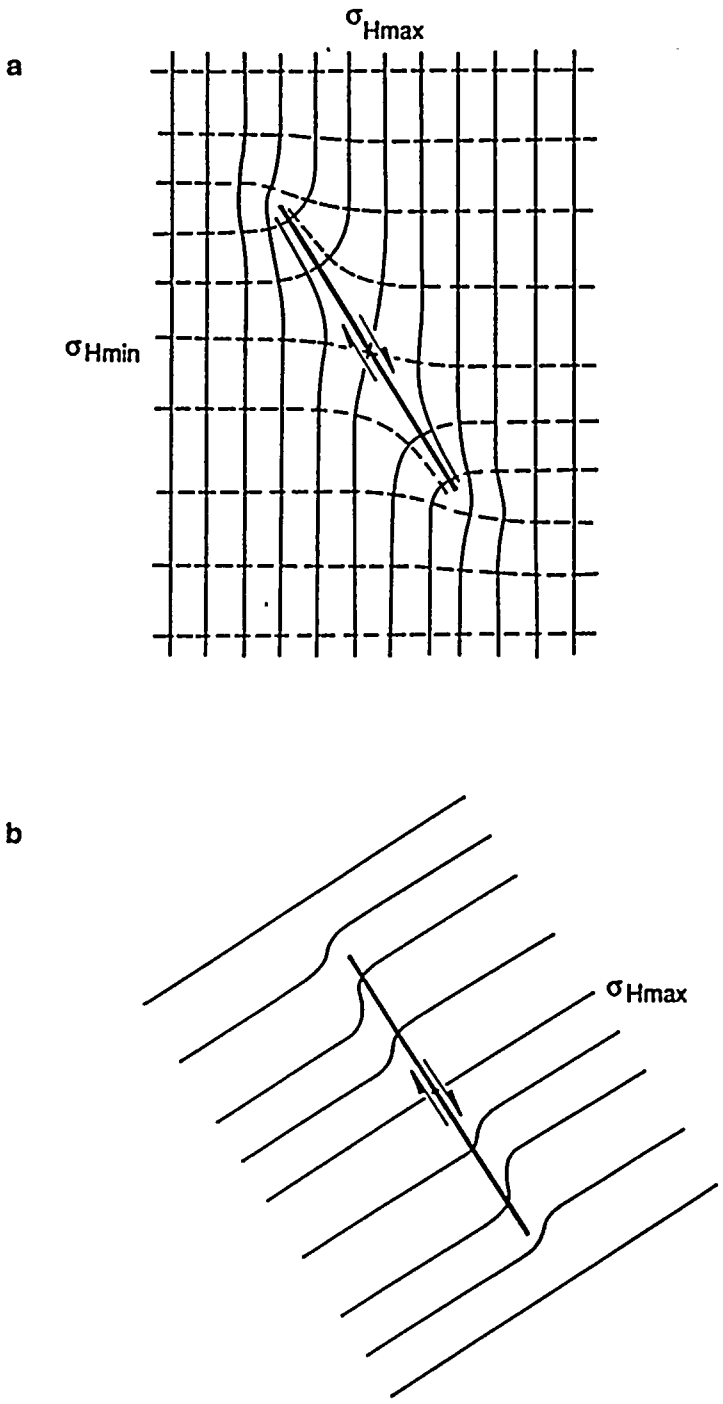

Figure LP Q7-7

(a) Predicted maximum and minimum stress trajectories around a wrench-style fault after an increment of slip at the center of the fault (after Anderson, 1951). (b) Schematic illustration of possible maximum horizontal stress trajectories around a weak fault after an increment of slip at the center of the fault. Stress trajectories are deformed near the fault tip by an increase in elastic strain.

Anderson (1951) modeled a Coulomb fracture in an ideal isotropic and homogeneous medium, thus implying the mechanical behavior of a wrench-style fault system. The concept could also apply to the Hosgri fault zone, even though the Hosgri fault zone may behave as a weak fault, because the relationship between lateral slip along the fault and the build-up of elastic strain near the fault tip remains unchanged. Strike-slip displacement produced by a single event at the center of the fault generally decreases toward the fault tip, as indicated by the geometry of the fault system resulting from repeated slip events over time. The decrease in slip is accommodated by an increase in elastic strain energy in the rock adjacent to the unslipped region of the fault. Because elastic strain by definition produces unrelieved stress in the form of potential energy, the ambient stress field deforms to accommodate the new stress regime at equilibrium. This effect is shown schematically for a weak fault in Figure LP Q7-7b.

Structural Interaction Between the Western Transverse Ranges, the Los Osos/Santa Maria Domain, and the Hosgri Fault Zone

Post-Miocene clockwise rotation of the western Transverse Ranges has also influenced the trend of compressive structures in the Los Osos/Santa Maria domain. Paleomagnetic data presented by Luyendyk and others (1980), and Hornafius (1985) indicate that this east/west-trending range has rotated approximately 90 degrees since early Miocene time. Data presented by these authors suggest two distinct periods of rotation separated by a hiatus of approximately 2 million years. The first phase began just prior to the middle Miocene and produced 50 to 60 degrees of rotation before the late Miocene, and the second phase produced 30 to 40 degrees of rotation between the late Miocene and the Quaternary.

Luyendyk and others (1980) present a kinematic model to explain these rotations in the context of the North American/Pacific plate transform boundary. The model consists of one set of nonrotating blocks parallel to the plate boundary separated by right-slip faults, and a second set of rotating blocks at a high angle to the plate boundary (Figure LP Q7-8a). Right-lateral simple shear along the boundary-parallel faults produces clockwise rotation of the transverse blocks (Figure LP Q7-8b). During rotation, gaps or areas of block overlap are created between the transverse faults and the boundary-parallel faults depending upon the location of the hinges connecting the two sets of blocks (Luyendyk and Hornafius, 1987).

Hornafius (1985) uses this model of right-lateral shear and rotation of the western Transverse Ranges to explain the development of northwest-southeast extensional basins in the Los Osos/Santa Maria domain during the first phase of rotation, followed by northeast-southwest compression of the basin during the second, current phase of rotation. Extensional basin formation is accomplished by assuming that the domain is divided into rigid, linear north-northwest-trending block elements separated by evenly spaced right-slip faults. Hornafius (1985) models the development of both fault-normal and fault-parallel basins during the middle to late Miocene clockwise rotation about a pole near the southern (present-day western) end of the western Transverse Ranges (Figure LP Q7-9a).

Compression of the domain is accomplished by a change in location of the pole of rotation to the eastern end of the western Transverse Ranges. The change in pole location produces a pattern of compressive structures that fan outward from the pole of rotation (Figure LP Q7-9b). Folds and thrust/reverse faults in the domain form nearly perpendicular to the Hosgri fault zone near the southern tip off Point Arguello, and form at progressively lower angles to the Hosgri fault zone northward to the Northern reach of the fault zone off Point Estero. In agreement with the weak fault concept for the Hosgri fault zone, Hornafius' (1985) model considers the Hosgri fault zone to be a vertical detachment between the Los Osos/Santa Maria domain and the offshore Santa Maria Basin, whereby deformation east of the fault zone due, in part, to rotation of the western Transverse Ranges occurs independently from deformation west

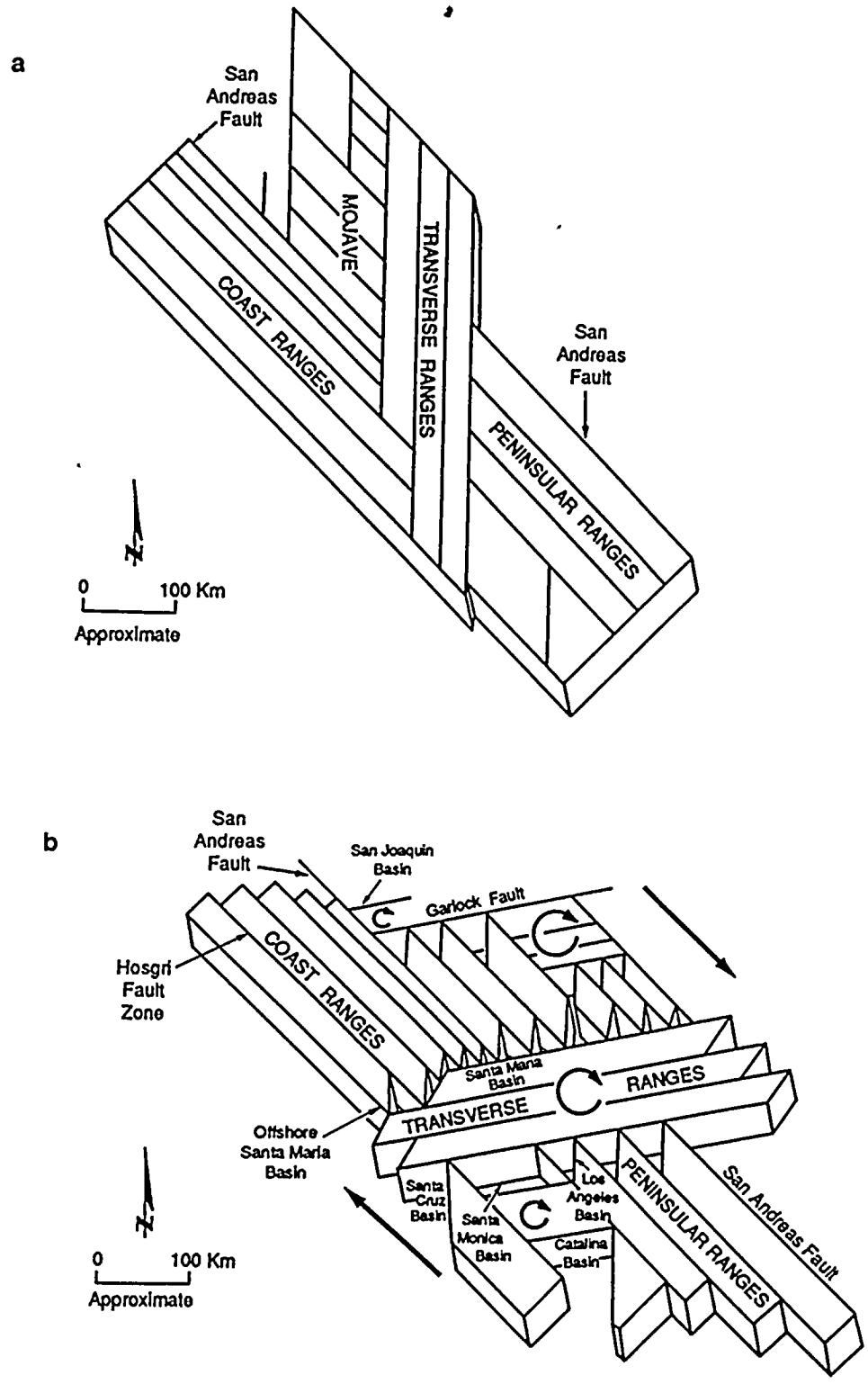

Figure LP Q7-8

Right-lateral shear block rotation model for central coastal California, according to Luyendyk and others (1980).

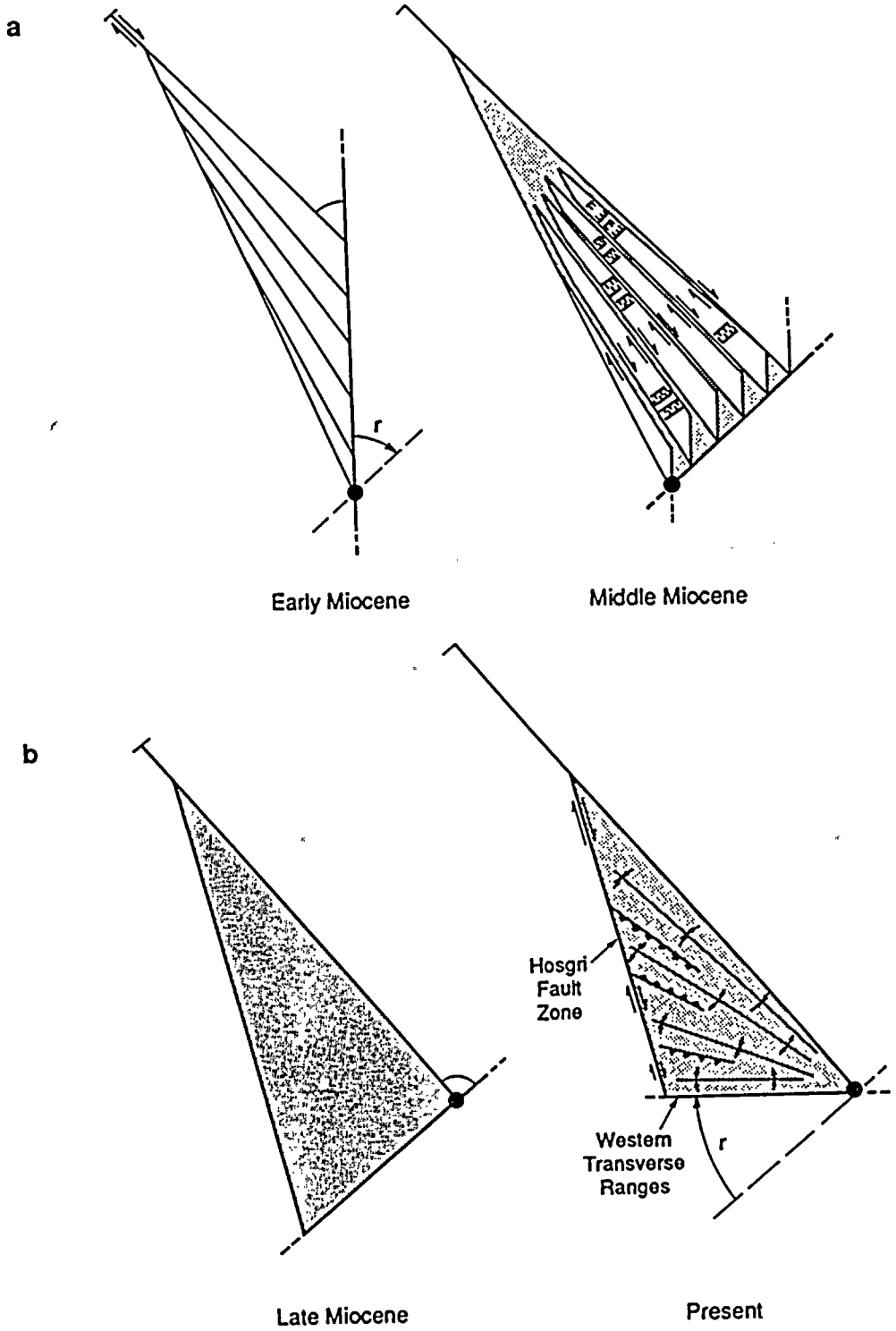

Figure LP Q7-9

Basin development and compression of the Los Osos/Santa Maria domain due to clockwise rotation of the western Transverse Ranges, according to Hornafius (1985).

of the fault zone. Decrease in slip on the Hosgri fault toward the south is accommodated by the development of compressive structures in the Los Osos/ Santa Maria domain, in agreement with the concept of an increase in elastic strain near the southern tip of the Hosgri fault zone as mentioned above.

CONCLUSIONS

The abrupt change in trend of folds and reverse/thrust faults across the Hosgri fault zone could be interpreted to be the result of a change in the direction of the maximum horizontal stress across a very narrow corridor. Trends east of the fault zone suggest a northeast/southwest-directed maximum principal stress direction, consistent with a wrench fault model for strike-slip deformation, and trends west of the fault zone suggest an east/west-directed maximum principal stress direction, consistent with the concept of strain-partitioning-style deformation in the Hosgri fault zone.

This apparent contradiction is resolved if the Hosgri fault zone is a weak, vertical, strike-slip fault and the relationship between stress and strain in the vicinity of the fault is ascribed to strain partitioning with some minor modification. This is supported by: (1) the stress trajectory map of Mount (in review) showing that the maximum horizontal compressive stress is oriented at a high angle to the main fault trace; (2) the fault-normal trend of compressive structures and earthquake focal mechanisms west of the Hosgri fault zone. The concept of strain partitioning predicts the development of subparallel strike-slip and reverse/thrust faults and folds. We observe this pattern of deformation between the Hosgri fault zone and the offshore Santa Maria Basin. East of the Hosgri fault zone, however, compressive structures in the Los Osos/Santa Maria domain trend obliquely to the Hosgri fault zone. This deviation from the concept of strain partitioning is explained by the influence of three tectonic mechanisms: noncoaxial stress and strain due to the influence of preexisting basement structures; local deformation of the regional stress field by elastic strain at the southern tip of the Hosgri fault zone; and post-Miocene clockwise rotation of the western Transverse Ranges.

The abrupt change in structural trends across the Hosgri fault zone, and the concept of strain partitioning produced by a weak Hosgri fault zone are consistent with our previous interpretations of the structural style, sense of slip, and neotectonic setting of the Hosgri fault zone. Therefore, the concepts and observations provided in this response are consistent with our interpretation of the seismic source characteristics of the Hosgri fault zone.

REFERENCES

Anderson, E. M., 1951, The dynamics of faulting: Oliver and Boyd, Ltd., Edinborough, Scotland.

Brune, J. N., Henyey, T. L., and Roy, R. F., 1969, Heat flow, stress, and rate of slip along the San Andreas fault, California: Journal of Geophysical Research, v. 74, p. 3821-3827.

Clark, D. H., Hall, N. T., Hamilton, D. H., and Heck, R. G., in press, Structural analysis of late Neogene deformation in the central offshore Santa Maria Basin, California: Journal of Geophysical Research, Paper 90JB00922.

Donath, F. A., 1961, Experimental study of shear failure in anisotropic rocks: Geological Society of America Bulletin, v. 72, p. 985.

Etheridge, M. A., 1986, On the reactivation of extensional fault systems: Philosophical Transactions of the Royal Society of London, v. A317, P. 179-194.

Hall, C. A., Jr., 1973a, Geology of the Arroyo Grande Quadrangle, California: California Division of Mines and Geology, Map Sheet 24, scale 1:24,000.

Hall, C. A., Jr., 1973b, Geologic map of the Morro Bay South and Port San Luis quadrangles, San Luis Obispo County, California: U.S. Geological Survey Miscellaneous Field Studies Map MF-511, scale 1:24,000.

Harding, T. P., 1974, Petroleum traps associated with wrench faults: American Association of Petroleum Geologists Bulletin, v. 58, p. 1290-1304.

Harding, T. P., 1976, Tectonic significance and hydrocarbon trapping consequences of sequential folding synchronous with San Andreas faulting, San Joaquin Valley, California: American Association of Petroleum Geologists Bulletin, v. 60, p. 365-378.

Hornafius, J. S., 1985, Neogene tectonic rotation of the Santa Ynez Range, western Transverse Ranges, California, suggested by paleomagnetic investigation of the Monterey Formation: Journal of Geophysical Research, v. 90, p. 12503-12522.

Hsu, K. J., 1969, Preliminary report and geologic guide to Franciscan melanges of the Morro Bay-San Simeon area, California: California Division of Mines and Geology Special Publication 35, 46 p.

Jaeger, J. C., and Cook, N. G. W., 1979, Fundamentals of rock mechanics: Chapman and Hall Ltd., London.

Lachenbruch, A. H., and Sass, J. H., 1980, Heat flow and energetics of the San Andreas fault zone: Journal of Geophysical Research, v. 85, no. B11, p. 6185-6222.

Lettis, W. R., and Hanson, K., 1990, Crustal strain partitioning; implications for seismic hazard assessment in western California: submitted to Geology.

Luyendyk, B. P., Kamerling, M. J., and Terres, R. R., 1980, Geometric model for Neogene crustal rotations in southern California: Geological Society of America Bulletin, v. 91, p. 211-217.

Luyendyk, B. P., and Hornafius, J. S., 1987, Neogene crustal rotations, fault slip, and basin development in southern California; in Ingersoll, R., and Ernst, G., eds., Cenozoic Basin Development in Coastal California: Rubey Volume VI, Pergammon Press, Elmsford, N. Y., p. 259-283.

McCulloch, D. S., 1987, Regional geology and hydrocarbon potential of offshore central California; in Scholl, D. W., Grantz, A., and Vedder, J., eds., Geology and Resource Potential of the Continental Margin of Western North America and Adjacent Ocean Basins, Beaufort Sea to Baja California: American Association of Petroleum Geologists, Circum Pacific Earth Science, v. 6, p. 353-401.

Means, W. D., 1976, Stress and strain: Springer-Verlag, N. Y.

Medwedeff, D., 1989, Growth fault-bend folding at southeast Lost Hills, San Joaquin Valley, California: American Association of Petroleum Geologists Bulletin, v. 73, p. 54-67.

Moody, J. D., and Hill, M. J., 1956, Wrench-fault tectonics: Geological Society of America Bulletin, v. 67, p. 1207-1246.

Mount, V. S., in review, Present-day stress directions in California: submitted to Journal of Geophysical Research.

Mount, V. S. and Suppe, J., 1987, State of stress near the San Andreas fault; implications for wrench tectonics: Geology, v. 15, p. 1143-1146

Namson, J. S., and Davis, T. L., 1988, Seismically active fold and thrust belt in the San Joaquin Valley, central California: Geological Society of America Bulletin, v. 100, p. 257-273.

Naylor, M. A., Mandl, G., and Sijpesteijn, C. H. K., 1986, Fault geometries in basement-induced wrench faulting under different initial stress states: Journal of Structural Geology, v. 8, no. 7, p. 737-752.

Pacific Gas and Electric Company, 1988, Final report of the Diablo Canyon Long Term Seismic Program: U. S. Nuclear Regulatory Commission Docket Nos. 50-275 and 50-323.

Page, B. M., 1981, Chapter 13 - The southern Coast Ranges; in Ernst, W. G., ed., The Geotectonic Development of California: Rubey Volume, v. 1, Prentice-Hall, Inc., Englewood Cliffs, New Jersey, p. 330-417.

Ramsay, J. G., 1967, Folding and fracturing of rocks: McGraw-Hill Book Company, New York, 560 p.

Stein, R. S., 1983, Reverse slip on a buried fault during the 2 May, 1983 Coalinga earthquake; evidence from geodetic data: in Bennett, J. H., and Sherburne, R. W., eds., The 1983 California Earthquakes, California Division of Mines and Geology, Special Publication 66 p. 151-164.

Sylvester, A. G., 1988, Strike-slip faults: Geological Society of America Bulletin, v. 100, p. 1666-1703.

Tchalenko, J. S., 1970, Similarities between shear zones of different magnitudes: Geological Society of America Bulletin, v. 81, p. 1625-1640.

Wilcox, R. E., Harding, T. P., and Seely, D. R., 1973, Basic wrench tectonics: American Association of Petroleum Geologists Bulletin, v. 57, p. 74-96.

Zoback, M. L., and Zoback, M. D., 1980, State of stress in the conterminous United States: Journal of Geophysical Research, v. 85, p. 6113-6156.

Zoback, M. D., Zoback, M. L., Mount, V. S., Suppe, J., Eaton, J. P., Healy, J. H., Oppenheimer, D., Reasenberg, P., Jones, L., Raleigh, C. B., Wong, I. G., Scotti, O., and Wentworth, C., 1987, New evidence on the state of stress of the San Andreas fault system: Science, v. 238, p. 1105-1111.

QUESTION LP 8

The logic tree parameters and weights used in the seismic source characterization result in the Hosgri being considered as primarily a strike-slip fault. As a means of assessing the impacts of differences of opinion, provide probabilistic seismic hazard calculations in which higher weights are put on reverse and oblique slips, such as 100 percent oblique slip; and 50 percent oblique slip, 40 percent strike slip, and 10 percent reverse slip. What is the effect on calculated seismically-induced core damage?

The logic tree for the Hosgri fault zone is presented in the Final Report (PG&E, 1988; Chapter 3), along with the basis for weighting of the various styles of faulting. Support for our assessment of the sense of slip on the Hosgri fault zone has been given in response to several previous questions (Questions GSG 4, SSC 2, and SSC 4, March 1990).

For purposes of sensitivity analysis, we present here the impact of alternative weights on the various styles of faulting, as requested in the question. Figure LP Q8-1 shows the mean seismic hazard curve (expressed as the probability of exceedance of various spectral accelerations in the 3.5 to 8 Hz frequency range) based on the weights for the sense of slip on the Hosgri fault zone (strike slip, 0.65; oblique, 0.30; reverse/thrust, 0.05) (PG&E, 1988). Also shown are the mean hazard curves for the two alternative weightings of the Hosgri sense of slip requested in the question. In the case where the weights are only slightly different from the Long Term Seismic Program weights (strike slip, 0.4; oblique, 0.5; reverse/thrust, 0.1), the hazard curve is very slightly less than the Program's curve at 2.0 g spectral acceleration. In the case where oblique-slip is given a 1.0 probability, the exceedance frequency is about two-thirds of that given by the Program's curve at 2.0 g spectral acceleration.

To understand the reason for these differences, we can consider the various seismic source characteristics and seismic hazard parameters that are related to the sense of slip (for example, empirical magnitude relations, fault slip rate, ground motion attenuation relations). In the case of the Hosgri fault zone, the most important parameter controlling the differences in the seismic hazard curves in Figure LP Q8-1 is the earthquake recurrence rate, which in turn, is directly related to the fault slip rate. As discussed in Chapter 3 of the Final Report (PG&E, 1988), the rate of slip on the Hosgri fault zone, assuming that it is a strike-slip fault, is 1 to 3 millimeters per year. If the fault is assumed to be an oblique-slip fault, the slip rate is about 0.2 to 0.8 millimeters per year. Recent detailed studies of the vertical component of slip on the Hosgri fault zone (see Response to Questions GSG 3 and GSG 4, March 1990) confirms that the slip rates for the oblique case given in the logic trees are appropriate.

The probability of seismically induced core damage is closely related to the probabilistic hazard results. Therefore, the decrease in seismic hazard for the cases given in Figure LP Q8-1 will likewise result in a decrease in the probability of seismically induced core damage.

REFERENCES

Pacific Gas and Electric Company, 1988, Final report of the Diablo Canyon Long Term Seismic Program: U. S. Nuclear Regulatory Commission Docket Nos. 50-275 and 50-323.

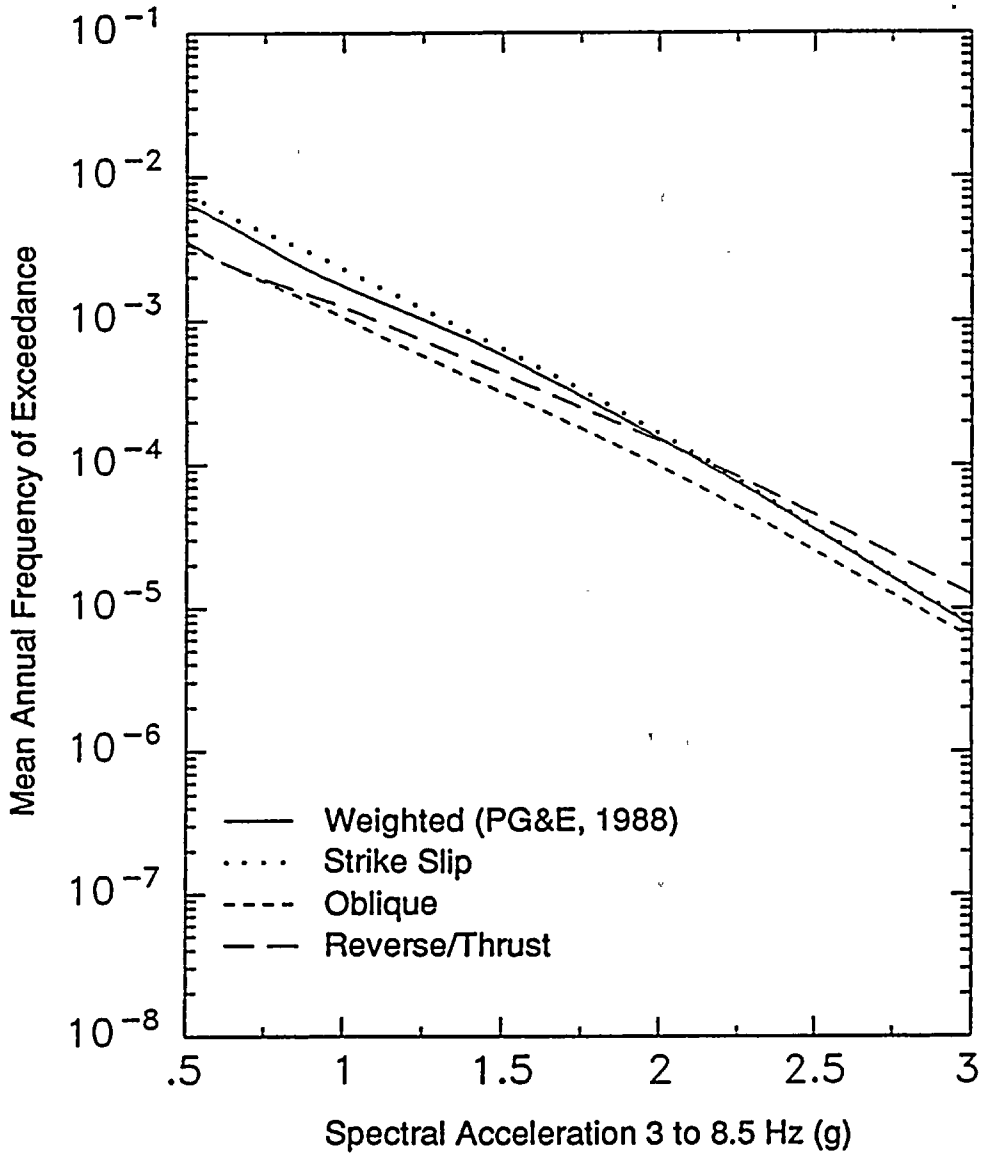

Figure LP Q8-1

Mean seismic hazard curves for alternative weights for the sense of slip on the Hosgri fault zone.

QUESTION LP 10

The characterization of the LTSP Hosgri earthquake is based heavily on trench observations of near surface strike-slip on the San Simeon fault 50 kilometers north of the plant site. As noted above, surface observations at similar distances from the Loma Prieta fault break also show evidence for strike-slip motion although that earthquake had oblique slip. Justify giving heavier weight to distant data from the San Simeon than to geologic and geophysical evidence (e.g., dipping blind thrusts, coincidence of the Hosgri zone with the break in the sea floor slope, and the juxtaposition of older Franciscan rock on the east side of the zone with the thick Pliocene - Pleistocene section on the west side of the zone) in the Hosgri fault zone tens of kilometers closer to the plant site which support the hypothesis of large vertical motions on the zone.

Question LP 10 requests that we justify giving "heavier weight" in our characterization of the Hosgri fault zone to trenching studies at San Simeon, 50 kilometers north of the Diablo Canyon site, than to other geologic and geophysical data nearer to the plant site that support "large vertical motions" on the Hosgri fault zone. We disagree both with the premise of the question that data near the power plant support the hypothesis of "large vertical motions" on the Hosgri fault zone, and with the stated assumption that we base our characterization of the Hosgri fault zone primarily on trenching studies at San Simeon. In this response, we first clarify the process and analytical techniques used during the Long Term Seismic Program to characterize the Hosgri fault zone, including individual data sets such as trench observations. Second, we describe evidence near the plant site for vertical displacement on the Hosgri fault zone and discuss this evidence in the context of the overall sense of slip on the fault.

CHARACTERIZATION OF THE HOSGRI FAULT ZONE

The process of characterizing a fault includes an assessment of the fault's physical (geometry, dimensions, and so forth) and behavioral (slip rate, sense of slip, recurrence, displacement per event, and so forth) properties. Although these properties are interrelated, no single geologic, seismologic or geophysical technique will fully assess the entire suite of properties. For example, detailed mapping and trenching studies are important for assessing displacement per event, whereas geophysical and seismologic studies are important for assessing down-dip geometry. Thus, a complete physical and behavioral description of a fault involves an integrated analysis of a wide variety of data sets, all of which are important for fault characterization but no one of which is solely or primarily the basis for the characterization.

By stating that we based our characterization of the Hosgri fault zone primarily on the results of a single study, the trenching investigations at San Simeon, Question LP 10 inaccurately portrays the process used in the Long Term Seismic Program to characterize the Hosgri fault zone. We characterized the Hosgri fault zone based on an integrated analysis of geologic, geophysical, seismologic and tectonic data from the entire length of the fault zone and the surrounding region. We did not base the characterization on one data set, nor did we inordinately weight one data set over another, as is indicated in the question.

The geologic, seismologic and geophysical data and analyses used in our characterization of the Hosgri fault zone are provided in the Final Report (PG&E, 1988) and in the responses to subsequent questions. Based on these data, we characterized the Hosgri fault zone as a strike- slip fault and established that the San Simeon and Hosgri fault zones are structurally related via the San Simeon/Hosgri pull-apart basin. As described in Response to Question LP 13, additional analyses were performed in response to NRC

questions and data requests subsequent to the submittal of the Final Report (PG&E, 1988), and included geologic and geophysical studies of the Hosgri fault zone near the power plant site. These studies significantly reduced our uncertainty in assessing sense of slip on the Hosgri fault zone and support the conclusion that the Hosgri fault zone is a strike-slip fault.

The geologic, seismologic, and geophysical investigations performed during the Long Term Seismic Program to characterize the Hosgri fault zone include the following:

- Paleoseismic investigations and detailed Quaternary mapping of the San Simeon fault zone (PG&E, 1988, p. 108-120; Response to Questions Q43i, j, and q, March 1989).
- Geophysical and geologic investigations of the San Simeon/Hosgri pull-apart basin (Response to Questions 41, March 1989, and GSG 12, March 1990).
- Geophysical and geologic investigations of the Piedras Blancas antiform and analysis of strain rates within the antiform (Response to Question GSG 13, March 1990).
- Analysis of high-resolution and common-depth-point seismic reflection data along the entire length of the Hosgri fault zone (PG&E, 1988, p. 2-10 to 2-14 and p. 2-94 to 2-86; Response to Questions 43f, g, h, n, o, t, u, v, y, March 1989, and GSG 1, Attachment GSG Q1-A - Montages, March 1990).
- Analysis of bathymetry along the entire length of the Hosgri fault zone (Response to Questions 43p, March 1989, and GSG 1, Attachment GSG Q1-A - Montages, March 1990)
- Analysis of lateral and vertical components of slip along the entire length of the Hosgri fault zone (Response to Questions GSG 3 and GSG 4, March 1990).
- Analysis of seismicity along and in regions bordering the Hosgri fault zone (PG&E, 1988, p. 2-46 to 2-86; Response to Question Q43x, March 1989).
- Comparison of the Hosgri fault zone to known strike-slip faults worldwide and to published diagnostic criteria for identifying strike-slip faults on seismic reflection data (Response to Question SSC 4, March 1990).
- Analysis of fault classifications (strike slip, oblique slip, and dip slip) and components of slip on the Hosgri fault zone (Response to Question SSC 2, March 1990).
- Development of the concept of strain partitioning to explain the occurrence of coeval, subparallel strike-slip and dip-slip faults (Response to Question GSG 2, March 1990).

Although the trench data obtained from the San Simeon fault zone are important, it has been our approach to integrate all the available geologic, geophysical, seismologic and tectonic data to provide a comprehensive characterization of the Hosgri fault zone. In this manner, we have provided an assessment of fault geometry and behavioral and physical fault characteristics that describe the entire length of the fault zone, and that also can be used to characterize any particular reach along the fault zone.

This approach allows for the recognition of spatial and temporal changes in fault behavior or geometry, such as the type of change in fault geometry that occurs along the Santa Cruz Mountains segment of the San Andreas fault. Our analysis indicates that, unlike the San Andreas fault, there are no large restraining bends anywhere along the Hosgri fault zone that would result in localized oblique slip along a specific fault segment (see Response to Question LP 11). There are, however, spatial and temporal variations in horizontal and vertical slip rates along the Hosgri fault zone. These rates are based on data from the San Simeon fault zone, the San Simeon/ Hosgri pull-apart basin, and the entire length of the Hosgri fault zone, together with information on the orientations and rates of crustal shortening in the Piedras Blancas antiform and Los Osos/Santa Maria domain. The ratio of horizontal to vertical slip generally ranges from 2:1 to 30:1, indicating that the Hosgri fault zone is a strike-slip fault along most, if not all its length (Response to Questions SSC 2 and GSG 4, March 1990). In particular, the ratios of horizontal to vertical slip along the San Luis/Pismo and San Luis Obispo Bay reaches, which are closest to the plant site, range from 10:1 to 30:1, and clearly indicate strike slip. The ratio of horizontal to vertical slip changes abruptly at specific locations along the fault, and these abrupt changes have been incorporated into our assessment of fault segmentation (Response to Question GSG 15, March 1990).

In considering the appropriateness of using data from San Simeon in the characterization of the Hosgri fault zone, it is important to note that, although the San Simeon area is 50 kilometers north of the plant site, the San Simeon fault zone is closely related structurally to the Hosgri fault zone. The San Simeon fault zone and Hosgri fault zone are part of the same fault system. They structurally interact in the near-offshore region between San Simeon Bay and Estero Bay and are related via the San Simeon/Hosgri pull-apart basin. We have extensively investigated and analyzed the pull-apart basin to document its dimensions, geometry, and age, and evaluate the rate of slip transferred between the bordering San Simeon and Hosgri fault zones (Response to Question GSG 12, March 1990). Thus our assessment of these two faults is not limited to the onshore San Simeon area.

Furthermore, it is important to note that our investigations at San Simeon entailed detailed Quaternary mapping of marine terraces, and geophysical characterization of the Piedras Blancas antiform, as well as paleoseismic trenching studies. The trench data provided site-specific slip- rate, displacement-per-event, and sense-of-slip data on individual fault strands; the Quaternary mapping and assessment of the Piedras Blancas antiform provided regional slip-rate and sense- of-slip data across the entire fault zone and potentially related structures. In this manner, we have assessed the distribution, style, and rates of strain across the entire region to minimize the potential for underestimating rate of slip and earthquake recurrence (see Response to Question LP 12).

EVIDENCE FOR VERTICAL DISPLACEMENT ON THE HOSGRI FAULT ZONE

Question LP 10 states that evidence near the plant site supports the "hypothesis of large vertical motions" on the Hosgri fault zone. If by "large vertical motions" the question is intended to imply that reverse or oblique slip is characteristic of the Hosgri fault zone in the vicinity of the plant site, we do not agree.

In the vicinity of the plant site, geophysical data generally indicate down-to-the-west vertical separation across the Hosgri fault zone, and the presence of one or more dipping fault strands west of the high-angle strands of the Hosgri fault zone. Taken separately, the geophysical data indicate vertical separation across the Hosgri fault zone. However, it is important to note that vertical separation is only one component of the net separation across the fault zone, and that vertical separation based on interpretation of geophysical and other data must be compared with the amount of horizontal separation to define the sense of slip on the fault. Therefore, we strongly disagree with the use of only one data set from a

limited geographic area to characterize the Hosgri fault zone. In addition, data near the plant site *do not* indicate a consistent break in the sea floor coincident with the surface trace of any strand of the Hosgri fault zone, in contrast to the evidence indicated in the question.

In our assessment of the Hosgri fault zone, we integrated the results of the geophysical investigations with the results of all other geologic, geophysical and seismologic investigations conducted both locally and regionally along the Hosgri fault zone to assess actual (not apparent) slip along the fault. In this assessment, we assumed that the dipping fault strands within the fault zone are active in the contemporary tectonic setting and that all the vertical separation observed across the fault zone is equal to the vertical component of actual slip. In addition, we assumed that uplift of the coast is occurring by vertical slip on the Hosgri fault zone. In the Responses to Questions GSG 3 and GSG 4, we provided a quantification of horizontal and vertical slip along the entire Hosgri fault zone, including the reaches of the fault closest to the plant site. These analyses indicate that the ratio of horizontal to vertical slip near the plant site ranges from about 10:1 to 30:1. These ratios indicate that although a component of vertical slip may be occurring along the Hosgri fault zone, the component of horizontal slip far exceeds the vertical slip, and that the fault zone is best classified as a strike-slip fault.

In this manner, our quantification of slip rate does not give inordinant weight to one data set or to one geographic locality. The data in the plant site region are just as important as data obtained at San Simeon or elsewhere along the Hosgri fault zone, and are given equal treatment. In addition, because the Hosgri fault zone does not extend onshore, we are limited in our ability to obtain site-specific behavioral data. Because of this inherent limitation in characterizing the fault zone, we would be remiss in our investigations if we did not consider data available to us from the San Simeon area.

CONCLUSIONS

Question LP 10 implies that by relying heavily on observations made at San Simeon, some 50 kilometers away from the plant site, we may be misinterpreting the sense of slip on the Hosgri fault zone to the south. We have shown that, although the trenching investigations at San Simeon are a valuable data set that can be used, in part, to assess behavioral characteristics of the Hosgri fault zone, the interpretation of sense of slip on the Hosgri fault zone is not based primarily on data gathered at San Simeon. Rather, our interpretations have been developed from a full suite of geologic, geophysical, and seismologic data sets from along the entire length of the Hosgri fault zone, including reaches of the fault zone closest to the site. Analyses of these data sets clearly indicate that although there is a component of vertical slip on the Hosgri fault zone, "large vertical motions" are not the dominant component of slip along the fault zone.

REFERENCES

Pacific Gas and Electric Company, 1988, Final report of the Diablo Canyon Long Term Seismic Program: U. S. Nuclear Regulatory Commission Docket Nos. 50-275 and 50-323.

QUESTION LP 11

Coastal uplift rates near Santa Cruz and near Diablo Canyon are similar at about 0.2 millimeters per year. Under some postulations both coastal areas could be on the hanging-wall blocks of blind thrust or reverse faults. The fault near Santa Cruz is defined by aftershocks of the Loma Prieta earthquake and that near Diablo Canyon by interpretation of seismic reflection data. In both areas the reverse fault appears to be joined at depths on the order of a kilometer or so by a near vertical fault that exhibits Holocene surface displacement (i.e. the San Andreas surface break near Loma Prieta and the sea floor Hosgri off Diablo Canyon). List and discuss the criteria that were used to judge that the blind reverse members of the Hosgri zone are incapable of producing an oblique slip earthquake like that at Loma Prieta and greater than that assumed in the LTSP.

Question LP 11 postulates that south-central coastal California is on the "hanging-wall block of a blind thrust or reverse fault" similar to the Santa Cruz coastal area. The question cites similarities of coastal uplift rates and the occurrence of reverse fault components along both the Santa Cruz Mountains segment of the San Andreas fault and the Hosgri fault zone to postulate that an oblique-slip earthquake similar to the Loma Prieta earthquake and "greater than that assumed in the LTSP" may occur on the Hosgri fault zone. As described in this response, we disagree with two assumptions implied in this question: (1) that the Loma Prieta earthquake is an appropriate analog for earthquakes that may occur along the Hosgri fault zone adjacent to the plant site; and (2) that we do not consider the possibility of an oblique-slip earthquake on the Hosgri fault zone.

We first discuss the criteria used to evaluate the sense of slip and slip rate along the Hosgri fault zone, including both the high- and low-angle components of the fault zone. Because the question focuses on the low-angle strands within the fault zone, we specifically address the characterization of these structures in terms of the concept of strain partitioning. Because the question also directly explores the implications of the Loma Prieta earthquake to the sense of slip on the Hosgri fault zone, we also discuss geometric and behavioral characteristics of the Santa Cruz Mountains segment of the San Andreas fault zone on which the Loma Prieta earthquake occurred, and assess its usefulness as an analog to the Hosgri fault zone.

We conclude that there are a number of significant geologic and geometric differences between the Santa Cruz Mountains segment of the San Andreas fault zone and the Hosgri fault zone, such that the former is not an appropriate analog to use in evaluating geometric characteristics along the Hosgri fault zone. Therefore, even in light of the Loma Prieta earthquake, our analyses indicate that the Hosgri fault zone is a strike-slip fault and, therefore, we have given this a higher probability in our characterization of the sense of slip. There is no geologic evidence to suggest that either the high-angle or low-angle components of the Hosgri fault zone are capable of producing an oblique-slip earthquake comparable to the 1989 Loma Prieta event. However, in contrast to the statement that we judge the Hosgri fault zone to be "incapable of producing an oblique slip earthquake," we do consider the possibility that the Hosgri fault zone may be oblique, in both the probabilistic and deterministic assessments of the Hosgri fault zone (PG&E, 1988, Chapter 3).

HOSGRI FAULT ZONE SENSE OF SLIP

The criteria used to assess the sense of slip and slip rate along the Hosgri fault zone have been described in several previous submittals. The Responses to Questions GSG 3 and GSG 4, March 1990, provide quantitative assessments of the rates of lateral and vertical slip along the zone. The Response to Question SSC 2, March 1990, provides a definition of fault classifications and classifies the Hosgri fault zone in terms of the ratio of horizontal to vertical slip. The Response to Question GSG 2, March 1990, describes the concept of strain partitioning and its implications for assessing fault behavior along the Hosgri fault zone. The concept of strain partitioning is particularly useful in addressing the relationship between the high-angle and low-angle components of the Hosgri fault zone and in evaluating their earthquake potential.

In both the Final Report (PG&E, 1988) and in subsequent responses to questions concerning the style and components of slip along the Hosgri fault zone, both high-angle and low-angle components within the fault zone were recognized as active structures within the contemporary tectonic setting. In our characterization of the Hosgri fault zone as a transpressional strike-slip fault having a subordinate component of dip slip (see Response to Question SSC 2), we considered the contribution of vertical and horizontal deformation associated with both the low-angle components and the high-angle components of the fault zone (see Response to Question GSG 4). In particular, quantification of the rates of vertical slip for the Hosgri fault zone (see Response to Question GSG 3) incorporates the total amount of vertical deformation across the entire fault zone and includes fold deformation related to low-angle components, as well as brittle fault deformation and folding associated with the high-angle components. The ratio of horizontal to vertical slip along the Hosgri fault zone adjacent to the Diablo Canyon power plant (10:1 to 30:1), as well as the associated rake angles, clearly meet the definition of a strike-slip fault, and do not indicate that oblique-slip earthquakes comparable to the Loma Prieta earthquake are typical events for this segment of the fault zone.

The seismogenic capability of the low-angle components of the Hosgri fault zone also have been considered in the context of strain partitioning (see Response to Question GSG 2). Recently proposed models of strain partitioning suggest that oblique strain in the lithospheric mantle and lower crust commonly partitions into tangential and normal strain components in the upper crust, producing subparallel strike-slip and dip-slip faults with associated fold belts. Regional strain partitioning originates beneath or within the lower part of the seismogenic crust in the region of high seismic moment release, where large earthquakes typically nucleate. Regionally partitioned structures, therefore, should be treated as independent seismic sources and characterized separately. Regional strain partitioning along the Hosgri fault zone is restricted to the Southern and Point Sal reaches, where it appears to be occurring within the offshore Santa Maria Basin (Response to Question GSG 2). This part of the basin lies within the South Basin compressional domain and is characterized by a series of late Cenozoic folds and underlying thrust faults that strike subparallel to the Hosgri fault zone. As discussed in the Response to Question GSG 4, horizontal to vertical ratios of slip along these two southernmost reaches of the Hosgri fault zone may be less than 2:1 in extreme scenarios, indicating that oblique slip may be occurring along the southern part of the fault zone.

Partitioning that occurs within the upper part of the crust in the region of low seismic moment release (upper 5 to 7 km) is referred to as local strain partitioning. Structures that partition at these shallow depths are not considered to be potential sources of large-magnitude earthquakes, but appear to be the upper-crustal expression of a single seismic source at depth. These shallow structures, therefore, must be characterized collectively to adequately describe the earthquake source parameters of the seismic

source at depth. Local strain partitioning along some but not all of the Hosgri fault zone is suggested by the presence of upward-diverging fault splays and localized folding and warping of Tertiary strata in close proximity to the fault zone. The low-angle fault strands typically converge with the high-angle strands at shallow crustal depths (2 to 4 kilometers) suggesting that they are not independent sources of seismicity. Our characterization of the Hosgri fault zone at seismogenic depths in these areas is based, therefore, on the sum of the slip components of both the low-angle and high-angle faults in the shallow section, as described in the Responses to Questions GSG 3 and GSG 4.

COMPARISON OF SANTA CRUZ MOUNTAINS SEGMENT OF SAN ANDREAS FAULT WITH THE HOSGRI FAULT ZONE

The 1989 Loma Prieta earthquake, which resulted from oblique slip along the Santa Cruz Mountains segment of the San Andreas fault, provides additional data and geologic observations that are important in characterizing fault behavior. Geodetic data suggest that the ratio of horizontal to vertical slip was about 1.3 to 1 (U.S. Geological Survey Staff, 1990). Aftershock data define a steeply southwest dipping fault plane and a rupture surface extending from about 6 to 18 kilometers in depth (U.S. Geological Survey Staff, 1990. Although the Loma Prieta earthquake did not produce surface rupture along the main trace of the San Andreas fault, the earthquake did produce permanent ground deformation, including surface fracturing, uplift, warping, and folding within the Santa Cruz Mountains, and contractional deformation along the northeastern flank of the Santa Cruz Mountains. Ground fracturing occurred at locations where similar fracturing occurred during the 1906 and prior earthquakes (for example, Highway 17 roadcut, Cotton and others, 1990). This recurrent ground deformation can be identified and evaluated in trench and road-cut exposures and is the subject of ongoing research by William Cotton and Associates, and Dan Ponti, Ray Wells, Steve Haugerud, David Schwartz, and Carol Prentice of the U.S. Geological Survey. Uplift and warping or folding of the Santa Cruz Mountains is reflected in the topographic relief of the range and can be quantified by detailed mapping of Quaternary surfaces such as coastal marine terraces. Anderson (in press), for example, shows that the marine terrace sequence from Point Año Nuevo to south of the Town of Aptos is deformed into two broad upwarps. One of these upwarps is centered in the epicentral region of the Loma Prieta earthquake and is coincident with geodetically defined and modeled coseismic uplift patterns. Recurrent Quaternary deformation along the northeastern range front of the Santa Cruz Mountains is topographically well expressed by the abrupt, linear range front, and is structurally expressed by several faults along the range front. These faults include the Shannon, Monte Vista, and Sargent-Berrocal faults. These types of ground deformation, therefore, produce features that can be identified and quantified by Quaternary mapping and paleoseismic investigations.

Comparison of the geometric and behavioral characteristics of the Loma Prieta earthquake, in addition to geomorphic and topographic expression of long-term deformation along the Santa Cruz Mountains segment of the San Andreas fault zone, indicates that there is a number of significant geometric and physical differences between this segment of the San Andreas fault and the San Simeon/Hosgri fault zone. Because of these differences, which are discussed below, it is not appropriate to use this earthquake as an analogy for the type of earthquake that would occur along the Hosgri fault zone.

Comparison of Fault Geometry

The Santa Cruz Mountains segment occupies a long, pronounced, 10- to 15-degree double restraining bend in the trend of the San Andreas fault (Figure LP Q11-1). Kinematic studies by several workers (for

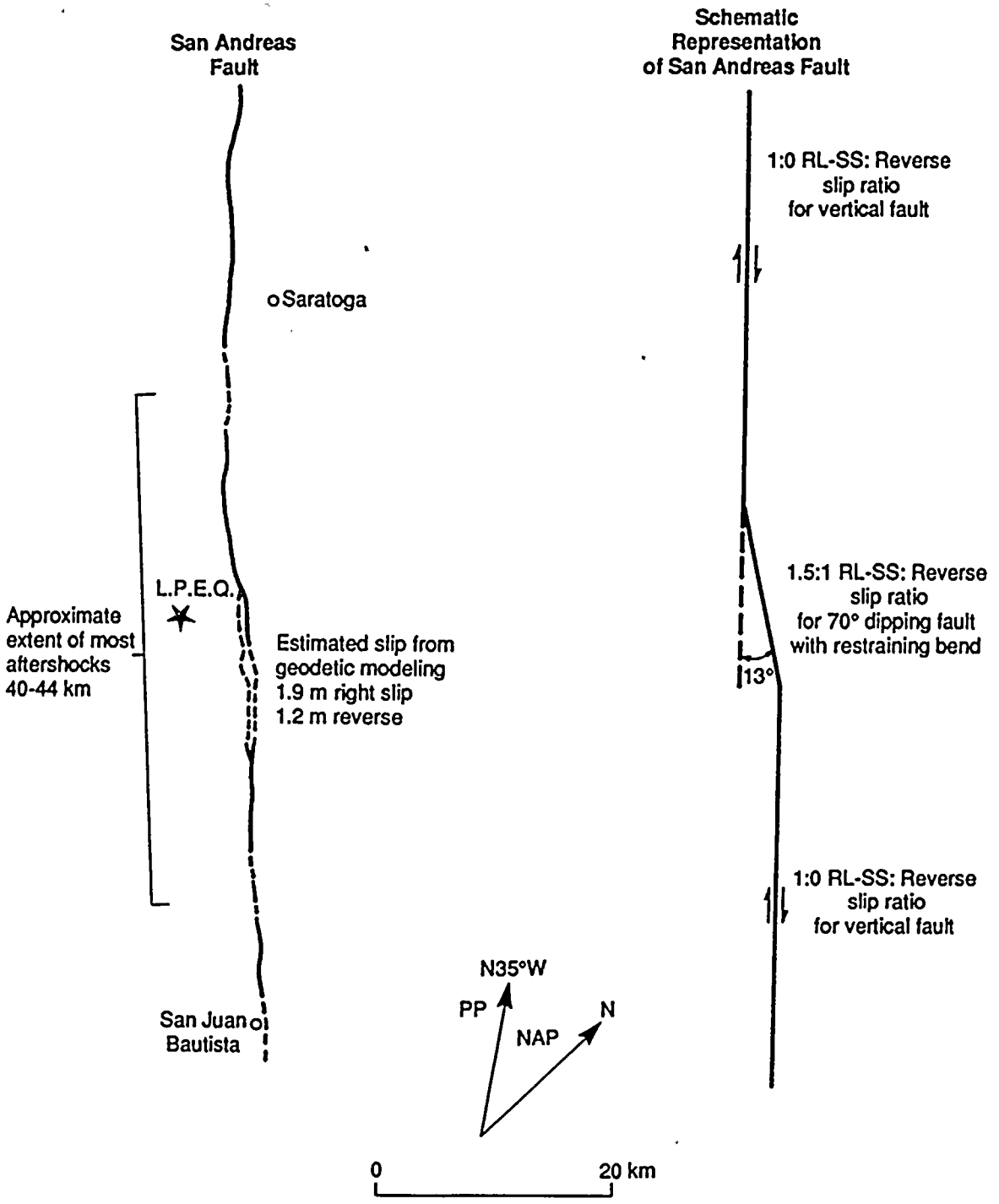

Figure LP Q11-1

Mapped trace of the San Andreas fault in the vicinity of the Loma Prieta earthquake, and schematic representation of the restraining double bend. Also shown is the relative direction of motion of the North American and Pacific plates.

example, Kadinsky-Cade and Barka, 1989) indicate that restraining bends will produce localized compression and oblique slip along a predominantly strike-slip fault. Furthermore, fault-specific assessments of the Loma Prieta rupture show that the oblique components of slip could have been predicted simply from the angle of the restraining bend and the 70-degree southwesterly dip of the fault (U. S. Geological Survey Staff, 1990; Dietz and Ellsworth, in press). There are no comparable restraining bends on the Hosgri fault zone (Figure LP Q11-2) that would produce oblique slip of the nature observed during the Loma Prieta earthquake. In fact, the northern three reaches of the Hosgri fault zone trend more nearly parallel to the plate motion vector than does the San Andreas fault. South of Point Sal, the Hosgri fault zone actually becomes more transtensional (northerly trending) relative to the plate motion vector.

Comparison of Components of Slip

Geodetic data from the Loma Prieta earthquake suggest that the ratio of horizontal to vertical slip was about 1.3 to 1 (U. S. Geological Survey Staff, 1990). In contrast, detailed studies to capture the long-term components of lateral and vertical slip along the Hosgri fault zone (see Response to Questions GSG 3 and GSG 4) indicate that the ratio of lateral to vertical slip ranges from 2:1 to 30:1, with the possible exception of the southernmost reaches of the fault south of Point Sal, which may be as low as 1:1. Ratios of 2:1 or greater are indicative of a strike-slip fault, following published definitions of styles of faulting (see Response to Question SSC 2). There is no evidence of oblique slip (that is, slip ratios of 2:1 to 1:2) along most of the length of the Hosgri fault zone, including the reaches of the Hosgri fault zone closest to the plant site.

Comparisons of Patterns and Rates of Uplift

The Santa Cruz Mountains segment of the San Andreas fault has topographic and geomorphic evidence of repeated oblique-slip events. The Santa Cruz Mountains are a linear range subparallel to the San Andreas fault, and reach elevations exceeding 3500 feet. The existence of the range is directly attributable to compression across the restraining bend and associated uplift (Anderson, in press; Schwartz and others, in press). In contrast, there is little or no relief across the Hosgri fault zone.

As noted in the question, both the Santa Cruz region, in the hanging wall of the southern Santa Cruz Mountains segment of the San Andreas fault, and several structural blocks within the Los Osos/Santa Maria domain east of and adjacent to the Hosgri fault zone have experienced late Quaternary uplift and are characterized by sequences of elevated coastal terraces. However, the rates and patterns of late Quaternary deformation differ considerably between the two areas.

A summary of the ages and deformation pattern of marine terraces in the Santa Cruz coastal region and their implications for repeat times of Loma Prieta earthquakes and for long term evolution of the Santa Cruz Mountains has been presented by Weber and Anderson (1990). As indicated by the profile of the present elevations of five marine terraces along the Santa Cruz coast (Figure LP Q11-3a), the rate of uplift has not been uniform in the Santa Cruz region. The lower three terraces have been uplifted at rates that range from approximately 0.2 to 0.7 millimeters per year, and have patterns of differential uplift that are similar and have persisted for at least the past 200,000 years. The pattern of uplift shows two distinct upwarps or bulges. The terraces all reach a peak elevation in the upwarp south of Santa Cruz. A comparison of the patterns of normalized uplift of these elevated marine terraces and the uplift resulting from the 1989 Loma Prieta earthquake (Figures LP Q11-3b and LP Q11-4) shows a marked similarity between the patterns of uplift. As noted by Anderson (in Weber and Anderson, 1990), this similarity

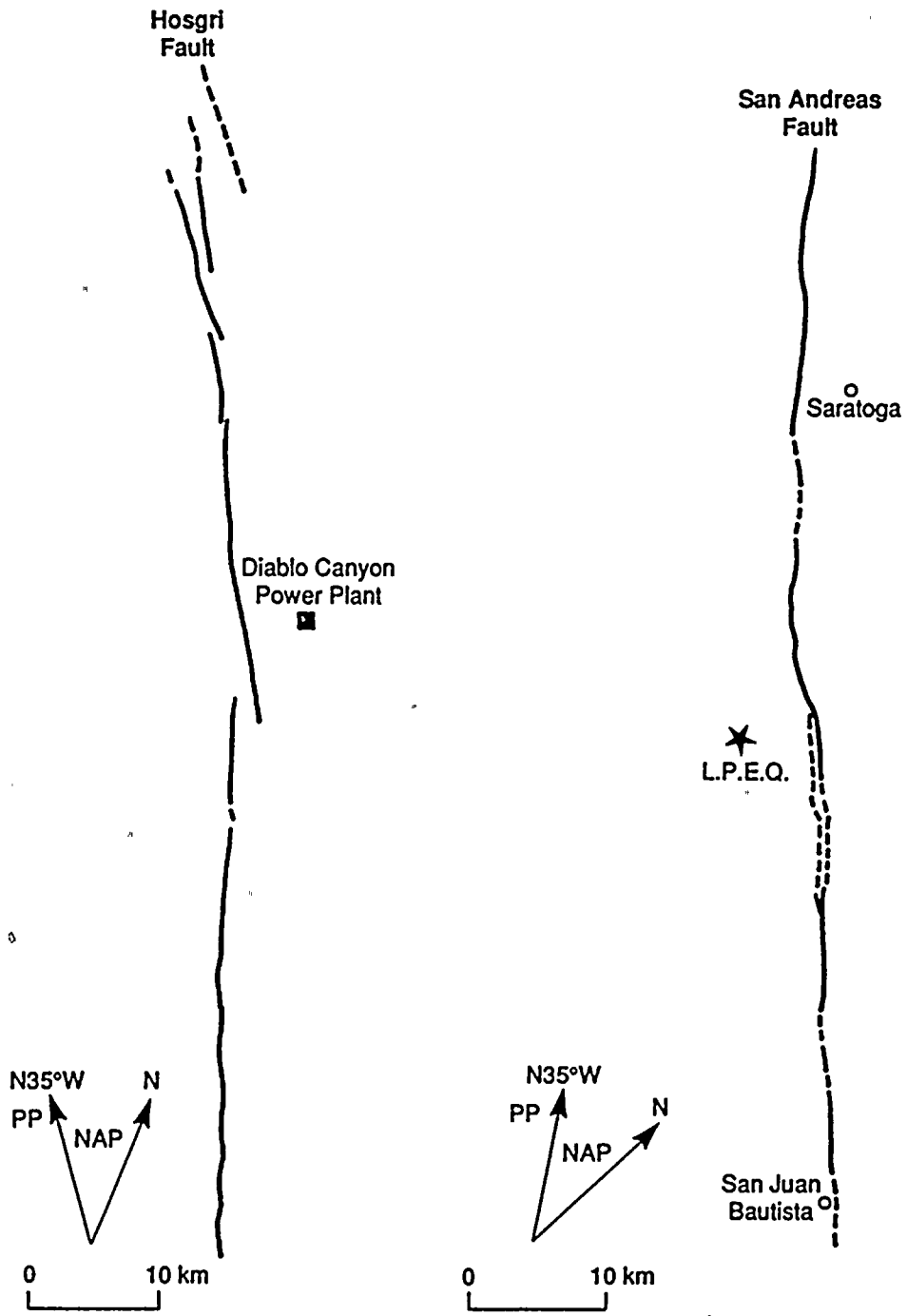

Figure LP Q11-2

Comparison of the major mapped trace of the Hosgri fault with the San Andreas fault. Also shown is the relative direction of motion of the North American and Pacific plates.

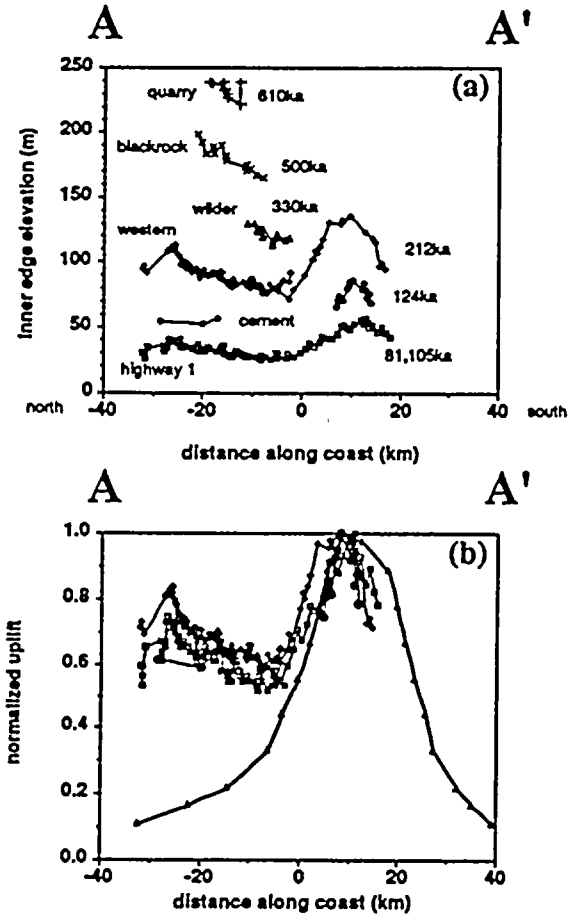

Figure LP Q11-3

(a) Longitudinal profile of marine terrace elevations in the Santa Cruz region (Section AA′, see Figure LP Q11-2); (b) Patterns of total uplift at terrace back edges (difference between terrace elevations and formation elevations) and Loma Prieta uplift (Figure LP Q11-2), each normalized to its maximum value to facilitate comparison of patterns (from Weber and Anderson, 1990).

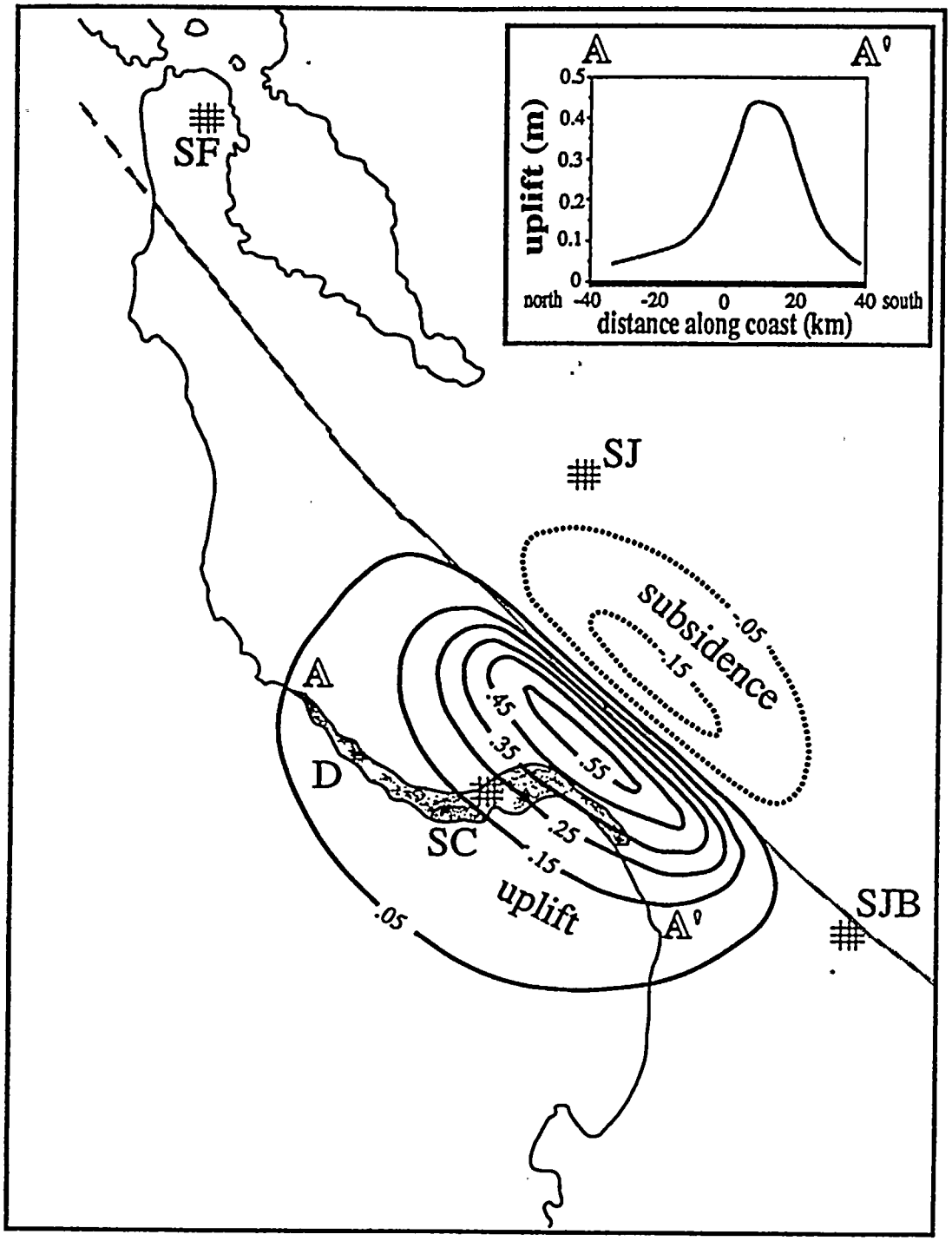

Figure LP Q11-4

Distribution of coseismic uplift and subsidence based upon laser geodometer and GPS measurements taken within days of the 1989 Loma Prieta earthquake. Shaded region along the coast depicts distribution of marine terrace deposits (from Weber and Anderson, 1990).

implies a strong genetic tie between coastal uplift and faulting along the San Andreas fault and suggests that uplift of the terraces in this region has been the result of repeated earthquakes comparable to the Loma Prieta earthquake.

In contrast to the epicentral region of the Loma Prieta earthquake, which is characterized by high topography and maximum late Pleistocene uplift rates of approximately 0.7 millimeters per year, the San Luis/Pismo structural block adjacent to the Hosgri fault zone has experienced considerably lower uplift rates of 0.06 to 0.22 $\pm$ 0.02 millimeters per year. Patterns of deformation also differ between the two regions. Unlike the Santa Cruz region, where elevations of marine terrace shoreline angles suggest regional folding, uplifting structural blocks in the Los Osos/Santa Maria domain east of the Hosgri fault zone show no internal fold deformation and are bordered by northwest-trending reverse faults that appear to have accommodated all the uplift.

In addition, the Hosgri fault zone is bordered on the east, in part, by subsiding or static structural blocks. The northern reach of the Hosgri fault zone is bordered by the Cambria structural block that is not uplifting in the vicinity of Estero Bay and is subsiding locally beneath Morro Bay. The San Luis Obispo Bay reach of the fault is bordered on the east by the Santa Maria structural block, which is subsiding at a rate of more than 0.01 millimeters per year. Subsiding regional blocks do not occur in the Santa Cruz region or Loma Prieta epicentral region. The occurrence of subsiding regional blocks on the "hanging wall" of the steeply dipping Hosgri fault zone is not consistent with and, in fact, precludes an interpretation that the Hosgri fault zone is a dip-slip or oblique-slip fault with northeast-side-up relative sense of slip.

Comparisons of Seismogenic Crustal Depths

The Loma Prieta earthquake and prior microseismicity indicate that the seismogenic part of the crust extends to a depth of more than 18 kilometers within the Santa Cruz Mountains. This differs from a more typical depth of about 10 to 12 kilometers for the seismogenic crust along most of the central San Andreas fault. The anomalously thick seismogenic crust is locally confined to the Santa Cruz Mountains restraining bend of the San Andreas fault (Figure LP Q11-5), and it has been concluded that the anomalous U-shaped zone of deep microseismicity prior to the event could have been used to anticipate the subsequent rupture area (U. S. Geological Survey, 1990; Olson, in press). A similar thickening of the seismogenic crust does not occur along the Hosgri fault zone. As shown in Figure LP Q11-6, microseismicity along and in regions directly bordering the Hosgri fault zone is confined to a depth of less than about 12 kilometers.

CONCLUSIONS

Our interpretation of sense of slip of the Hosgri fault zone is based on an integrated analysis of a full suite of geologic, geophysical, and seismologic data sets along the entire Hosgri fault zone (see Response to Question LP 10). The weight of the evidence provided by this integrated analysis strongly supports a conclusion that the Hosgri fault zone is a strike-slip fault. Therefore, in our characterization of the Hosgri fault zone, we considered the probability that the fault zone is a strike-slip fault to be 0.65 (PG&E, 1988, Chapter 3). Investigations and analyses performed in response to NRC questions subsequent to the Final Report support this interpretation and indicate a greater probability that the Hosgri fault zone is a strike-slip fault (see Response to Question LP 13). Our assessment of the style of faulting and slip rate of the Hosgri fault zone is based on cumulative horizontal and vertical components of slip across the entire fault zone, including high- and low-angle ("blind reverse") fault strands, and structural

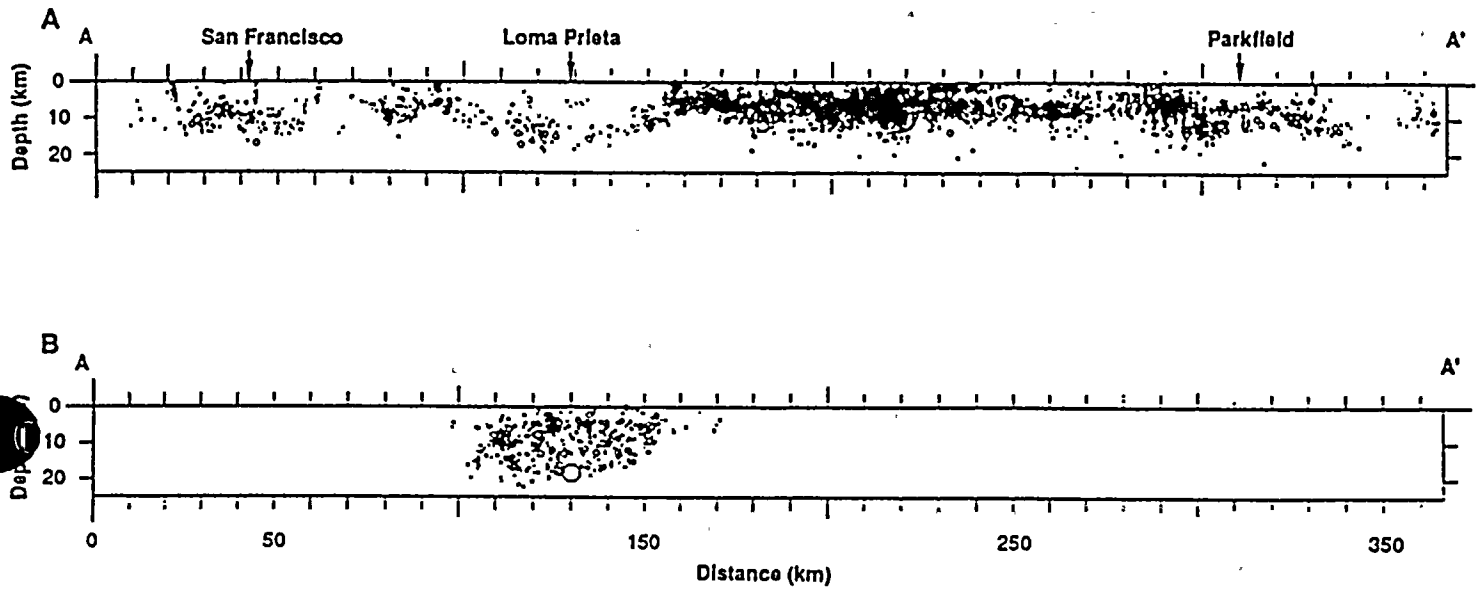

From U.S.G.S. staff, 1990

Figure LP Q11-5

(a) Cross section of seismicity of the San Andreas fault from 1969 to 1989 prior to the Loma Prieta earthquake; (b) Loma Prieta mainshock and aftershocks (from U. S. Geological Survey Staff, 1990).

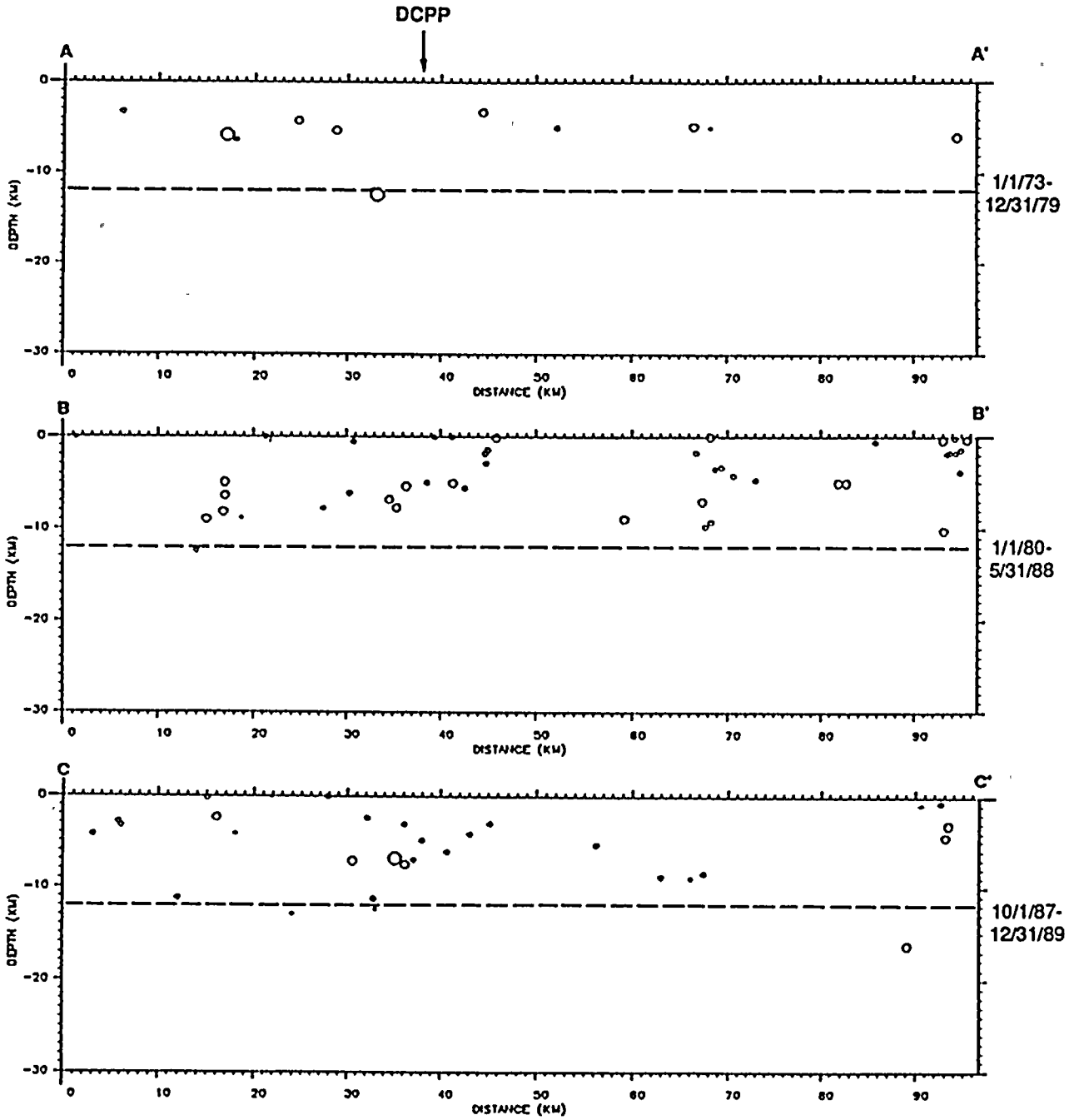

Figure LP Q11-6

Cross section of seismicity along the Hosgri fault for three time periods. DCPP denotes the Diablo Canyon site and the dashed line is a depth of 12 kilometers.

relief due to folding proximal to the fault zone. Thus, our estimates of slip encompass all coeval intra-fault-zone (local) strain partitioning. If strain partitioning is occurring, which implies that the vector sum of the slip components near the surface is occurring at seismogenic depths, the rate of vertical separation on low-angle components is much less than the rate of horizontal separation on high-angle components. When combined at seismogenic depths, these estimates of slip yield ratios of horizontal to vertical slip greater than 2:1 for nearly the entire length of the fault zone, including the reaches closest to the plant site. Thus, the slip-rate estimates indicate that the Hosgri fault zone is a strike-slip fault, following published definitions of styles of faulting (see Response to Question SSC 2).

Our characterization of the Hosgri fault zone incorporates the potential for an oblique-slip earthquake. In contrast to the statement in the question that we consider the Hosgri fault zone to be "incapable of producing an oblique-slip earthquake," we consider the possibility that the Hosgri fault zone may be oblique in the logic tree for the fault as well as in our deterministic assessment of the Hosgri fault zone (PG&E, 1988, Chapter 3). In those assessments, we considered the probability that the Hosgri fault zone is an oblique-slip fault to be 0.3. Further, in our Responses to Questions GSG 3, GSG 4, and SSC 2, we quantified the components of horizontal and vertical slip along the Hosgri fault zone and noted that under certain conditions the zone may have an oblique sense of slip along its southernmost reaches south of Point Sal.

Drawing analogies between the Hosgri fault zone and the Santa Cruz Mountains segment of the San Andreas fault is simply inappropriate. Sense of slip along the Santa Cruz Mountains segment is directly related to a large, double restraining bend in the San Andreas fault. Associated regional compression is expressed by Quaternary uplift, topographic relief of the Santa Cruz Mountain range, and thickening of the seismogenic zone. These phenomena clearly indicate the profound influence that the restraining bend has on the regional tectonics. In contrast, the Hosgri fault zone does not undergo any significant restraining bends and, as a consequence, is not associated with diagnostic indicators of major compression such as uplift and mountain-building.

In response to the question of whether the Loma Prieta earthquake would lead us to a conclusion that the maximum magnitude on the Hosgri fault zone might be "greater than that assumed in the LTSP," we see no reason why it would. One way to test the implications of this event is to compare the rupture dimensions, which would be used to assess the magnitude of the event, with the dimensions and magnitudes of other earthquakes. The Loma Prieta earthquake did not rupture the surface, so data on historical surface rupture lengths are obviously not applicable. However, when we compare the magnitude and subsurface rupture length defined by aftershocks, and rupture area of the Loma Prieta event with other earthquakes, we see that the rupture dimensions are very compatible with those of other earthquakes having similar magnitudes (Figures LP Q11-7 and LP Q11-8). In other words, available empirical relations would have provided a good estimate of the magnitude of this event if we knew only the rupture dimensions before the event. It follows that there is nothing about the Loma Prieta event that would cause us to revise our empirical magnitude relationships such that we would change our estimates of the maximum magnitude on the Hosgri fault zone.

REFERENCES

Anderson, R. S., in press, Evaluation of the Santa Cruz Mountains by advection of crust past a restraining bend on the San Andreas fault: Science.

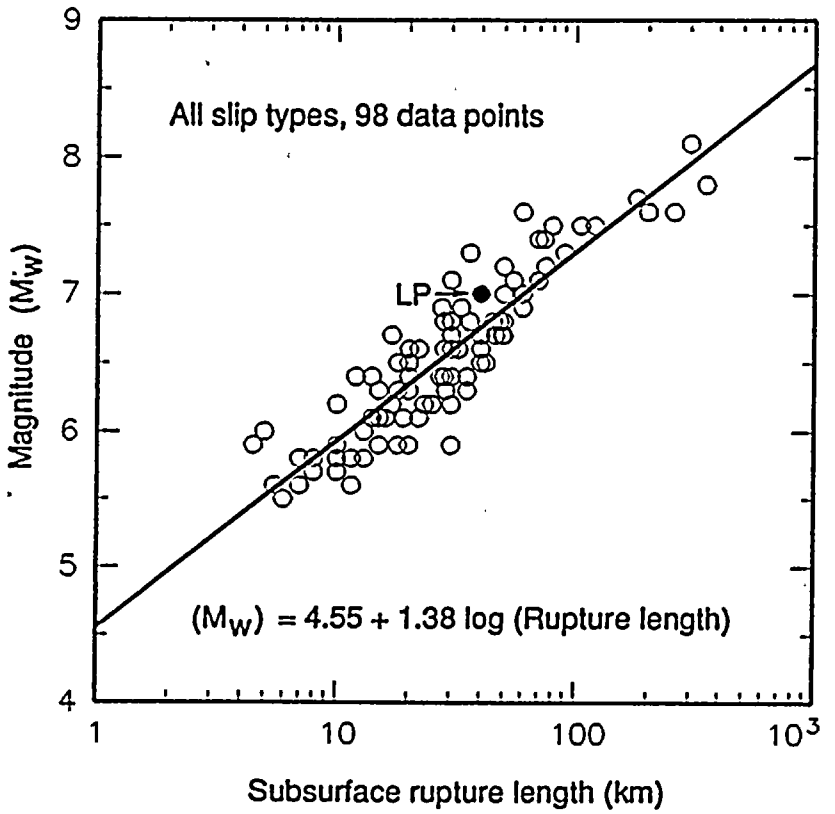

Figure LP Q11-7

Empirical relationship between subsurface fault rupture length and moment magnitude (from Wells and others, in preparation). The subsurface rupture length and magnitude of the Loma Prieta earthquake is indicated by LP.

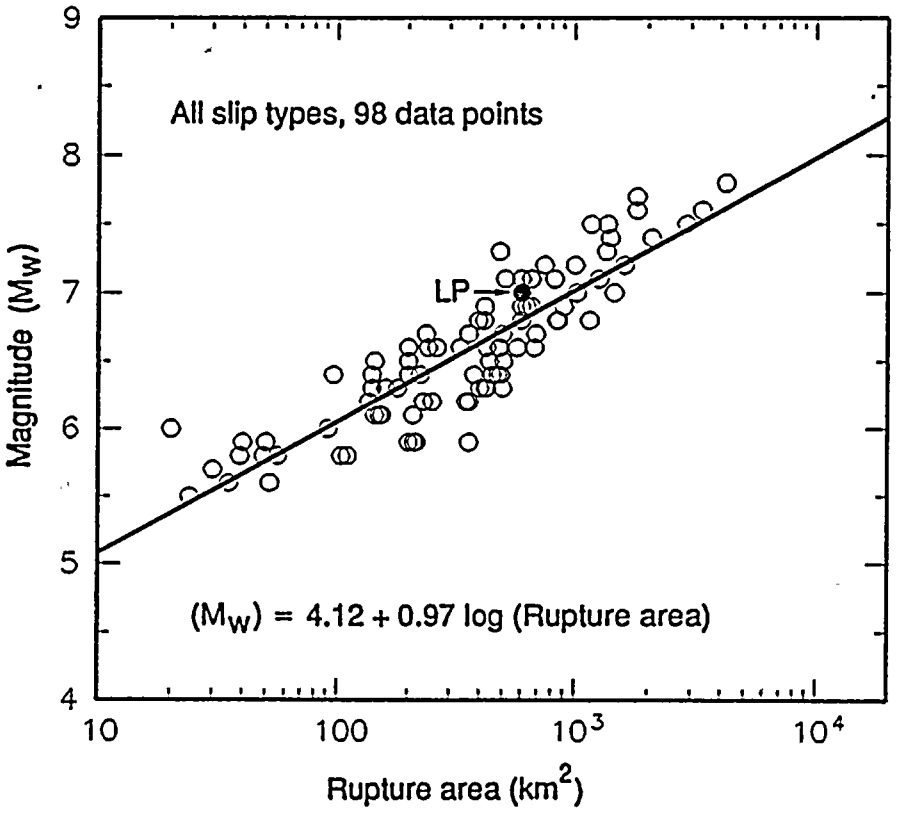

Figure LP Q11-8

Empirical relationship between rupture area and moment magnitude (from Wells and others, in preparation). The rupture area and magnitude of the Loma Prieta earthquake is indicated by LP.

Cotton, W. R., Fowler, W. L. and Van Velsor, J. E., 1990, Coseismic bedding plane faulting associated with the Loma Prieta earthquake of October 17, 1989 (abs.): Seismological Research Letters, v. 61, p. 16.

Dietz, C. D., and Ellsworth, W. L., in press, The October 17, 1989 Loma Prieta, California earthquake and its aftershocks; geometry of the sequence from high-resolution location: Geophysical Research Letters.

Kadinsky-Cade, K., and Barka, A. A., 1989, Effects of restraining bends on the rupture of strike-slip earthquakes; in Schwartz, D. P., and Sibson, R. H., (eds.), Fault Segmentation and Controls of Rupture Initiation and Termination: U. S. Geological Survey Open File Report 89-315, p. 181-192.

Lettis, W. R., and Hanson, K. L., in review, Strain partitioning; implications for seismic hazard assessment in western California: Geology (submitted May, 1990).

Olson, J. A., in press, Seismicity in the twenty years preceding the 1989 Loma Prieta, California earthquake: Geophysical Research Letters.

Pacific Gas and Electric Company, 1988, Final report of the Diablo Canyon Long Term Seismic Program: U. S. Nuclear Regulatory Commission Docket Nos. 50-275 and 50-323.

Schwartz, D. P., Orange, D. L., and Anderson, R. S., in press, Complex fault interactions in a restraining bend on the San Andreas fault, southern Santa Cruz Mountains: Geophysical Research Letters.

U. S. Geological Survey Staff, 1990, The Loma Prieta, California, earthquake: an anticipated event: Science, v. 247, p. 286-293.

Weber, G. E., and Anderson, R. S. 1990, Marine terrace deformation pattern: Its implications for repeat times of Loma Prieta earthquakes and for the long term evolution of the Santa Cruz Mountains; in D.P. Schwartz and D.J. Ponti, eds., Field Guide to Neotectonics of the San Andreas Fault System, Santa Cruz Mountains, in Light of the 1989 Loma Prieta Earthquake: U. S. Geological Survey Open-File Report 90-274, p. 6-14.

Wells, D. L., Coppersmith, K. J., Slemmons, D. B., and Zhang, X., in preparation, Earthquake source parameters; updated empirical relationships among magnitude, rupture length, rupture area, and surface displacement: for submittal to Seismological Society of America Bulletin.

QUESTION LP 12

The maximum deterministic and probabilistic earthquakes on the Hosgri fault are anchored to geologic slip measured in the trenches at San Simeon. The Whittier, Coalinga, and Loma Prieta earthquakes demonstrate that large, damaging earthquakes may occur without leaving a record of discernible tectonically induced fault rupture in trench exposures. How does the LTSP compensate for this potential undercounting of earthquakes and minimal estimate of geologic slip on the Hosgri, the Los Osos, and the San Luis Bay faults?

Question LP 12 makes the observation that moderate-to-large earthquakes have occurred recently at Coalinga, the Whittier Narrows, and Loma Prieta, leaving no evidence of fault rupture. The question implies that the Hosgri, Los Osos, and San Luis Bay faults may have behaved similarly, and asks how our investigations compensated for this potential under-estimation of seismic hazard from these faults.

Prior to addressing this issue, it is important to note that the question makes an incorrect assertion that the maximum deterministic and probabilistic earthquakes on the Hosgri fault zone are anchored to geologic slip measured in the trenches at San Simeon. There is a potential for "undercounting of earthquakes and minimal estimates of geologic slip" if fault evaluations are based solely on site-specific trenching investigations. As described in this response, we based our estimation of maximum magnitude and recurrence on a much more extensive suite of data. In addition, the question implies that the Coalinga, Whittier Narrows, and Loma Prieta earthquakes were not associated with discernible ground deformation. In fact, although these earthquakes were not associated with surface fault rupture, there is discernible ground deformation preserved in the Quaternary stratigraphic and geomorphic record. In this response, we first discuss each of these issues and then address the more general issue regarding potential underestimation of geologic slip and undercounting of earthquakes on the Hosgri, Los Osos, and San Luis Bay faults.

MAXIMUM EARTHQUAKE MAGNITUDE ANCHORED TO GEOLOGIC SLIP MEASURED IN TRENCHES AT SAN SIMEON

As discussed in Response to Question LP 10, we based our characterization of the Hosgri fault zone, including estimates of maximum magnitude, on a comprehensive suite of geologic, geophysical, seismologic, and tectonic data collected along the entire length of the Hosgri fault zone and in the surrounding region. Characterization of fault behavior and geometry is not based on one data set or data from one geographic locality.

We estimated maximum magnitude based on a number of empirical relationships that have been established between magnitude and various fault parameters, including fault length, rupture length, rupture area, amount of displacement per event, and seismic moment (Wells and others, in preparation). The rate of earthquake recurrence is based on the estimated slip rate of the Hosgri fault zone, not on the number of earthquakes deduced from trench exposures across the San Simeon fault zone. The use of fault slip rate to assess earthquake recurrence is described in the Final Report (PG&E, 1988, p. 3-33 to 3-39). We quantified slip rate across the Hosgri/San Simeon fault system using a variety of data including: (1) displaced marine terraces that cross the entire San Simeon fault zone; (2) displaced drainages; (3) displaced stratigraphic horizons in trench exposures; (4) evaluation of the San Simeon/Hosgri pull-apart basin; (5) vertical separation across the Hosgri fault zone based on seismic reflection data and coastal uplift rates; and (6) rates and orientations of crustal shortening in the Piedras Blancas antiform,

the offshore Santa Maria Basin, and the Los Osos/Santa Maria domain. These techniques capture the potential range in slip rate across the entire Hosgri fault zone and are not limited to local slip-rate estimates from trenches across individual fault traces (see Response to Question LP 10). Thus, estimates of maximum magnitude, slip rate, and earthquake recurrence are *not* anchored to the trenching studies performed at San Simeon.

PERMANENT GROUND DEFORMATION DURING THE COALINGA, WHITTIER NARROWS, AND LOMA PRIETA EARTHQUAKES

Although the Coalinga, Whittier Narrows, and Loma Prieta earthquakes did not have evidence of surface fault rupture, permanent ground deformation did occur and can be identified and quantified by Quaternary mapping and paleoseismic investigations. Permanent ground deformation during the Coalinga and Whittier Narrows earthquakes included uplift and folding of the Coalinga and Elijian Park anticlines, respectively. These anticlines deform Quaternary deposits and geomorphic surfaces, and have clear topographic expression. Quaternary studies in these areas by Stein and Ekström (1990) and Bullard and Lettis (1990), among others, indicate that the Quaternary record of structural deformation can be used to evaluate the geometry, dimensions and behavior of the underlying thrust faults.

Permanent ground deformation during the Loma Prieta earthquake included surface fracturing, uplift, warping, and folding within the Santa Cruz Mountains, and contractional deformation along the northeastern flank of the Santa Cruz Mountains. Ground fracturing occurred at locations where similar fracturing occurred during the 1906 and prior earthquakes (for example, Interstate 880 roadcut, Cotton and others, 1990). This recurrent ground deformation can be identified and evaluated in trench and road-cut exposures and is the subject of ongoing research by William Cotton and Associates, and Dan Ponti, Ray Wells, Steve Haugerud, David Schwartz, and Carol Prentice of the U. S. Geological Survey. Uplift and warping or folding of the Santa Cruz Mountains is reflected in the topographic relief of the range and can be quantified by detailed mapping of Quaternary surfaces such as coastal marine terraces. Anderson (in press), for example, shows that the marine terrace sequence from Point Año Nuevo to south of the Town of Aptos is deformed into two broad upwarps (see Response to Question LP 11 for discussion). One of these upwarps is centered in the epicentral region of the Loma Prieta earthquake and is coincident with geodetically defined and modeled coseismic uplift patterns. Recurrent Quaternary deformation along the northeastern range front of the Santa Cruz Mountains is topographically well expressed by the abrupt, linear range front and is structurally expressed by the occurrence of several faults along the range front. These faults include the Shannon, Monte Vista, and Sargent-Berrocal faults.

Ground deformation associated with the Coalinga, Whittier Narrows, and Loma Prieta earthquakes, therefore, produces features that can be identified and quantified by Quaternary mapping and paleoseismic investigations. It is incorrect to assume that simply because an earthquake was not associated with tectonic surface rupture that the repeated occurrence of such slip events does not produce a record of Quaternary surface deformation that can be identified and evaluated by thorough, comprehensive geologic investigations.

Underestimation of Earthquake Potential

The occurrence of the 1983 Coalinga, 1987 Whittier Narrows, and 1989 Loma Prieta earthquakes underscores the need to conduct thorough, comprehensive investigations to fully characterize fault behavior and geometry. These investigations should include integrated geologic, geophysical, and seismologic analyses and should not rely on any single technique such as paleoseismic trenching

investigations. As described in Response to Question LP 10, we adopted such a comprehensive approach to assess fault activity in south-central coastal California. We did not rely on just one investigative technique or analysis to characterize fault behavior or geometry.

Although surface fault rupture was not associated with the Coalinga, Whittier Narrows, and Loma Prieta earthquakes, permanent ground deformation did occur and is associated with Quaternary deformation that is well-expressed at the earth's surface. As stated in the previous discussion, the Loma Prieta earthquake was associated with ground deformation that, in part, could be recognized in trenches as well as in regional Quaternary surfaces. The Coalinga and Whittier Narrows earthquakes were associated with coseismic uplift and folding. This coseismic deformation is generally coincident with the locus of Quaternary anticlines and indicates that the anticlines have grown, at least in part, by repeated coseismic uplift. These folds are clearly expressed topographically and Quaternary surfaces and deposits are involved in the deformation. Thus, although there is no evidence of surface fault rupture, the earthquakes were associated with permanent ground deformation that can be recognized by appropriate geologic and geophysical investigative techniques. This deformation can be used both to identify the locations of potential seismic sources (Stein and Ekstrom, 1990) and to characterize the long-term behavior of these seismic sources in terms of sense of slip, slip rate, probable fault length and down-dip geometry (sense of vergence).

Can fault-slip events comparable to the Loma Prieta event occur on the Hosgri, Los Osos, and San Luis Bay faults without producing surface fault rupture? Based on aftershock data, fault rupture during the Loma Prieta earthquake appears to have terminated below a depth of 2 kilometers. Geodetic modeling suggests that the fault displacement extended no shallower than 10 kilometers (Lisowski and others, in press). Lack of fault rupture at the surface is most likely directly related to the deep (18 kilometers) nucleation of the event at the base of the seismogenic crust along the Santa Cruz Mountains segment of the San Andreas fault (U. S. Geological Survey Staff, 1990). Fault rupture simply did not propagate to the surface from this great depth. If the event had nucleated at a depth of 12 kilometers or less, fault rupture probably would have intersected the ground surface, given the rupture dimensions that are interpreted for the event. The base of the seismogenic crust along south-central coastal California is about 12 kilometers (see Response to Question LP 10). Therefore, large earthquakes will likely nucleate at or above the base of the seismogenic crust in the depth range of 7 to 12 kilometers. Given the magnitude and rupture dimensions of the Loma Prieta earthquake, similar events occurring in the depth range of 7 to 12 kilometers on the Hosgri or Los Osos faults would produce surface fault rupture and/or near-surface deformation (folding, tilting, distributed shearing, surface fissuring, and so forth). The smaller-magnitude Coalinga and Whittier Narrows earthquakes have correspondingly smaller rupture dimensions than the Loma Prieta earthquake. These earthquakes were nearly pure dip-slip events on shallow-dipping faults. As described in the Final Report (PG&E, 1988) and in the Responses to Questions GSG 3, GSG 4 and SSC 2, the Hosgri fault zone is a strike-slip fault and will not produce moderate-to-large magnitude, dip-slip earthquakes. The Los Osos and San Luis Bay faults, however, are reverse faults and may produce dip-slip earthquakes near the threshold of tectonic surface fault rupture. Multiple events through time, however, will result in cumulative deformation of strain indicators such as marine terraces. As a result, there will not be a significant undercounting or underestimation of earthquake behavior based on paleoseismic investigations and Quaternary mapping of surface deformation.

CONCLUSIONS

In characterizing the behavior of the Hosgri, Los Osos, and San Luis Bay faults, we conducted a variety of geologic, geophysical, and seismologic investigations. Paleoseismic trenching studies were an

important element of this program, but were not the sole or primary basis for characterizing the behavior or geometry of any potential seismic source in the south-central coastal California region.

As described earlier, estimates of the maximum earthquake magnitude were based on a variety of techniques that relate magnitude to fault parameters, and the rate of earthquake recurrence was assessed on the basis of fault slip rate. The major advantages in using fault slip rate are that we capture the total strain across the fault zone (and thus do not rely on data from individual fault strands), and that we conservatively assume all the strain is the result of coseismic slip at depth. Estimates of sense of slip and slip rate across the San Simeon, Los Osos, San Luis Bay, and Olson faults are based, in part, on detailed regional mapping of Quaternary marine terraces. Marine terraces were mapped along the coast across the entire width of these fault zones. The terraces provide excellent long-term strain gauges from which to evaluate cumulative displacement, sense of slip, and slip rate. Mapping these terraces enabled us to define brittle surface fault displacement, distributed shear across a broad zone, near-surface tilting or folding within and bordering the fault zone, and subparallel faulting that may result from local strain partitioning (see Response to Question GSG 2). In this manner, our characterization of each of these faults includes the potential for near-surface permanent ground deformation such as that which occurred during the 1983 Coalinga earthquake, the 1987 Whittier Narrows earthquake, and the 1989 Loma Prieta earthquake.

We therefore conclude that because our estimates of earthquake recurrence were developed for fault slip rate across the entire zone of deformation, we are not subject to "undercounting of earthquakes" or to "minimal estimates of geologic slip." In fact, we provide conservative estimates of earthquake recurrence, because we assume that all the deformation near the surface represents seismogenic slip at depth, and that no aseismic deformation is occurring or has occurred during the Quaternary.

REFERENCES

Anderson, R. S., in press, Evaluation of the Santa Cruz Mountains by advectionof crust past a restraining bend on the San Andreas fault: Science.

Bullard, T., and Lettis, W. R., 1990, Characterization of Quaternary surface deformation in the vicinity of the 1987 Whittier Narrows earthquake, Los Angeles Basin, California: Geological Society of America Abstracts with Program, v. 22, no. 3, p. 11.

Cotton, W. R., Fowler, W. L. and Van Velsor, J. E., 1990, Coseismic bedding plane faulting associated with the Loma Prieta earthquake of October 17, 1989 (abs.): Seismological Society of America, Eastern Section, Seismological Research Letters, v. 61, no. 1, p. 16.

Lisowski, M., Prescott, W. H., Savage, J. C., and Johnston, M. J., 1990, Geodetic estimate of coseismic slip during the 1989 Loma Prieta, California, earthquake: submitted to Geological Research Letters Special Issue.

Pacific Gas and Electric Company, 1988, Final report of the Diablo Canyon Long Term Seismic Program: U. S. Nuclear Regulatory Commission, Docket Nos. 50-275 and 50-323.

Stein, R. S., and Ekstrom, G., 1990, Anatomy of a 100-km-long blind thrust fault in central California, from short and long period seismology, geodesy, and seismic reflection profiles (abs.): Seismological Society of America, Eastern Section, Seismological Research Letters, v. 61, no. 1, p. 23.

U. S. Geological Survey Staff, 1990, The Loma Prieta, California, earthquake; an anticipated event: Science, v. 247, p. 286-293.

Wells, D. L., Coppersmith, K. J., Slemmons, D. B., and Zhang, X., in preparation, Earthquake source parameters; updated empirical relationships among magnitude, rupture length, rupture area, and surface displacement: for submittal to the Seismological Society of America Bulletin.

QUESTION LP 13

List and describe differences between findings in the 1988 LTSP Final Report and those arrived at as a result of subsequent investigations and analyses.

PG&E submitted the Final Report of the Long Term Seismic Program to the U.S. Nuclear Regulatory Commission (NRC) on July 31, 1988. The final report provides the data and results of a comprehensive three-year program to address the conditions to the operating license of the Diablo Canyon Power Plant. Subsequent to this submittal, PG&E conducted a series of follow-up investigations and analyses in response to data requests and questions raised during the NRC's review of the Final Report. The data and interpretations generated by these subsequent studies are provided in written responses to NRC questions submitted to PG&E on December 13, 1988; August 1, 1989; October 13, 1989; and February 22, 1990.

Most of these responses provide data that augment or clarify information provided in the Final Report. Several responses required additional focused investigations and analyses or involved updating the technical data base as a result of ongoing research in the region by others. In addition, the 1989 Loma Prieta earthquake occurred during the NRC review process and provided additional information on the process of earthquake nucleation along strike-slip faults, the distribution of strain along strike-slip faults, and the seismotectonic setting of the Pacific/North American plate margin. Our investigations, analyses, and review of new technical data, including those of the 1989 Loma Prieta earthquake, support the principal conclusions of the Final Report regarding all four elements of the license condition, including tectonic models, seismic source characteristics, ground motions, and adequacy of seismic margins at Diablo Canyon. An important result of the NRC review process and our subsequent studies is that the degree of uncertainty in many of the conclusions of the Final Report has been reduced significantly.

Although our studies did not produce substantive changes in the principal conclusions of the Final Report, we have significantly clarified our interpretation of potential seismic sources in three main areas: (1) strike-slip characterization of the Hosgri fault zone; (2) location and source structure of the 1927 earthquake; and (3) potential existence and characterization of a blind thrust fault beneath the San Luis/Pismo structural block. Each of these revised interpretations is summarized below. In addition, we describe other, less significant issues that reflect updating of geologic, seismologic, and source characterization data sets.

STRIKE-SLIP CHARACTERIZATION OF THE HOSGRI FAULT ZONE

In addressing the first two elements of the license condition, we concluded in the Final Report (PG&E, 1988) that the Hosgri fault zone is a strike-slip fault separating the offshore Santa Maria Basin to the west from the Los Osos/Santa Maria domain to the east. In response to NRC questions and concerns, we conducted several additional investigations and analyses that bear directly or indirectly on the style of faulting on the Hosgri fault zone. These studies included the following:

- Quantification of components of horizontal and vertical slip, which indicate ratios of horizontal to vertical slip of 2:1 to 30:1 (Response to Questions GSG 3 and GSG 4).

- Definition of fault classifications and use of fault rake and ratios of horizontal to vertical slip to classify style of faulting (Response to Question SSC 2). The ratio of horizontal to vertical slip of 2:1 to 30:1 indicates that the Hosgri fault zone is a strike-slip fault.

- Development of the concept of strain partitioning to explain the occurrence of subparallel strike-slip and reverse faults and folds, both worldwide and along the Hosgri fault zone (Response to Question GSG 2).

- Evaluation of the orientation and rates of regional crustal shortening in the Piedras Blancas antiform, offshore Santa Maria Basin and Los Osos/Santa Maria domain, and the contribution to rate of strain along the Hosgri fault zone (Response to Questions GSG 4 and GSG 13). These rates are incorporated in the assessment of horizontal and vertical slip on the Hosgri fault zone in Response to Question GSG 4.

- Documentation of the San Simeon/Hosgri pull-apart basin and use of basin geometry and age to evaluate slip rate on the bordering San Simeon and Hosgri fault zones (Response to Question GSG 12). An estimated right-slip rate of 1 to 4 millimeters per year on the San Simeon and Hosgri fault zones is required to form the pull-apart basin.

- Interpretation of high-resolution and common-depth-point seismic reflection data across the Hosgri fault zone, incorporating a refined velocity model and the techniques of retrodeformable structural modeling, and use of these interpretations to assess down-dip geometry and lateral and vertical variation in sense of vertical separation (Response to Question GSG 1, Attachment GSG Q1-A, Montages).

- Review of published criteria to identify and characterize strike-slip faults as they are imaged on seismic reflection data and comparison of the Hosgri fault zone to known strike-slip faults worldwide imaged on seismic reflection data, including the San Gregorio fault zone (Response to Question SSC 4). These analyses indicate that the Hosgri fault zone is comparable to other geophysically imaged strike-slip faults worldwide.

- Recognition of small, subsiding structural basins at releasing, en echelon steps of the Hosgri fault zone (Response to Question GSG 1).

- Recognition of upward-diverging fault splays and potential intra-fault-zone partitioning of dip slip and strike slip along the Hosgri fault zone (Response to Questions GSG 1, GSG 2, and GSG 3).

- Analysis of focal mechanisms for additional earthquakes that have occurred in the south-central coastal California region (Response to Question 43x). The epicenters of several earthquakes are along the surface trace of the Hosgri fault zone near the plant site. The focal mechanism solutions for these small- magnitude earthquakes are nearly pure strike slip.

These analyses confirm our interpretation of style of faulting along the Hosgri fault zone presented in the Final Report. The Hosgri fault zone is a strike-slip fault. The reach of the fault closest to Diablo Canyon, the San Luis/Pismo reach, has a ratio of horizontal to vertical slip ranging from 10:1 to 30:1. This ratio progressively decreases southward as lateral slip is lessened by crustal shortening within the Los Osos/Santa Maria domain east of the fault. In some scenarios, the ratio of horizontal to vertical slip

may decrease to less than 2:1 south of Point Sal, suggesting that the fault may become an oblique-slip fault along its southernmost reaches.

Our interpretation of the Hosgri fault zone differs from the Final Report only in the degree of certainty regarding the style of faulting. In the Final Report, we assigned relative weights of 65 percent for strike-slip faulting, 30 percent for oblique-slip faulting and 5 percent for reverse-slip faulting (PG&E, 1988, p. 3-19 to 3-22). The analyses performed subsequent to the Final Report have greatly reduced the uncertainty in classifying the style of faulting, especially along the northern three reaches of the fault, the Northern, San Luis/Pismo, and San Luis Obispo Bay reaches. All lines of evidence described above indicate that the fault zone is a strike-slip fault. Alternative interpretations that the Hosgri fault zone is a thrust, reverse or oblique-slip fault are not consistent with an integrated analysis of the multiple data sets used in the Long Term Seismic Program.

RELOCATION AND STRUCTURAL ASSOCIATION OF THE 1927 EARTHQUAKE

Subsequent to the Final Report and in response to NRC questions, we performed several analyses to refine and better document the epicentral location of the 1927 earthquake offshore of Point Arguello. These analyses included:

- Analysis of teleseismic and regional body wave data using recordings from the De Bilt and Pasadena seismograph stations (Response to Questions 46, 47 and GSG 8).
- Analysis and modeling of tsunami data using marigrams recorded at Hilo, Hawaii, San Francisco (Fort Point) and La Jolla, California (Response to Question GSG 5).
- Evaluation of Rossi Forel intensity data compiled by Byerly (1930) and used by Everndon and others (1981) to model the location of the 1927 earthquake (Response to Questions GSG 6 and GSG 7).

Analyses of these data sets constrain the location of the 1927 earthquake to be about 35 kilometers southwest of Point Arguello at approximately 34.35°N, 120.90°W (see Response to Question GSG 9 for discussion, Figure GSG Q9-1). This revised epicentral location is about 10 kilometers south of the location provided in the Final Report at 34.5°N, 120.9°W. The total uncertainty in the revised location is estimated to be 25 kilometers (Response to Question 46, p. 5).

The constraints on this location do not permit an interpretation of an epicenter near Point Sal nor in association with either the Hosgri fault zone or faults associated with the Casmalia block. In addition, the epicentral location is well south of the southern end of the Lompoc fold, thus precluding any postulated association with this structure.

Because of its far offshore location and epicentral uncertainty, it is difficult to associate the 1927 Lompoc earthquake with a known specific geologic structure. As discussed in Response to Question GSG 9, however, the epicentral location is along the southwestern projection of the structural boundary between the Santa Lucia Bank High and the southern offshore Santa Maria Basin. To the north, this boundary is structurally controlled by the Santa Lucia Bank fault. In the epicentral location of the 1927 earthquake, a structural boundary between the Santa Lucia Bank and offshore Santa Maria Basin has not been described in the literature. Recent work by Nicholson and others (1989), however, indicates that several late Cenozoic reverse faults are present in the epicentral region. The trend and recency of activity of

these faults is not known. These faults may be, in part, the southeastern continuation of the Santa Lucia Bank fault zone, suggesting that the 1927 earthquake may be associated with the southwestern structural margin of the offshore Santa Maria Basin.

In Response to GSG 9, we provided an assessment of the Santa Lucia Bank fault zone for seismic hazards at the plant site. In all cases, the ground motions estimated for the Hosgri fault zone far exceed those associated with a possible repeat of the 1927 earthquake anywhere along the Santa Lucia Bank fault, or along faults within the Santa Lucia Bank.

BLIND THRUST FAULT BENEATH SAN LUIS/PISMO STRUCTURAL BLOCK

In the Final Report, we concluded that an active blind thrust fault is not present beneath the San Luis/Pismo structural block (PG&E, 1988, p. 2-34 to 2-36). This interpretation is based on the following lines of reasoning:

- Blind thrust faults are associated with anticlines in the hanging wall above the thrust ramp. Mapping of marine terraces along the northwestern, western and southwestern margins of the San Luis/Pismo block indicate that the block is rising as a rigid structure, and has no internal fold deformation. Absence of folding is supported by mapping of fluvial terraces along San Luis Obispo Creek by Killeen (1988).

- Uplift of the block can be accommodated by recognized Quaternary reverse faults along the northeastern and southwestern margins of the block and by the Hosgri fault zone along the western margin of the block. A blind thrust fault beneath the block is not needed to account for uplift of the block and, if present, would produce uplift rates that far exceed actual uplift rates when combined with rates from the bordering block-margin faults.

- Rather than an active anticline, the San Luis/Pismo block contains the Pismo syncline. Mapping of marine terraces across the synclinal axis indicates that fold deformation ceased prior to 500,000 years ago and probably at least one million years ago.

Subsequent to submittal of the Final Report, Namson and Davis (1990) performed a retrodeformable structural analysis of the Santa Maria region. One of their structural sections crosses the San Luis/Pismo block. Applying the theories and techniques of fault-bend folding and fault-propagation folding (Suppe, 1983), they interpret the regional structure as a system of active southwest-verging blind thrust faults above a basal detachment at a depth of 11 to 14 kilometers. They postulate that the San Luis/Pismo block is underlain by one of these thrust faults.

The modeling technique applied by Namson and Davis can be a powerful quantitative tool for modeling crustal deformation in regions of crustal shortening, and may provide useful insights concerning the neotectonic development of south-central coastal California. However, as described in Response to Question GSG 10, the structural model developed by Namson and Davis violates many of the assumptions inherent in the modeling technique developed by Suppe (1983), and is not consistent with the known stratigraphic and structural relationships in the region. Therefore, in our opinion, their model does not portray the contemporary style of deformation occurring in south-central coastal California, and their interpretation of crustal structure and rates of deformation is not appropriate for assessing seismic hazard in the contemporary tectonic setting.

As requested by the NRC, we have provided alternative retrodeformable cross sections through the San Luis/Pismo structural block, in Response to Question GSG 11. Although these cross sections are based on assumptions inherent in the modeling technique, they are better constrained by and are consistent with the known geology in the region. These cross sections show that the San Luis/Pismo block may be underlain by active blind thrust faults. These modeled thrust faults could produce uplift of the block and localized folding along the margins of the block. The pattern and rates of uplift implied by these cross sections are consistent with the pattern and rates of uplift recorded by the marine terraces.

Based on these retrodeformable structural analyses, there is some probability that an active blind thrust fault underlies the San Luis/Pismo structural block. We have provided deterministic and probabilistic assessments of the postulated blind thrust fault in Response to Question GSG 11. As documented in the response, earthquakes associated with the blind thrust fault are not significant for either deterministic or probabilistic assessments of ground motions at the site.

OTHER ISSUES

In addition to the differences in interpretation described above, analyses performed in response to NRC questions have led to a number of minor refinements to conclusions in the Final Report. These include:

- *Reevaluation of the character and location of faults along the southwestern boundary of the San Luis/Pismo structural block.* The Final Report states that the San Luis Bay fault branches into two fault traces, the Rattlesnake trace and the Olson trace. Based upon studies conducted subsequent to the Final Report, we interpret these traces to be two distinct faults. In Response to Question SSC 5, we provide a seismic source characterization of each of these faults.

- *Assessment of focal mechanism solutions for earthquakes in the south-central coastal California region.* Subsequent to the Final Report, several additional small magnitude earthquakes have occurred. In Response to Question 43x, we provide focal mechanism solutions for earthquakes within 50 kilometers of the plant site.

- *Assessment of maximum magnitude.* The Final Report provides an assessment of maximum magnitude for potential seismic sources based on published regressions that relate magnitude to various fault parameters. Subsequent to the Final Report, new regressions were developed based on an updated and more extensive empirical data base. These regressions support the estimates of maximum earthquake magnitudes for potential seismic sources in the plant site region, and confirm the conclusions provided in the Final Report.

- *Rate of deformation within and bordering the Casmalia Hills structural block.* Subsequent to the Final Report, research conducted by D. Clark at the University of Nevada, Reno, provided improved estimates of the pattern and rates of deformation within the Casmalia Hills in the vicinity of Point Sal. We have incorporated these data into our assessment of rates of deformation occurring within the Los Osos/Santa Maria domain and along the Hosgri fault zone (see Response to Questions GSG 3 and GSG 4). These rates of deformation provide improved resolution and quantification of rates of slip along the Point Sal reach of the Hosgri fault zone and support the interpretation presented in the Final Report that the Hosgri fault zone is a strike-slip fault, potentially becoming an oblique-slip fault south of Point Sal.

CONCLUSIONS

Subsequent to submittal of the Final Report (PG&E, 1988), we conducted a number of follow-up investigations and data analyses in response to NRC questions and data requests. Most of these studies provide data that augment or clarify information and conclusions provided in the Final Report. Several studies, however, have led to an improved understanding and interpretation of several technical conclusions presented in the Final Report. In particular, a number of studies has been conducted to further evaluate source characteristics of the Hosgri fault zone. These studies conclusively indicate that the Hosgri fault zone is characterized by right slip along most of its length, including that part of the fault nearest the Diablo Canyon Power Plant. In addition, studies performed subsequent to the Final Report have led to an improved location of the 1927 Lompoc earthquake in the offshore region southwest of Point Arguello, and to an improved understanding of deformation within the San Luis/Pismo block and the potential for an active blind thrust fault beneath the block.

Although we have revised some of our interpretations of potential seismic sources in the plant site region, our investigations and revised interpretations support the principal conclusions of the Final Report. The controlling source for deterministic ground motions at the site is the Hosgri fault zone. The Hosgri fault zone is characterized by right slip occurring at a rate of 1 to 3 millimeters per year. The fault is an integral part of the more regional San Gregorio/San Simeon/Hosgri fault system, and structurally separates the offshore Santa Maria Basin to the west from the Los Osos/Santa Maria domain to the east. Other potential seismic sources in the region, including the Los Osos fault zone, San Luis Bay and Olson faults, postulated blind thrust faults beneath the San Luis/Pismo block, and potential source structures for the 1927 Lompoc earthquake have been considered in the deterministic analysis and included in the probabilistic ground motions at the Diablo Canyon site.

REFERENCES

Byerly, P., 1930, The California earthquake of November 4, 1927: Seismological Society of America Bulletin, v. 20, p. 53-66.

Everndon, J. F., Kohler, W. M., and Clow, G. D., 1981, Seismic intensities of earthquakes of conterminous United States--their prediction and interpretation: U. S. Geological Survey Professional Paper 1223, 56 p.

Killeen, K. M., 1988, Timing of folding and uplift of the Pismo syncline, San Luis Obispo County, California: M.S. Thesis, University of Nevada, Reno, 75 p. (unpublished).

Namson, J. S., and Davis, T. L. 1990, Subsurface study of the late Cenozoic structural geology of the Santa Maria Basin, western Transverse Ranges and southern Coast Ranges, California: American Association of Petroleum Geologists, v. 74, p. 467-492.

Nicholson, C., Sorlien, C., and Luyendyk, B. P., 1989, Reprocessing of the Line RU-10, Offshore southern Santa Maria Basin, California (abs.): EOS Transactions, American Geophysical Union, v. 70, no. 43, p. 1214-1215.

Pacific Gas and Electric Company, 1988, Final report of the Diablo Canyon Long Term Seismic Program: U. S. Nuclear Regulatory Commission Docket Nos. 50-275 and 50-323.

Suppe, J., 1983, Geometry and kinematics of fault-bend folding: American Journal of Science, v. 283, p. 684-721.

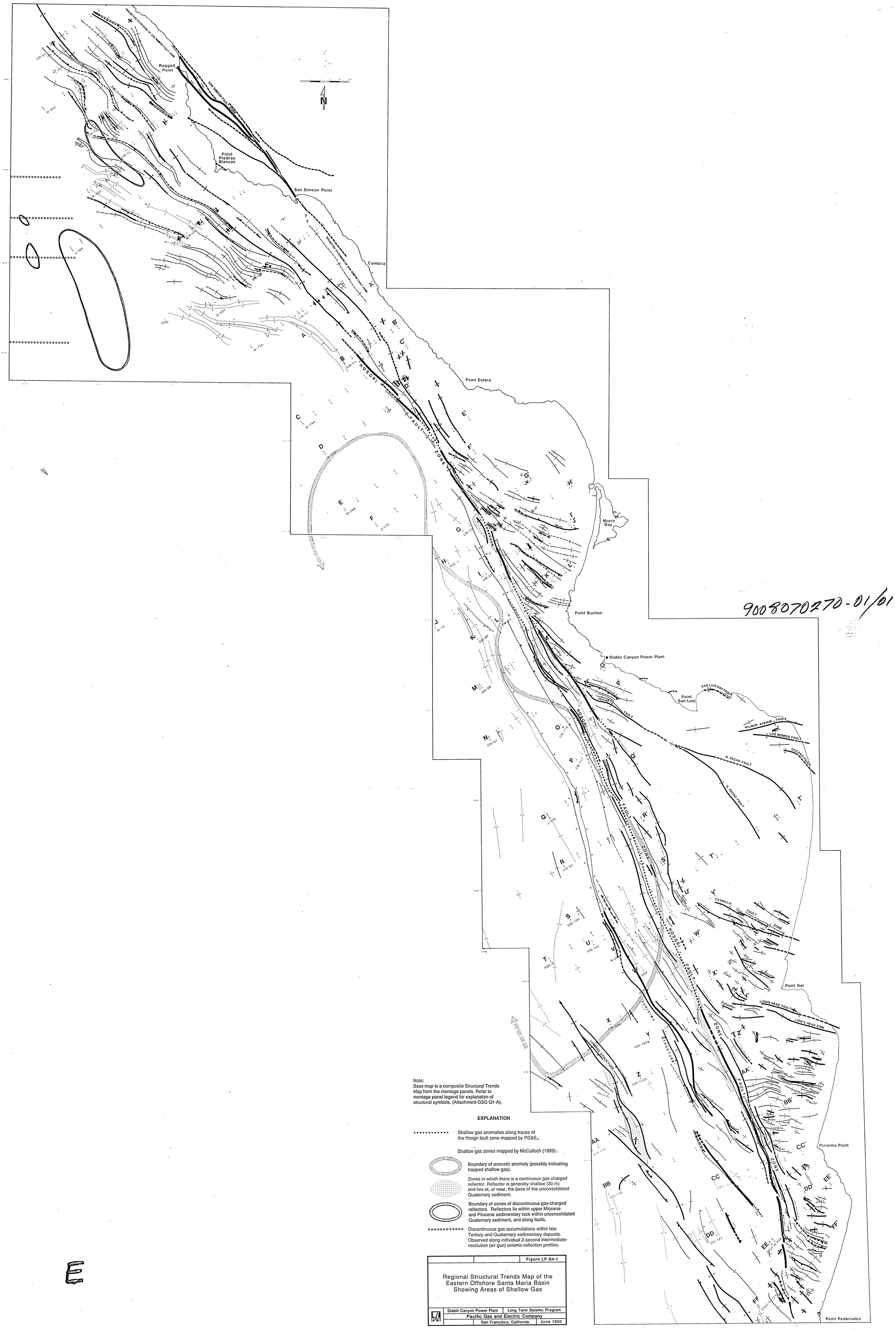

Note:
Base map is a composite Structural Trends Map from the montage panels. Refer to montage panel legend for explanation of structural symbols. (Attachment GSG Q1-A).

EXPLANATION

Shallow gas anomalies along traces of the Hosgri fault zone mapped by PG&E.

Shallow gas zones mapped by McCulloch (1989):

- Boundary of acoustic anomaly (possibly indicating trapped shallow gas).
- Zones in which there is a continuous gas-charged reflector. Reflector is generally shallow (30 m) and lies at, or near, the base of the unconsolidated Quaternary sediment.
- Boundary of zones of discontinuous gas-charged reflectors. Reflectors lie within upper Miocene and Pliocene sedimentary rock within unconsolidated Quaternary sediment, and along faults.
- Discontinuous gas accumulations within late Tertiary and Quaternary sedimentary deposits. Observed along individual 2-second intermediate-resolution (air gun) seismic-reflection profiles.

Figure LP Q4-1

Regional Structural Trends Map of the Eastern Offshore Santa Maria Basin Showing Areas of Shallow Gas

Diablo Canyon Power Plant	Long Term Seismic Program
Pacific Gas and Electric Company	
San Francisco, California	June 1990

9008070270-01/01

E

9008070270-01